SYNTHESIS AND IMPROVEMENT OF HIGH PERFORMANCE

PVC AND PVDF ULTRAFILTRATION MEMBRANES

A Dissertation
Presented to
The Academic Faculty

by

Chen Chen

In Partial Fulfillment
of the Requirements for the Degree
Doctor of Philosophy in Environmental Engineering

Georgia Institute of Technology
May, 2015

SYNTHESIS AND IMPROVEMENT OF HIGH PERFORMANCE

PVC AND PVDF ULTRAFILTRATION MEMBRANES

Approved by:

Dr. John Crittenden, Advisor
School of Civil and Environmental
Engineering
Georgia Institute of Technology

Dr. Yongsheng Chen
School of Civil and Environmental
Engineering
Georgia Institute of Technology

Dr. Ching-Hua Huang
School of Civil and Environmental
Engineering
Georgia Institute of Technology

Dr. William J. Koros
School of Chemical and Biomolecular
Engineering
Georgia Institute of Technology

Dr. Yonathan Thio
School of Chemical and Biomolecular
Engineering
Georgia Institute of Technology

Date Approved: March 12, 2015

To my parents, wife

ACKNOWLEDGEMENTS

First and foremost, I would like to express my sincere gratitude to Dr. John Crittenden and Dr. Yongsheng Chen for their continuous support of my graduate study and research, for their patience, enthusiasm, and intelligence. I cannot thank them enough for the countless help and I feel extremely lucky to have two such wonderful mentors for my PhD study.

I would also like to thank my committee members, Dr. Ching-Hua Huang, Dr. William J. Koros and Dr. Yonathan Thio for their time and guidance. Their valuable comments and advice were of great help to polishing my research.

My thanks also go to Dr. Guangxuan Zhu, who offered to help me whenever I was in need. I also wish to thank Ms. Martha Lindsay, Ms. Susan Ryan, Mr. Robert Simon, Ms. Jenny Eaton and other staff in the CEE department for their consistent support. I am grateful to the former and current research group members for helping me in the lab and the office. Also, many thanks to my friends Kunggang Li, Peizhe Sun, Biao Chang, Zhongming Lu, Arka Pandit, Jean-Ann James and Liz Minne.

Lastly, I would like to thank my family. My mother, Man Chen, my father, Lianggang Chen and my wife, Xuewei Yu, supported me with endless love and encouragement.

TABLE OF CONTENTS

LIST OF TABLES

LIST OF FIGURES

Page

LIST OF SYMBOLS

X_S^{PEGMA} The near-surface mole fraction of PEGMA [mol%]

A_{CF_2} The areas of the fitted CF_2 [cm^2]

A_{COO} The areas of the fitted COO [cm^2]

$\phi_{w,s}^{PEGMA}$ The near-surface weight fraction of PEGMA [wt%]

$D_{average}$ Average pore diameter [nm]

D_{max} Maximum pore diameter [nm]

ε Surface porosity [%]

LIST OF ABBREVIATIONS

PVDF	Polyvinylidene fluoride
PTFE	Polytetrafluoroethylene
PES	Polyethersulfone
PP	Polypropylene
PVC	Polyvinyl chloride
PSF	Polysulfone
MF	Microfiltration
UF	Ultrafiltration
NF	Nanofiltration
RO	Reverse osmosis
NOM	Natural organic matter
PAN-g-PEO	Polyacrylonitrile-graft-poly(ethylene oxide)
PSF-g-PEG	Polysulfone-graft-poly(ethylene glycol)
PEGMA	Poly(ethylene glycol) methyl ether methacrylate
PVDF-g-PEGMA	PVDF-graft-PEGMA
MBRs	Membrane bioreactors
EPSs	Extracellular polymeric substances
AFM	Atomic force microscopy
PVP	Poly(vinyl pyrrolidone)
DMAc	N,N-dimethylacetamide
XPS	X-ray photoelectron spectroscopy
SEM	Scanning electron microscopy

TMP	Transmembrane pressure
RMS	Root mean square
ATRP	Atomic transfer radical polymerization
THF	Tetrahydrofuran
DMF	N,N-dimethylformamide
CuCl	Copper(I) chloride
DMDP	4-4′-dimethyl-2-2′-dipyridyl
NMP	1-methyl-2-pyrrolidinone
HCl	Hydrochloric acid
$CaCl_2$	Calcium chloride
SA	Sodium alginate
SRHA	Suwannee River humic acid
TOC	Total organic carbon
FTIR	Fourier transform infrared spectrometer
ATR	Attenuated total reflection

SUMMARY

The applications of membrane technologies have dramatically increased during the last few decades due to technology improvement and significant cost reduction. Membrane applications can be found in water and wastewater treatment, pharmaceutical industry, chemical processing industry, food industry, etc. However, the membrane technology still faces two major challenges: membrane fouling and membrane lifetime. During the membrane filtration process, membrane fouling caused by natural organic matter (NOM) is an inevitable phenomenon, and physical or chemical cleaning is required for recovering the performance of membrane. As a result of these cleaning processes, membrane lifetime is shortened. For this reason, it is necessary to improve membrane's fouling resistance and lifetime in order to apply membrane technology in large-scale facilities.

The objective of this dissertation is to improve the fouling resistance and flux performance of polyvinyl chloride (PVC) and polyvinylidene fluoride (PVDF) membranes. We choose PVC and PVDF materials to synthesize membrane because of their outstanding physical properties (e.g., robust mechanical strength), chemical properties (e.g., acid and base resistance) and low cost.

This dissertation contains four sections. First, I prepared PVC membranes by adding different amounts of the amphiphilic copolymer (Pluronic F 127) into PVC casting solutions. The results show that the increase of the Pluronic F 127 content from 0 to 10 wt% increases the oxygen content on the membrane surface, reaching an asymptote when 8 wt% or greater Pluronic F 127 is used. Both pore size and pore density decrease

dramatically as Pluronic F 127 content increases. The PVC membrane exhibits remarkable antifouling characteristics even at 2 wt% Pluronic F 127 addition. Second, I prepared PVDF membranes by adding PVDF graft poly(ethylene glycol) methyl ether methacrylate (PEGMA) (PVDF-g-PEGMA) as additive in casting solutions via the phase inversion method. The results show that the prepared PVDF membranes have unique pillar-like structures on surfaces. The fabricated membranes exhibit an intriguing morphology with ~200 nm diameter of pillar-like structures connected by a porous mesh, high flux of 5170 $L/m^2/h/bar$ under low transmembrane pressure (0.07 MPa), and high removal efficiencies of sodium alginate (SA) (over 87%) and Suwannee River humic acid (SRHA) (over 72% with calcium). Third, I explored the formation mechanism of pillar-like structures from aspects of solvent and additive. Based on the experimental results and analysis of the ternary diagram, both NMP and PVDF-g-PEGMA must coexist in casting solution to form pillar-like structures. When NMP is in the solvent, PEGMA segments have enough time to migrate to the surface and repel each other during the phase inversion process. Furthermore, I investigated how the performance of PVDF membranes changes when different amounts of PEGMA are added to the casting solutions. The results show that the dose of PEGMA additive significantly influences not only the properties of the membrane, but also its performance. Both the hydrophilicity and the surface roughness of prepared PVDF membranes increase as more PEGMA is added to the casting solution. The surface porosity and pore size tend to decrease with higher PEGMA dose. The addition of PEGMA improves the hydrophilicity of the membrane, which leads to improved membrane fouling resistance property and flux recovery ratio.

Overall, this study significantly improved the fouling resistance and flux of PVC and PVDF membranes. Especially for PVDF membranes, it has advanced out understanding of the forming mechanism of pillar-like structure on the surface of our synthesized PVDF membrane. The results of this study may provide useful casting conditions and guidance for synthesizing higher performance PVC and PVDF membranes.

CHAPTER 1

INTRODUCTION

1.1 Background and motivation

A membrane is a selective barrier that has different selectivity between species. Different types of membranes have been developed for specific applications. Membranes such as microfiltration (MF), ultrafiltration (UF), nanofiltration (NF) and reverse osmosis (RO) are pressure driving membranes (Mulder 1991). When comparing membrane technology with conventional treatment, membrane technology has several advantages such as less land use, less by-product, consistent and high quality permeate (Baker 1991).

Membrane technologies have been increasingly applied in water and wastewater treatment (Judd and Judd 2011), pharmaceutical industry (Pabby, Rizvi et al. 2008), food industry (Daufin, Escudier et al. 2001) during the last few decades because of the technology improvement and cost reduction (Baker 1991, Petersen 1993, Brindle and Stephenson 1996, Baker and Dudley 1998, Childress and Elimelech 2000, Van der Bruggen, Everaert et al. 2001, Rasanen, Nystrom et al. 2002, Bartels, Wilf et al. 2005, Frenzel, Stamatialis et al. 2006, Manttari, Viitikko et al. 2006, Bellona and Drewes 2007, Judd 2008). According to research by Freedonia Group, the global membrane filtration market will reach \$25 billion in 2017, on 9.2 percent annual growth (http://www.thomasnet.com/journals/fluid-gas-flow/global-membrane-filtration-market-will-surpass-25-billion-in-2017/). However, there are two major challenges faced by membrane technology. The first challenge is membrane lifetime. The second challenge is membrane fouling during the filtration process (Mulder 1991).

Membrane lifetime is the period that membrane can be used for filtration without replacing with new membrane (Goosen, Sablani et al. 2004). The membrane lifetime is related to the properties of membrane backbone material. Membrane backbone material is the main material used to cast the membrane. During the membrane filtration process, membrane fouling will happen because of the accumulation of colloids, microorganisms and natural organic matter (NOM) (Mulder 1991, Wang, Tan et al. 2001, Asatekin, Kang et al. 2007). Membrane fouling is an undesirable phenomenon since it decreases the efficiency of the membrane filtration process (Listiarini, Chun et al. 2009, Zhou, Liu et al. 2009). In order to maintain the performance of membrane, cleaning process is needed. Due to the necessary cleaning process (e.g., air flush, backward flush and chemical cleaning) to maintain the performance of membrane, the intrinsic properties of membrane backbone material is essential for membrane lifetime (Mulder 1991). An outstanding backbone membrane material should have excellent physical properties (e.g., robust mechanical strength) and chemical properties (e.g., acids and base resistance). The common polymers used to prepare membrane include polyvinylidene fluoride (PVDF), polytetrafluoroethylene (PTFE), polyethersulfone (PES), polypropylene (PP) polyvinyl chloride (PVC), polysulfone (PSF) and et.al (Yang, Xu et al. 2005, Chakrabarty, Ghoshal et al. 2008, Teoh and Chung 2009, Zhang, Chen et al. 2009, Darvishmanesh, Tasselli et al. 2011, Pezeshk, Rana et al. 2012, Liu, Chen et al. 2013). In recent years, PVC and PVDF membranes have been used in many applications due to their good physical and chemical properties (Deshmukh and Li 1998, Xu and Xu 2002, Yeow, Field et al. 2002, Yeow, Liu et al. 2004, Kim, Lee et al. 2005, Fontananova, Jansen et al. 2006, Tan, Tan et

2

al. 2006, Van der Bruggen 2009, Tian, Chen et al. 2010, Liu, Chen et al. 2012). Therefore, I choose PVC and PVDF as backbone material for this study.

Membrane fouling is another major challenge for the membrane filtration technology (Baker 2012). During membrane operation, the accumulation of colloids, microorganisms and natural organic matter (NOM) is the main cause for fouling. Flux declines and operation pressure increases as membrane fouling builds up. More frequent physical and chemical cleaning is needed if the membrane fouls easily, and this eventually leads to a shorter membrane lifetime. Therefore, much research has been devoted to improve the fouling resistance of membranes. According to past studies, membrane fouling is mainly caused by the intrinsic hydrophobicity of the backbone material (Rana and Matsuura 2010). Several studies have shown that membrane fouling resistance can be improved by increasing the hydrophilicity of membranes (Asatekin, Kang et al. 2007, Kang, Asatekin et al. 2007). Several methods have been proved to improve the hydrophilicity of membranes. These methods can be classified into surface coating (Chiag, Chang et al. 2012), surface grafting (Taniguchi and Belfort 2004) and interfacial polymerization (Liu, He et al. 2011). However, those methods have several disadvantages. For instance, surface coating uses physical adsorption to coat a thin layer of water-soluble polymers or surfactants on the membrane from a solution. The coating is usually unstable and can be washed away during membrane operation. To introduce functional groups on the membrane surface, surface grafting requires an extra step, such as UV photoinitiation, redox initiation, gamma-ray initiation, or plasma initiation, which makes surface grafting inapplicable in large-scale industrial manufacturing (Schäfer, Fane et al. 2005, Liu, Xu et al. 2009, Zhou, Liu et al. 2009). Interfacial polymerization is

3

often carried out under highly hazardous conditions (Rana and Matsuura 2010). Another method recently applied to improve the hydrophilicity of membranes is blending modification (Zhang, Xu et al. 2013). In the blending modification method, additives (e.g., hydrophilic polymer, amphiphilic polymer and zwitterionic polymer) are added in the membrane casting solution during membrane preparation (Yi, Zhu et al. 2012, Venault, Liu et al. 2014, Yu, Kang et al. 2014). When comparing the blending modification method with other modification methods, the blending modification method is simple and applicable for large-scale industrial manufacturing.

In blending modification, copolymers have been used to improve the hydrophilicity of ultrafiltration membranes. Several studies show that by adding copolymers into the casting dopes, the hydrophilicity and fouling resistance of membranes casted by the phase inversion technique had been dramatically improved (Asatekin, Kang et al. 2007, Kang, Asatekin et al. 2007, Phillip, O'Neill et al. 2010).

Amphiphilic copolymers are usually used in the blending modification method because the hydrophobic segments in this type of copolymer can physically combine with the membrane backbone matrix, while the hydrophilic segments will extend on the membrane surface to increase membrane hydrophilicity.

The self-assembly of copolymers can lead to uniform pore size distribution and high flux owing to high pore density. A membrane with uniform pore size can exhibit better selectivity than one with a wide distribution of pore sizes (Gin and Noble 2011). Usually the fabrication of a membrane without any structural defects is not easy. If defects such as large pores exist, most of the particles or molecules will pass through these pores first because they have the least resistance (Gin and Noble 2011). Self-

4

assembly is the next generation of ultrafiltration membrane fabrication because it can form defect-free membranes with high pore density. Such membranes have high flux and superior molecular weight cut-offs (Phillip, Hillmyer et al. 2010).

Both amphiphilic block copolymer and amphiphilic graft copolymer have been used to improve membranes hydrophilicity (Bates and Fredrickson 1999, Wang and Li 2011, Zavala-Rivera, Channon et al. 2012).

Block copolymers dissolved in certain solvents can form micelles or other self-assembled superstructures depending on: (1) the concentration (Smart, Lomas et al. 2008, Nunes, Sougrat et al. 2010), (2) block copolymer composition (Phillip, Hillmyer et al. 2010, Phillip, O'Neill et al. 2010), (3) block-block and block-solvent interactions, (4) the ratio of block lengths (Smart, Lomas et al. 2008, Nunes, Sougrat et al. 2010), (5) overall copolymer molecular weight (Phillip, O'Neill et al. 2010), (6) solvent composition and solvent selectivity (Phillip, O'Neill et al. 2010), (7) solvent evaporation rate (Phillip, Hillmyer et al. 2010, Phillip, O'Neill et al. 2010), and (8) evaporation time (Peinemann, Abetz et al. 2007, Phillip, Dorin et al. 2011). Through the rational control of these conditions, we can prepare a self-assembling ultrafiltration membrane.

Several amphiphilic graft copolymers have been successfully applied in the membrane casting process to improve membrane hydrophilicity (Hester, Banerjee et al. 2002, Chen, Ying et al. 2003, Akthakul, Salinaro et al. 2004, Zhao, Zhu et al. 2007, Zhao, Qian et al. 2008, Hashim, Liu et al. 2009, Li, Zhao et al. 2009, Liu, Xu et al. 2009). For instance, polyacrylonitrile-graft-poly(ethylene oxide) (PAN-g-PEO) was fabricated by free radical polymerization (Kang, Asatekin et al. 2007). Then PAN-g-PEO was used as an additive in the fabrication of a PAN/PAN-g-PEO membrane. This membrane exhibits

antifouling properties (Asatekin, Kang et al. 2007, Kang, Asatekin et al. 2007) and prevents the irreversible adhesion of bacteria (Adout, Kang et al. 2010). Polysulfone-graft-poly(ethylene glycol) (PSF-g-PEG) was used as an additive in PSF membrane fabrication to improve its resistance to fouling by proteins (Park, Acar et al. 2006). Several studies have reported that the hydrophilicity of PVDF membranes were significantly improved by adding the amphiphilic copolymer PVDF-graft-poly(ethylene glycol) methyl ether methacrylate (PEGMA) into the membrane casting solution (Hester, Banerjee et al. 2002, Asatekin, Menniti et al. 2006, Chen, Liu et al. 2006, Hashim, Liu et al. 2012). Addition of PVDF-g-PEGMA to PVDF has produced membranes with good fouling resistance (Hester, Banerjee et al. 2002).

1.2 Research objectives

The overall goal of this research is to improve the fouling resistance and flux performance of PVC and PVDF membranes with a simple and easy method, which would render the results more applicable to large-scale production.

The specific objectives of this research are:

1) To improve the performance of PVC membrane by using amphiphilic copolymer of Pluronic F 127;

2) To improve the performance of PVDF membrane by using amphiphilic copolymer of PVDF-g-PEGMA;

3) To investigate the forming mechanism of pillar-like structure on PVDF membrane based on our previous work;

4) To investigate the influence of PEGMA dose on the PVDF membranes.

6

The rest of the thesis is organized as follow.

Chapter 2 describes the influence of Pluronic F 127 on PVC membranes. I prepared flat PVC membrane by adding different amounts of Pluronic F 127 (from 0 wt% to 10 wt%) to casting solutions and characterized the synthesized membranes using XPS, SEM, AFM, contact angle, and flux measurements.

Chapter 3 describes the research of using amphiphilic graft copolymers of PVDF-g-PEGMA as additive to synthesize PVDF membranes. The membrane characteristics and performance were systematically examined when adding different molecular weights ($PVDF_{275K}$-g-PEGMA, $PVDF_{534K}$-g-PEGMA) and the amounts (5 wt%, 10 wt%, and 15 wt%) of copolymer.

Chapter 4 describes the research on exploring the formation mechanism of pillar-like structures from aspects of solvent and additive.

Chapter 5 describes the research of investigating the influence of PEGMA dose on PVDF membrane.

Chapter 6 presents the conclusions based on the results from this study. Furthermore, recommendations for future research are made based on current results.

CHAPTER 2

LOW-COST ANTIFOULING PVC ULTRAFILTRATION MEMBRANE FABRICATION WITH PLURONIC F 127: EFFECT OF ADDITIVES ON PROPERTIES AND PERFORMANCE

2.1 Introduction

Membrane fouling poses a grand challenge for increasing the performance of membrane filtration technology (Shannon, Bohn et al. 2008). Fouling is caused mainly by the accumulation of natural organic matter (NOM), colloids, and microorganisms during long-term operation. Particularly, fouling in membrane bioreactors (MBRs) occurs when microbe-generated extracellular polymeric substances (EPSs), such as polysaccharides, proteins, and NOM, progressively build up on the membrane (Shannon, Bohn et al. 2008, Herzberg, Kang et al. 2009). Membrane fouling may lead to a decline in flux, increased operation pressure, a need for frequent physical and chemical cleaning, and even a shorter membrane life. Thus, developing antifouling membrane materials is one of the most important tasks in improving the sustainability of membrane filtration technology.

Of the many modern membrane fabrication approaches, membrane surface modification has been successful in preventing fouling through grafting of various types of polymers onto the membrane surface (Zhou, Liu et al. 2009). For example, poly(ethylene oxide) (PEO) has been used for the effective prevention of bacterial adhesion. Features of PEO include its hydrophilicity, large excluded volume, electroneutrality, and unique ability to coordinate surrounding water molecules in an

9

aqueous medium (Kang, Asatekin et al. 2007), (Hamilton-Brown, Gengenbach et al. 2009), (Su, Cheng et al. 2009), (Pasche, Textor et al. 2005). Previous studies using atomic force microscopy (AFM) revealed that steric repulsion made the polyacrylonitrile-graft-poly(ethylene oxide) (PAN-g-PEO) membrane resistant to bacterial adhesion (Adout, Kang et al. 2010). Amphiphilic graft/comb copolymers with hydrophobic backbones and hydrophilic PEO side chains have been successfully employed as surface-modifying additives for polyvinylidene fluoride (PVDF) (Hester, Banerjee et al. 1999), (Hester, Banerjee et al. 2002), (Hester and Mayes 2002) and polysulfone (PSf) ultrafiltration (UF) membranes. PEO-containing Pluronic F 127 was added into poly(ether sulfone) (PES) membrane to reduce irreversible fouling (Wang, Wang et al. 2005). Such additives can change the hydrophilicity, surface roughness, and flux performance of the membrane (Rana and Matsuura 2010).

Backbone materials and additives are both important for improving membrane performances. Cellulose acetate (CA), PSF, PAN, polyethylene (PE), PES, PVC, and PVDF are commonly used as backbone materials of membranes for water treatment. Particularly, PVC is an outstanding candidate due to its robust mechanical strength, low cost, and other excellent physical and chemical properties such as high resistance to acids, bases, solvents, and chlorine (Xu and Xu 2002), (Zhang, Chen et al. 2009). Moreover, PVC membranes can maintain a long membrane life and remain intact after repeated cleaning with a wide variety of chemical agents. Therefore, a chlorine disinfection process can be combined with membrane filtration processes (Huang, Schwab et al. 2009). Although both PVC and PVDF membranes have excellent performance when compared with other organic membranes, PVC is considerably

10

cheaper than PVDF. The PEO-containing amphiphilic polymer has been successfully used in the PVDF membrane to increase the hydrophilicity and fouling-resistance, as mentioned above; however, few studies explored this using the PVC membrane with amphiphilic copolymer, except two studies using poly(vinyl pyrrolidone) (PVP) or poly(ethylene glycol) (PEG) as additives (Xu and Xu 2002), (Mei, Xiao et al. 2011). Among the amphilic copolymers, Pluronic F127 or PEO-poly (propylene oxide) (PPO)-PEO is a cheap one with the molecular formula of $H(OCH_2CH_2)_{98}$-$(OCHCH_3CH_2)_{67}$-$(OCH_2CH_2)_{98}OH$ and a molecular weight of 12,528. The PEO segment of Pluronic F 127 is highly hydrophilic, while the PPO segment of Pluronic F 127 is hydrophobic (Alexandridis, Athanassiou et al. 1994, Wang, Wang et al. 2005). Using Pluronic F 127 as the solution additive for PVC membrane presents a potential for creating low-cost antifouling ultrafiltration membranes.

In this study, we fabricated PVC membranes with different additions of Pluronic F 127 and systematically characterize the performance and properties of the modified PVC membranes. XPS was used to investigate the elemental composition on the membrane surface and oxygen content. SEM was used to characterize the pore size and pore distribution or density. Contact angle measurements were conducted to investigate hydrophilicity. AFM was used to map the topography and to quantify the surface roughness. Overall, the study provides detailed insight into the PVC membrane casting using Pluronic F 127 as additives.

2.2 Materials and methods

2.2.1 Chemicals and materials

Unless otherwise specified, all reagents and chemicals were analytical grade. PVC (CAS No. 9002-86-2), PEG 6000 (CAS No. 25322-68-3), Pluronic F 127 (CAS No. 9003-11-6), sodium alginate, and N,N-dimethylacetamide (DMAc) were purchased from Sigma-Aldrich (St. Louis, MO). NaCl was purchased from Fisher Scientific (Pittsburgh, PA). Sodium alginate was used as the model organic foulant. Stock solution was prepared by adding sodium alginate to deionized water and mixing until completely dissolved. The stock solution of 2 g/L sodium alginate was stored in a sterilized glass bottle at 4°C.

2.2.2 Membrane casting by phase inversion method

Membranes were prepared from casting solutions containing PVC, PEG, Pluronic F 127, and DMAc according to the compositions listed in Table 3.1. The casting solution was prepared in a 125-mL conical flask and heated to approximately 60°C while being stirred with stir bars of 7.9×25.4 mm (diameter × length) at 600 rpm using a digital stirring hot plate (Corning, MA). Casting solution preparation at 60°C was chosen because several trial experiments were conducted and revealed that PVC (with the compositions specified in Table 1) can dissolve completely in DMAc within 24 hours. After polymers were dissolved completely and stirred for at least 24 hours, the resulting solution was degassed, while it was no longer being mixed, for at least 30 minutes until no gas bubbles were visible. The solution was cast on a first-grade surface optical mirror

using an 8-inch–wide doctor blade (Universal blade applicator, Paul N. Gardner Company, Inc.; Pompano Beach, FL) that was set with a membrane thickness of ~ 200 µm. The mirror was immersed in a bath of deionized water at room temperature, 24 ± 1°C. The membrane was left in the coagulation bath for 10 minutes until the membrane detached from the mirror, and subsequently was immersed in the deionized water bath for 24 hours, after which the membrane was air dried for 24 hours before use in experiments.

Table 2.1 Compositions of PVC membrane casting solutions.

Membrane	PVC(g)	PEG (g)	DMAc (g)	Pluronic F 127 (g)	Pluronic F 127/PVC wt/wt (%)
No.1	12.8	3.2	84	0	0
No.2	12.8	3.2	83.744	0.256	2
No.3	12.8	3.2	83.488	0.512	4
No.4	12.8	3.2	83.232	0.768	6
No.5	12.8	3.2	82.976	1.024	8
No.6	12.8	3.2	82.720	1.280	10

2.2.3 X-ray photoelectron spectroscopy (XPS)

XPS is an analytic technique that directs a monochromatic beam of X-rays onto a sample and detects the characteristic electrons that are ejected. The energies and number of these electrons can be used to determine not only the elements present on the sample surface but also their abundance and chemical bonding state. All elements except hydrogen can be detected (Tang, Kwon et al. 2007).

In the present study, XPS (Thermo K-Alpha XPS system) was used to analyze the fraction of modified membrane of depth less than 5 nm in the near surface. Survey XPS spectra were obtained by sweeping over electron binding energies of 0–1350 eV with a resolution of 1 eV. For all membranes, XPS analysis was conducted on the side of the membrane opposite to the side in contact with the mirror, which had been exposed to the feed solution during membrane operation (Hester, Banerjee et al. 2002). The relative elemental composition was determined on the basis of the intensity (area) of the peaks.

2.2.4 Scanning electron microscopy (SEM) analysis

Scanning electron microscopy (SEM) (Zeiss Ultra 60; Carl Zeiss NTS, LLC North America) was used for imaging the membrane surface and cross-sectional morphologies. The flat membranes were cut into small slices and then immersed in liquid nitrogen for approximately 10 minutes. The frozen membrane was then fractured and flexed using tweezers to obtain the cross section for imaging. The membranes were fixed on stubs with carbon dots and then sputter coated with a ~2 nm gold layer. Coated samples were examined at different magnifications at an acceleration voltage of 5 kV.

2.2.5 Liquid sessile drop contact angle analysis

Water contact angle measurement of the membranes was performed using a Ramé-hart Model 250 goniometer (Ramé-hart Instrument Co.). The membranes were air dried at least 24 hours before the measurements. Ten to fifteen repeat measurements were taken for the dynamic contact angle variations over 180 seconds immediately after the droplet was placed on the membrane. The dynamic water contact angle was measured by placing 2 µL of deionized water on the membrane surface. Values and statistical analysis are reported as a box and whisker plot (Frigge, Hoaglin et al. 1989).

2.2.6 Flux performance

The experimental setup for flux evaluation was similar to those previously described (Listiarini, Chun et al. 2009). Briefly, the filtration experiment was conducted using an Amicon 8200 stirred dead-end filtration cell (Millipore) and the membranes had an effective area of 28.7 cm^2. The filtration cell, with a cell volume of 200 mL, attached to a 5.0-L dispensing vessel. Permeate was collected and weighted using Ohaus Adventurer Pro Balance AV8101. Data on permeate mass were collected every minute using Collect 6.1 software.

Filtration cells were stirred at 300 rpm using a stirring plate (PC-410D; Corning, MA) to minimize the concentration polarization. Fouling experiments were performed at a transmembrane pressure (TMP) of 0.07 MPa (10 psi).

The experimental procedures adopted for each fouling experiment are as follows. First, the membranes were soaked in deionized water for 48 hours prior to the

experiment; they were then compacted with deionized water at 10 psi for approximately 2 hours until the flux was stable. The membranes were then conditioned with a NaCl solution that had an ionic strength of 10 mM for 2 hours. Subsequently, the feed solution was added to the filtration cell to initiate the fouling test; this solution contained 20 mg/L sodium alginate solution and 10 mM NaCl. Each fouling test ran for at least 14 hours and was repeated in triplicate. Reported data are average values. At the end of the fouling runs, physical cleaning was conducted as follows: the foulant solution in the feed tank was disposed of, the tank was rinsed with deionized water then with electrode solution; the fouled membrane was flushed under deionized water followed by electrode solution for 5 times at room temperature (cleaning time of about 1 minute). To determine the flux after physical cleaning, the cleaned membrane was then exposed to foulant-free electrolyte solution according to standard conditioning practices (Kang, Asatekin et al. 2007). The sodium alginate concentration was determined by Beckman DU 7400 spectrophotometer at a wavelength of 220 nm. The particle size distribution of raw water and water after membrane filtration were determined by Zetasizer Nano ZS (Malvern Instruments Ltd, UK).

2.2.7 Atomic force microscopy (AFM) analysis

AFM was conducted with an Agilent 5500 AFM (Agilent Technologies, Inc., US) to map the morphology of the membrane surface and to quantify surface roughness. The acoustic AC tapping mode of AFM was used to characterize the membrane morphology, and image acquisition and processing was performed with PicoView software (Version 6.1.3). Silicon cantilever probes (BudgetSensors, Bulgaria) with a nominal resonant

frequency of 150 kHz and a force constant of 5 N/m were used for sample scanning. The cantilever probes were oscillated at an amplitude of approximately 2.5 V before engagement, and the piezo scanner stopped moving the sample toward the probe when the amplitude decreased by 10% due to tip-sample interactions. Once engaged, the servo system automatically adjusted the oscillation amplitude to 1.0–2.0 V for optimal imaging quality. The typical scan rate was 0.1–0.3 line/second with a scan size of 5 by 5 μm^2. At least 10 replicates were performed for each membrane sample.

2.2.8 Membrane cost analysis

PVC backbone material is less than 10% of the price of PVDF, and PVC membranes have shown outstanding physical and chemical properties (Zhang, Chen et al. 2009). Pluronic F 127 is an inexpensive commercial amphiphilic copolymer and has almost the same price as PVC; thus, PVC modified with different additions of Pluronic F 127 holds great promise in making low-cost and antifouling membranes.

2.3 Results and discussion

2.3.1 XPS analysis of membrane near-surface composition

The near-surface compositions of PVC membranes containing 0–10 wt% Pluronic F 127 were determined by XPS as shown in Figure 2.1. XPS survey results show that all membrane surfaces contain the elements carbon (C), chlorine (Cl), and oxygen (O). From the scan results, the oxygen content increased from 4.05% in PVC membrane without Pluronic F127 to 10.35% in PVC membrane with 10 wt% Pluronic F127. The 4.05% oxygen in the PVC membrane is probably from PEG in the casting solution. The survey scan detected no nitrogen, indicating that DMAc were not present or in a very low concentration on the PVC membrane surface. When XPS is used to analyze the membrane surface, it creates extremely low pressure of ~ 10^{-8} mbar; thus, if a small amount of DMAc is in the membrane, it evaporates and becomes undetectable because the vapor pressure of DMAc is ~2.0 mbar at 20°C. When Pluronic F 127 was increased in the present study, the oxygen content on the membrane surface first increased then reached an asymptote at approximately 8 wt% Pluronic F 127 (Figure 2.1). If Pluronic F 127 occupied all the area on the membrane surface, the oxygen content would be 33.72%. However, for Pluronic F 127 concentrations greater than 10%, only 10.35% oxygen and 23.19% chlorine were observed; this suggests that Pluronic F 127 only partially occupied the membrane surface. The PPO segment of Pluronic F 127 is hydrophobic and tends to interlacing with PVC. Accordingly, increasing Pluronic F 127 on the PVC membrane surface can increase the hydrophilicity. As noted above, DMAc is a solvent for PVC and PEG, whereas water is a non-solvent for PVC in the phase inversion process. When

19

casting thin film solution immersed in water, PVC remains in its original position. Conversely, PEG, which is a water-soluble polymer, tends to move to the water phase (Delgado, Francis et al. 1992). Pores form when PEG moves from polymer to water. When exposed to water, DMAc dissolves, and the polymer becomes more concentrated, forming a stable structure.
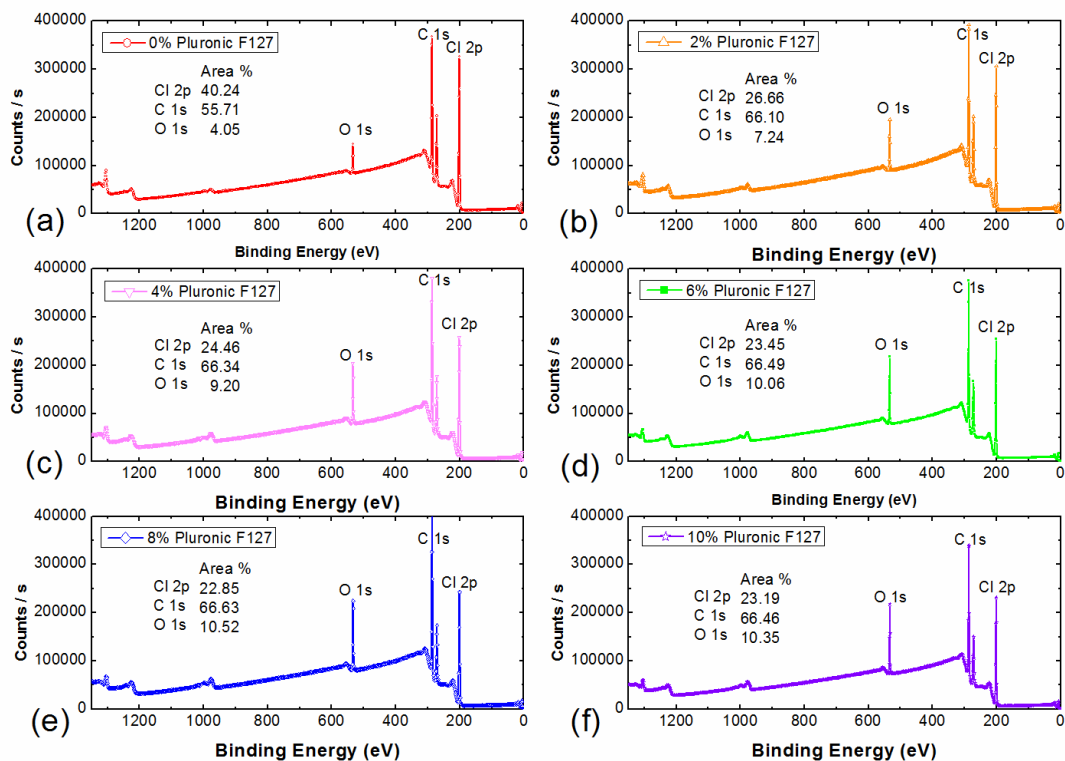
Figure 2.1. Survey of elements on the surface of the PVC membranes with additions of Pluronic F 127 at levels of (a) 0 wt%, (b) 2 wt%, (c) 4 wt%, (d) 6 wt%, (e) 8 wt%, and (f) 10 wt%.

2.3.2 Morphology

Figure 2.2 shows SEM images of membrane surfaces (left) and cross sections (right) of PVC membrane alone and with added Pluronic F 127. The PVC membrane not containing Pluronic F 127 has a pore size of 10–140 nm. As the Pluronic F 127 content increases, the pore size of the PVC membrane tends to become smaller. Few pores appeared on the membrane surface with 4 wt%, 6 wt%, 8 wt%, and 10 wt% Pluronic F 127. The pore size of PVC membrane with 8 wt% or 10 wt% of Pluronic F 127 is less than 10 nm. Macrovoids formed in the bottom layer of the PVC membrane, which is probably because of instantaneous liquid–liquid demixing during membrane immersion in the coagulation bath (Hester and Mayes 2002). When Pluronic F 127 concentrations were 0 wt% or 2 wt% in the casting solution, the cross section displayed finger-like structures. As the amphiphilic copolymer Pluronic F 127 content increased, the finger-like structure disappeared gradually. These phenomena are probably because the amphiphilic copolymer delays the rate of phase inversion, which decrease the formation of finger-like structure.
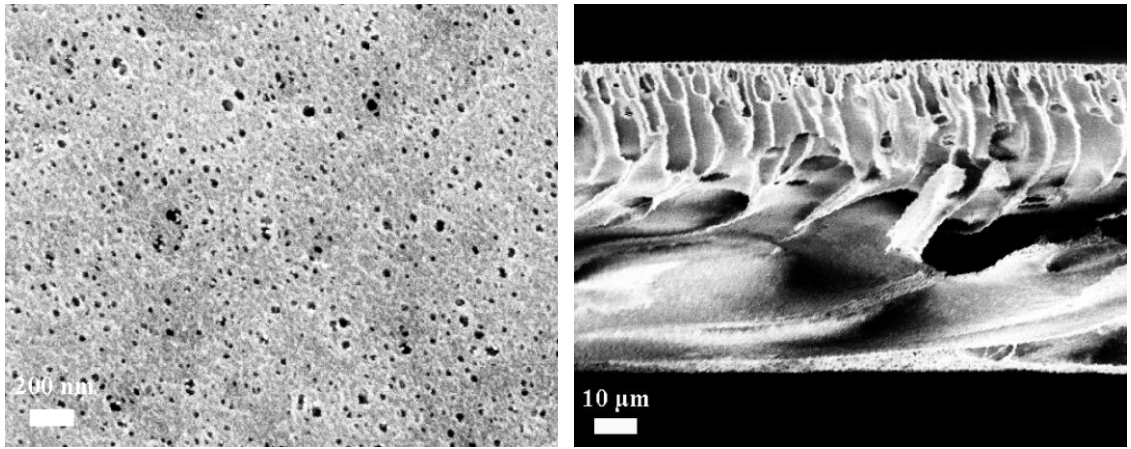
(a)
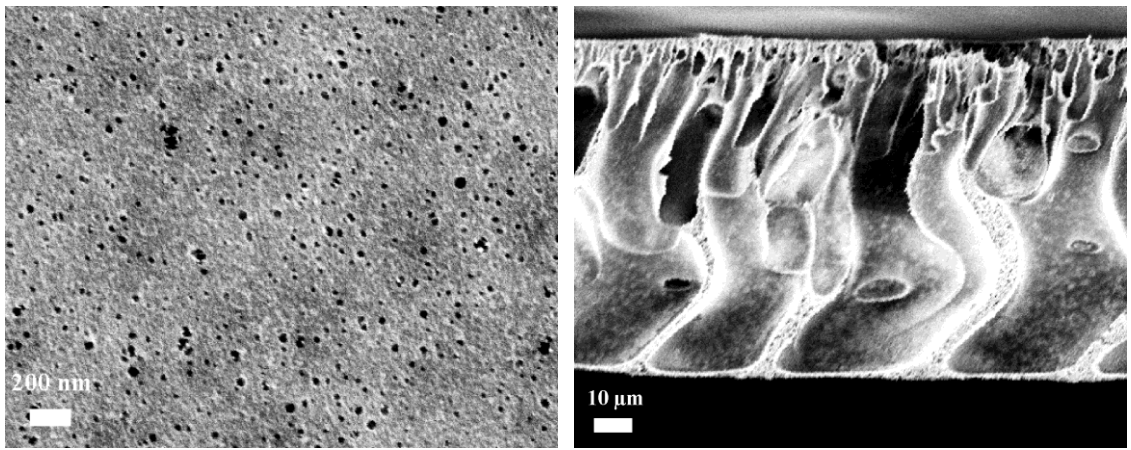
(b)
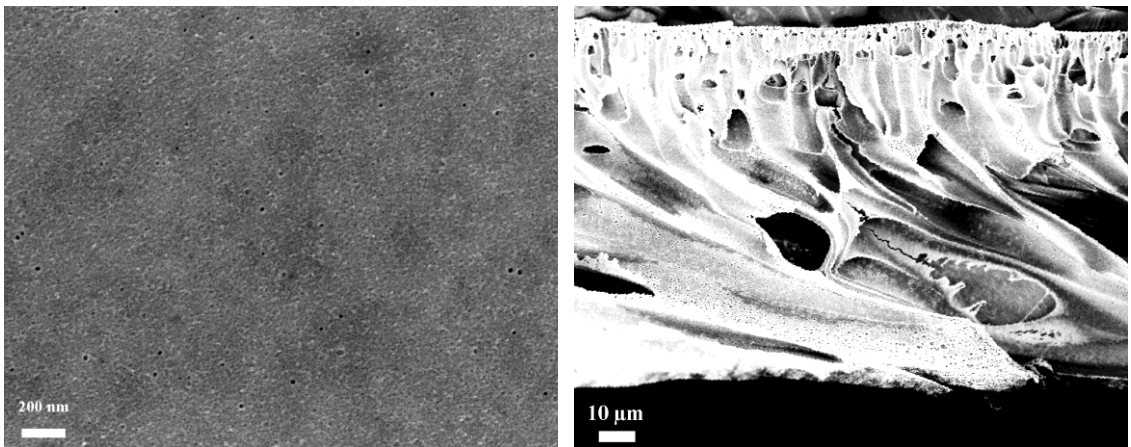
(c)
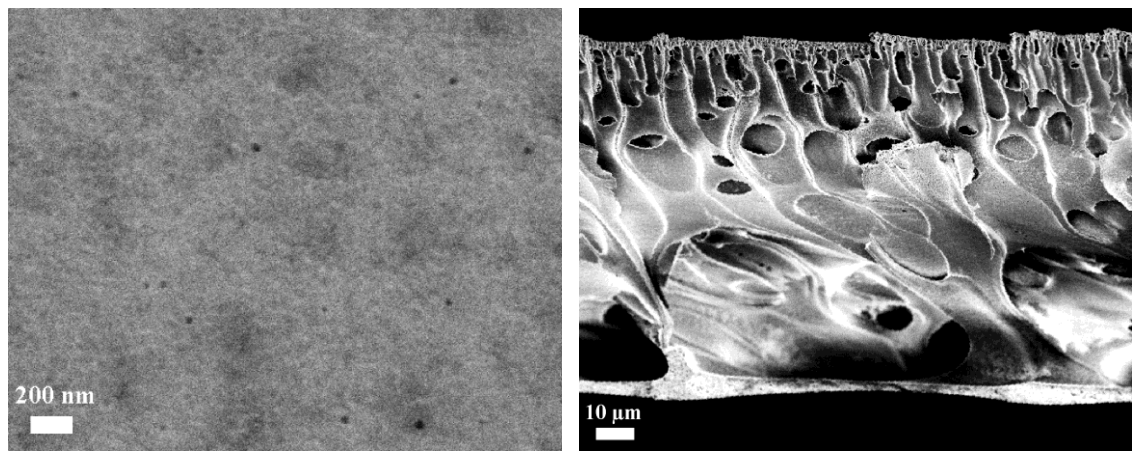
(d)
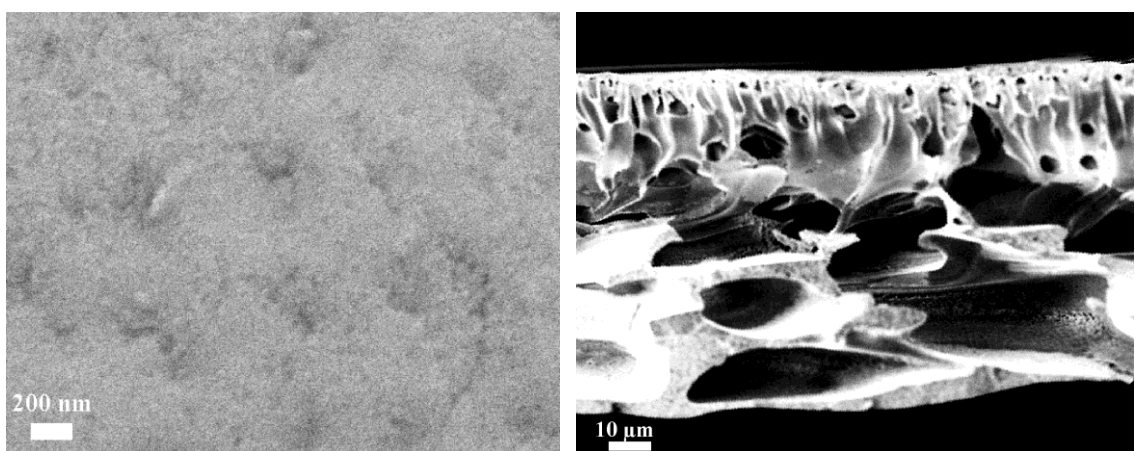
(e)
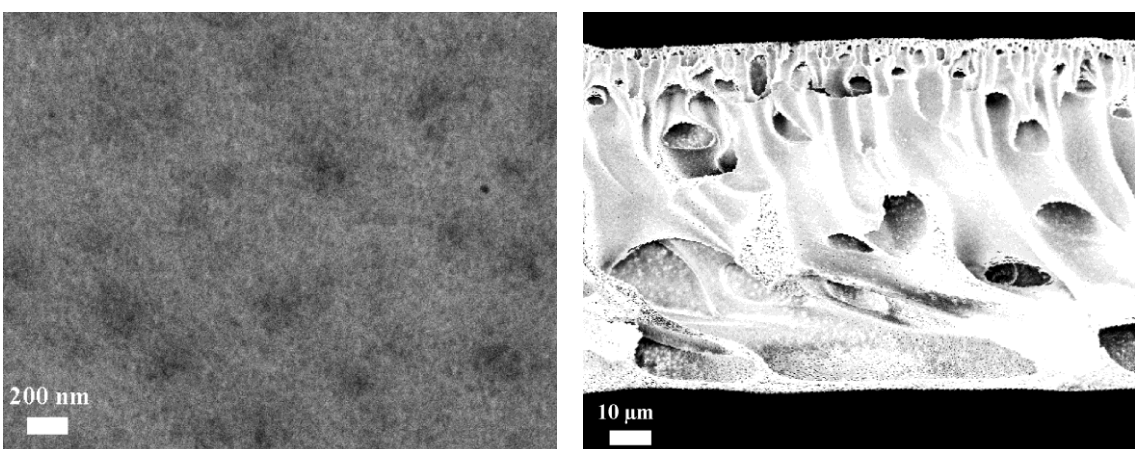
(f)

Figure 2.2. SEM images of the separation surfaces (left) and cross sections (right) of (a) pure PVC membrane and membranes containing Pluronic F 127 concentrations at (b) 2 wt%, (c) 4 wt%, (d) 6 wt%, (e) 8 wt%, and (f) 10 wt%.

24

2.3.3 Hydrophilicity

The dynamic water contact angle presented in Figure 2.3 indicates that the PVC membrane became more hydrophilic with increased addition of Pluronic F 127. The contact angle decreased linearly with increasing time. Figure 2.3 shows the contact angle variation in correlation with increasing Pluronic F127 content. The PVC membrane has an average contact angle of 86.38°, which decreases to 69.93° when 10 wt% of Pluronic F 127 is added. It appears that the contact angle becomes smaller as the surface oxygen content increases. However, the surface oxygen content plateaued after an 8 wt% concentration of Pluronic F 127.
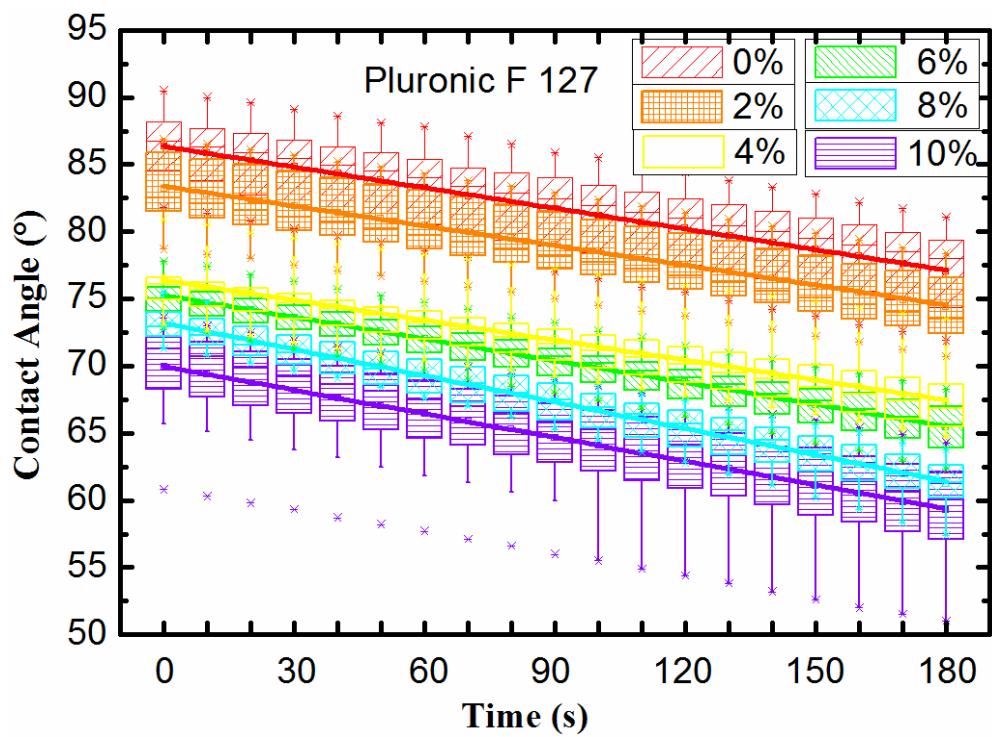
Figure 2.3. The effect of Pluronic F 127 content on contact angle versus time at $T = 25°C$.

2.3.4 Surface roughness

The Pluronic F 127 content did not affect the roughness of the PVC membrane significantly (Table 2.2). Figure. 2.4 shows the morphology of the PVC membrane with the increase of Pluronic F 127 content. The measured roughness of the PVC membrane had a root mean square (RMS) of 9.49 ± 0.71 nm. The RMS roughness of the PVC membrane with added Pluronic F 127 was slightly lower. As more Pluronic F 127 was added to the casting solution, smaller pores were found on the membrane surface as shown in Figure 2.2, possibly reducing the roughness.

Table 2.2 Root mean square (RMS) roughness of polyvinyl chloride membrane with differing contents of Pluronic F 127 in the casting solution.

Pluronic F 127 content (%)	0	2	4	6	8	10
RMS roughness (nm)	9.5 ± 0.7	8.0 ± 0.4	8.9 ± 0.3	8.3 ± 0.4	8.8 ± 0.3	8.5 ± 0.3
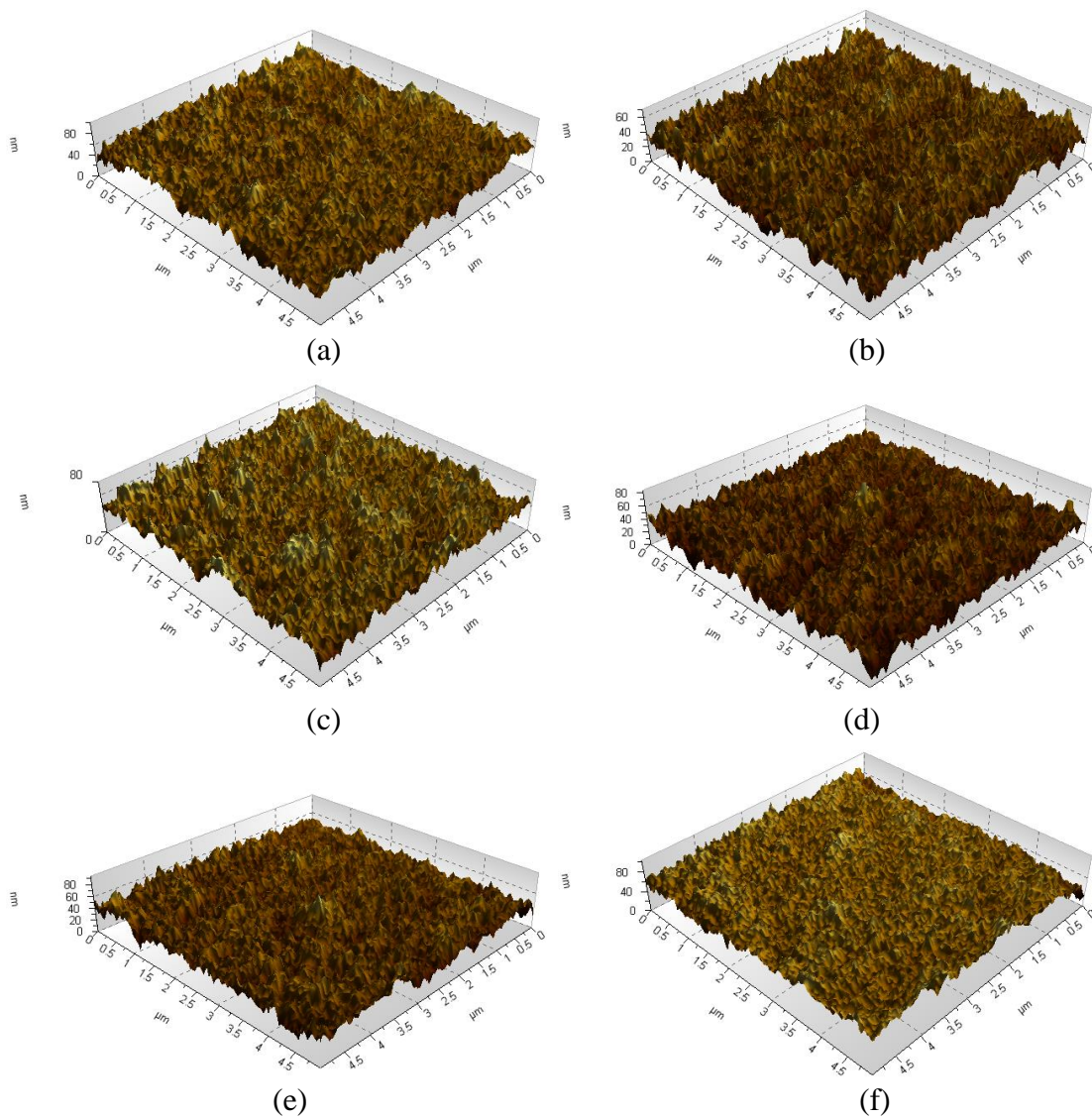
Figure 2.4. Atomic force microscopy image of PVC membrane at 25°C with added Pluronic F 127 at wt% (a) 0%, (b) 2%, (c) 4%, (d) 6%, (e) 8% and (f) 10%.

2.3.5 Membrane permeate flux

As shown in Figure 2.5, when a constant pressure was applied (10 psi), the permeate flux declined over time. With more Pluronic F 127 added, the membrane exhibited less reduction in the normalized permeate flux. For instance, the virgin PVC membrane had a permeate flux decline by approximately 65% over a period of 740 minutes. The permeate flux of the PVC membrane with 10% Pluronic F127 declined by approximately 52% over 740 min, which indicates that Pluronic F 127 addition reduced membrane fouling. After physical cleaning, the PVC membrane flux declined by approximately 25%, but the membrane with 2 wt% Pluronic F 127 did not decline at all. The absolute permeate flux of PVC membranes with additions of 0, 2, 4, 6, 8, and 10 wt% Pluronic F 127 are 227, 189, 184, 180, 164, and 157 $L/(m^2 \cdot h)$, respectively (under the same TMP of about 10 psi). The absolute permeate flux dropped approximately 30% when the additive increased from 0 wt% to 10 wt%. The flux decreased with increased additive, mainly because of pore size and/or pore density decreased. However, the antifouling property of the membrane was enhanced with increased Pluronic F 127. After physical cleaning, the flux of PVC membrane with 4 wt% and 6 wt% Pluronic F 127 were higher than the flux of the membrane without Pluronic F 127 addition, which could be due to the breakdown of the thin layer of copolymer that was formed by the Pluronic F 127 or the formation of large pores during the fouling experiments.
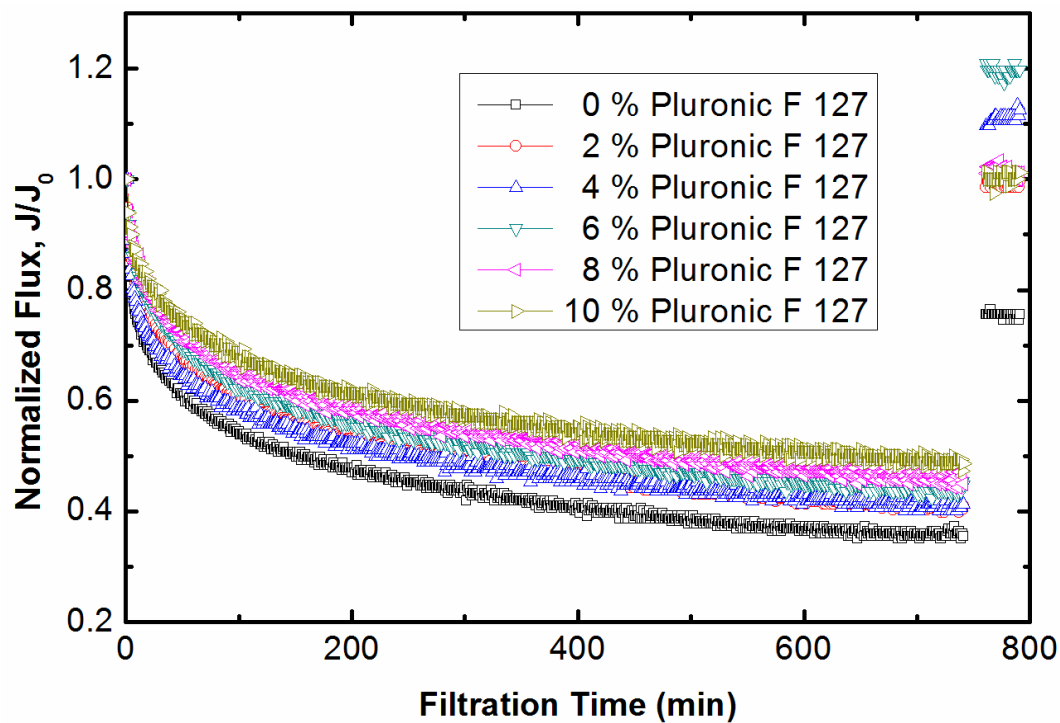
Figure 2.5. Normalized flux of PVC membranes containing different amounts of additives. Operating conditions: 24°C feed solution, TMP of 10 psi, 10 mM NaCl, and 20 mg/L sodium alginate.
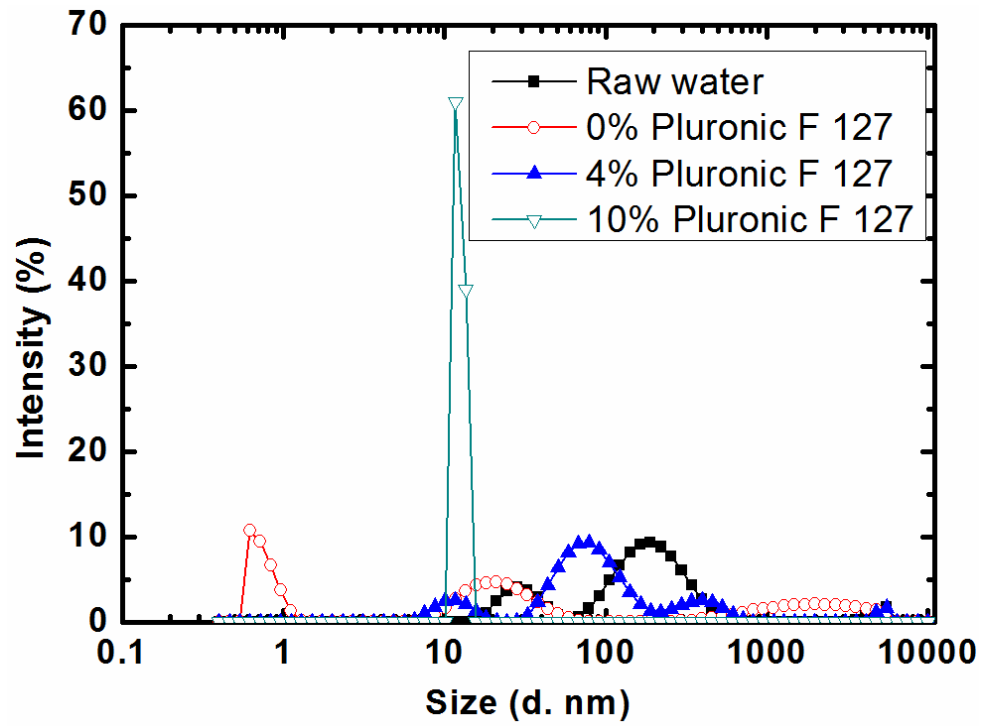
Figure 2.6. Particle size distribution by intensity of raw water and filtered water by PVC with 0 wt% Pluronic F 127, 4 wt% Pluronic F 127, and 10 wt% Pluronic F 127.

The model foulant rejections of PVC membranes with 0, 2, 4, 6, 8, and 10 wt% Pluronic F 127 were 28%, 32%, 35%, 45%, 49%, and 51%, respectively. All of these are higher than the rejection of 12% for the PAN-g-PEO ultrafiltration membrane (Asatekin, Kang et al. 2007). As shown in Figure 2.6, raw water comprises 20 mg/L sodium alginate and 10 mM NaCl, which has a large particle size distribution. The filtered water by PVC membrane with 10 wt% Pluronic F 127 has one small particle size distribution range near 10–15 nm, which means that fabricated PVC membrane containing 10 wt% Pluronic F 127 can easily remove particles larger than 10–15 nm.

2.4 Conclusions

We have fabricated a low-cost antifouling PVC membrane by adding different amounts of additive Pluronic F 127 to casting solutions and have characterized the synthesized membranes using XPS, SEM, AFM, contact angle, and flux measurements. Higher concentrations of Pluronic F 127 appeared on the membrane surface as the additive content in the casting solution was increased from 0 to 10 wt%, but plateaued after 8 wt%. Pore size decreased and pore density decreased dramatically as Pluronic F 127 content increased. The PVC membrane exhibited remarkable antifouling characteristics even at 2 wt% Pluronic F 127 addition. The flux declined by approximately 30% at 10 wt% Pluronic F 127 with a flux of 157 L/(m^2·h) under 10 psi TMP. Combining PVC and 8 wt% Pluronic F 127 exhibited optimized antifouling and flux performance. This improvement in PVC membrane fabrication could lead to broad applications in water and wastewater treatment owing to the low cost, high flux, and antifouling characteristics.

CHAPTER 3

HIGH PERFORMANCE ULTRAFILTRATION MEMBRANE COMPOSED OF PVDF BLENDED WITH ITS DERIVATIVE COPOLYMER PVDF-G-PEGMA

3.1 Introduction

Kato et al. (Kato, Kamigaito et al. 1995) and Wang and Matyjaszewski (Wang and Matyjaszewski 1995) independently discovered atomic transfer radical polymerization (ATRP). This method has enabled a great many copolymers to be fabricated. The synthesized block copolymers are tunable over a broad variety of molecular weights, architectures, chemical compositions, and functionalities (Smart, Lomas et al. 2008) owing to advances in ATRP and anionic polymerization. Poly(vinylidene fluoride)-graft- poly(ethylene glycol) methyl ether methacrylate (PVDF-g-PEGMA) (also termed PVDF-g-POEM in Mayes group's original description of such membranes) and poly(vinylidene fluoride)-graft-poly(methacrylic acid) (PVDF-g-PMAA) have been successfully fabricated using the ATRP method and characterized. Addition of PVDF-g-PEGMA to PVDF has produced membranes with good fouling resistance (Hester, Banerjee et al. 2002).

In another study, polyacrylonitrile-graft-poly(ethylene oxide) (PAN-g-PEO) was fabricated by free radical polymerization (Kang, Asatekin et al. 2007). Then PAN-g-PEO was used as an additive in the fabrication of a PAN/PAN-g-PEO membrane. This membrane exhibits antifouling properties (Asatekin, Kang et al. 2007, Kang, Asatekin et al. 2007) and prevents irreversible adhesion of bacteria.

Polysulfone-graft-poly(ethylene glycol) (PSf-g-PEG) was used as an additive in PSf membrane fabrication to improve its resistance to fouling by proteins (Park, Acar et al. 2006). To sum up, the above successful fabrication methods consists of blending the base polymer with derivatives of the base polymer, the amphiphilic copolymer.

Another emerging and promising path to improve membrane performance is the formation of a mesoporous membrane via block copolymer self-assembly (Jackson and Hillmyer 2010, Phillip, Dorin et al. 2011). Block copolymers can form periodic arrangements of spherical, cylindrical, gyroid, and lamellar microdomain morphology (Bates and Fredrickson 1999) under the phase separation method, or form ordered materials (Zavala-Rivera, Channon et al. 2012) under ultraviolet light exposure followed by immersion in solvents.

Block copolymers dissolved in certain solvents can form micelles or other self-assembled superstructures depending on: (1) the concentration (Smart, Lomas et al. 2008, Nunes, Sougrat et al. 2010), (2) block copolymer composition (Phillip, Hillmyer et al. 2010, Phillip, O'Neill et al. 2010), (3) block-block and block-solvent interactions, (4) the ratio of block lengths (Smart, Lomas et al. 2008, Nunes, Sougrat et al. 2010), (5) overall copolymer molecular weight (Phillip, O'Neill et al. 2010), (6) solvent composition and solvent selectivity (Phillip, O'Neill et al. 2010), (7) solvent evaporation rate (Phillip, Hillmyer et al. 2010, Phillip, O'Neill et al. 2010), and (8) evaporation time (Peinemann, Abetz et al. 2007, Phillip, Dorin et al. 2011). Through the rational control of these conditions, we can prepare a self-assembling ultrafiltration membrane.

Self-assembly of copolymers can lead to uniform size pore distribution and high flux owing to high pore density. A membrane with uniform pore size can exhibit better

selectivity than one with a wide distribution of pore sizes (Gin and Noble 2011). Usually fabrication of a membrane without any defects is not easy. If defects such as large pores exist, most of the particles or molecules will pass through these pores first because they have the least resistance (Gin and Noble 2011). Self-assembly is the next generation of ultrafiltration membrane fabrication because it can form membranes that are defect-free and have high pore density. Such membranes have high flux and superior molecular weight cut-offs (Phillip, Hillmyer et al. 2010).

Self-assembled thin films from the diblock copolymer polystyrene-block-poly(methyl methacrylate) (PS-b-PMMA) have been fabricated on a spin-coated silicon oxide sacrificial template; however, this method requires long annealing times and the tedious transfer of a fragile thin film from the primary substrate to a secondary support membrane (Yang, Ryu et al. 2006, Yang, Park et al. 2008, Yang, Yang et al. 2010). The block copolymer poly(styrene-b-lactide) has been cast onto a microporous membrane to form a self-assembled membrane with monodisperse pores of 24-nm diameter (Phillip, O'Neill et al. 2010). A new thin film composite nanofiltration (NF) membrane is composed of the self-assembling amphiphilic graft copolymers, poly(vinylidene fluoride)-graft-poly(oxyethylene methacrylate) (PVDF-g-POEM) coated on a commercial PVDF UF membrane (Akthakul, Salinaro et al. 2004, Asatekin, Menniti et al. 2006). The composite or coated self-assembly membranes require multiple and complicated fabrication steps, and the two layers may separate in the long run. The polystyrene-block-poly(4-vinylpyridine) (PS-b-P4VP) diblock copolymer was synthesized by sequential anionic polymerization of the respective monomers in tetrahydrofuran (THF) in the presence of lithium alkoxides (Auschra and Stadler 1993) at -62°C, and then this

copolymer was used to fabricate an asymmetric self-assembled membrane via phase separation (Peinemann, Abetz et al. 2007). However, the copolymer was used as both the active layer (where the pore structure is) and as support layers, so the membranes fabricated using this technique are expensive (Phillip, Hillmyer et al. 2010).

The main purpose of this research is to synthesize defect-free high performance ultrafiltration membrane using relatively simple method and cheap materials, blending the base polymer with derivatives of the polymer and tailoring the membrane casting conditions just like block copolymers required to form micelles or other self-assembled superstructures. We first make PVDF-g-PEGMA copolymers with two molecular weights $PVDF_{275K}$ and $PVDF_{534K}$ and a casting solution by dissolving the parent PVDF polymer into the mixture of N,N-dimethylformamide (DMF) and THF solvents, which is different from those used before (Hester, Banerjee et al. 2002, Hashim, Liu et al. 2009), respectively. Then different amounts of the copolymers were added to the PVDF casting solution. As a result, a periodic pillar-like or sphere structural membrane can be formed. Different molecular weights and the amounts of copolymer were employed to systematically examine their impact on membrane characteristics and performance such as flux and particle size rejection. The membrane characteristics were comprehensively investigated by XPS for the elemental composition of the membrane surface, SEM for the pore size and the pore distribution of synthesized membranes, and AFM for mapping the topography and the surface roughness. In addition, contact angle measurements were conducted to reveal the impact of copolymer percentage on the hydrophilicity of the membrane. Overall, the goal of our study is to provide insight into the fabrication of the

defect-free high performance ultrafiltration PVDF membranes for water treatment applications.

3.2 Experimental

3.2.1 Chemicals and materials

All reagents and chemicals are analytical grade unless stated otherwise. Poly(vinylidene fluoride) (PVDF), poly(ethylene glycol) methyl ether methacrylate (PEGMA), copper(I) chloride (CuCl), 4-4′-dimethyl-2-2′-dipyridyl (DMDP), silicone oil, 1-methyl-2-pyrrolidinone (NMP), tetrahydrofuran (THF), hydrochloric acid (HCl), calcium chloride ($CaCl_2$) and N,N-dimethylformamide (DMF) were purchased from Sigma-Aldrich (St. Louis, MO). NaCl and $Ca(OH)_2$ were purchased from Fisher Scientific (Pittsburgh, PA). Deionized (DI) water was supplied by a Thermo Scientific Barnstead Nanopure ultrapure water system (Dubuque, IA) and the water had a resistivity of 18.2 Mohm cm.

3.2.2 Model foulants

Two model foulants were used, sodium alginate (SA) used as model for extracellular polymeric substances (EPS) and Suwannee River humic acid (SRHA) used as model for natural organic matter (NOM). The sodium alginate was obtained from Sigma-Aldrich (St. Louis, MO), and the molecular weight of sodium alginate was in the range of 12–80 kDa (Katsoufidou, Yiantsios et al. 2007, Listiarini, Chun et al. 2009). SRHA was obtained from the International Humic Substances Society (St. Paul, MN). Stock solutions of sodium alginate and SRHA were prepared in separate flask. The stock solutions of each 2 g/L sodium alginate and SRHA were prepared by adding either

sodium alginate or SRHA to DI water and the solutions were mixed until completely dissolved and then stored at 4°C. In all fouling experiments, the sodium alginate and SRHA concentrations were determined using a Shimadzu total organic carbon (TOC) analyzer (Shimadzu Co.).

3.2.3 Synthesis of the graft copolymer PVDF-g-PEGMA

The synthesis of copolymer PVDF-g-PEGMA was similar to those previously described (Hester, Banerjee et al. 2002, Hashim, Liu et al. 2009). $PVDF_{275K}$ (275K MW by gel permeation chromatography (GPC)) or $PVDF_{534K}$ (534K MW by GPC) (5 g) was dissolved in 1-methyl-2-pyrrolidinone (NMP) (40 mL) in a conical flask at 50°C. PEGMA (50 mL), CuCl (0.04 g), and the initiator DMDP (0.23 g) were added to the solution until it was cooled to a room temperature of 25°C, and the flask was then sealed with a rubber septum. Nitrogen gas was bubbled through the reaction mixture for 30 minutes, while the mixture was stirred. The reaction vessel was then placed in a silicon oil bath that was preheated to 90°C, and the reaction was allowed to proceed for 19 hours. After cooling, the copolymer mixture was stored at room temperature. The copolymer concentrations were estimated from the actual weight of copolymer that could be precipitated from the polymerization mixture, this amount of copolymer was then used to estimate the amount in the preparation of the membrane solution (Hashim, Liu et al. 2009). A PEGMA conversion of 20% was obtained (Hester, Banerjee et al. 2002).

3.2.4 Membrane casting

Membranes were prepared from casting solutions containing $PVDF_{534K}$, PVDF-g-PEGMA copolymer mixture additives (which included NMP, unreacted PEGMA, the catalyst CuCl, and the ligand DMDP), tetrahydrofuran (THF), and N,N-dimethylformamide (DMF) according to the compositions listed in Table 3.1. The solution of PVDF and PVDF-g-PEGMA copolymer mixture additives in THF and DMF were prepared in 125-mL conical flasks and heated to approximately 60°C while being stirred at 500 rpm using digital stirring hot plates (Corning, MA). After the polymers were dissolved completely and stirred for at least 24 hours, the resulting solution was degassed with no mixing for at least 2 hours until no gas bubbles were visible. The solution was cast on a first-grade surface optical mirror using a 8-inch-wide doctor blade (Universal blade applicator, Paul N. Gardner Company, Inc., Pompano Beach, FL) that was set with a gate height of ~200 μm. The mirror was left in air to allow the solvents to evaporate for 60 s before it was immersed in a bath of deionized water at room temperature, 25 ± 1°C. The cast membranes were left in the coagulation bath for 48 hours, and then the air-dried for 24 hours before be characterized.

Table 3.1 The composition of the casting solutions.

Membrane	Additive type	PVDF (g)	THF (g)	DMF (g)	Additive (g)	Additive/PVDF wt/wt (%)
1	—	18	24.60	57.40	0.0	0
2	$PVDF_{275K}$-g-PEGMA	18	24.33	56.77	0.9	5
3	$PVDF_{275K}$-g-PEGMA	18	24.06	56.14	1.8	10
4	$PVDF_{275K}$-g-PEGMA	18	23.79	55.51	2.7	15
5	$PVDF_{534K}$-g-PEGMA	18	24.33	56.77	0.9	5
6	$PVDF_{534K}$-g-PEGMA	18	24.06	56.14	1.8	10
7	$PVDF_{534K}$-g-PEGMA	18	23.79	55.51	2.7	15

Note: The density of THF is 0.890 g/cm^3; the density of DMF is 0.944 g/cm^3

3.2.5 XPS analysis

X-ray photoelectron spectroscopy (XPS) (Thermo K-Alpha XPS system) was used to analyze membrane surface to a depth less than 5 nm. Survey XPS spectra were obtained by sweeping over 0–1350 eV electron binding energy with a resolution of 1 eV. High-resolution scans were also conducted which have a resolution of 0.1 eV. Each survey spectrum and high-resolution scan were the average of three and five scans, respectively.

3.2.6 SEM analysis

Scanning electron microscopy (SEM) (Zeiss Ultra 60, Carl Zeiss NTS, LLC North America) was used for imaging the membrane surface morphologies. The membranes were fixed on stubs with carbon dots and then sputter coated with an ~2 nm gold layer. Coated samples were examined at the accelerating voltage of 5 kV at different magnifications.

3.2.7 Liquid sessile drop contact angle analysis

Water contact angle measurement was performed on membranes using a Ramé-hart Model 250 goniometer (Ramé-hart Instrument Co.). For each membrane, five to ten repeat measurements at different locations were taken of the dynamic contact angle variations for 200 s, immediately after the droplet was placed on the membrane. The dynamic water contact angle was measured by placing 2 µL of DI water on the

membrane surface. Values and statistical analysis are reported as a box and whisker plot (Frigge, Hoaglin et al. 1989, Liu, Chen et al. 2012).

3.2.8 Flux performance

The filtration experiment was conducted using an Amicon 8200 stirred dead-end filtration cell (Millipore) using cast membranes that had a diameter of 63.5 mm and an effective area of 28.7 cm^2. The filtration cell (Millipore) had a cell volume of 200 mL and attached to a 5.0-L dispensing vessel. Permeate was collected and weighed using an Ohaus Adventurer Pro Balance AV8101. The permeate mass, that collected every minute and recorded using Collect 6.1 software.

The experimental procedures adopted for each fouling experiment are as follows. First, the cast membranes were soaked in DI water for 48 hours prior to the experiment. Second, the membranes were compacted using DI water with a transmembrane pressure of 0.07 MPa for 2 hours or a filtration volume of ~ 4 liters. Third, the membrane was conditioned by passing a 10 mM NaCl solution through it for 2 hours or a filtration volume of ~4 L.

For the fouling tests, the feed solution was added into the filtration cell and each fouling test ran for at least 5 hours or a filtration volume of ~ 4 L and each fouling test was replicated. The reported data are average values for the 2 tests. The filtration cell was stirred at 450 rpm using a stirring plate (PC-410D, Corning, MA) during the conditioning and fouling stages to minimize concentration polarization. Fouling experiments were performed at a transmembrane pressure (TMP) of 0.07 MPa (10 psi). The fouling tests involved filtering a solution containing sodium alginate in 10 mM NaCl solution and

solutions containing SRHA in 10 mM NaCl, 2 mM $CaCl_2$ and 10 mM $Ca(OH)_2$ solution, in separate tests. At the end of the fouling runs, physical cleaning was conducted as follows: the foulant solution, in the feed tank, was disposed of, the tank was rinsed with DI water then with electrode solution; the fouled membrane was flushed under ultrapure water outlet of Thermo Scientific Barnstead Nanopure ultrapure water systems, followed by electrode solution for 5 times at room temperature of cleaning time of about 1 min (except cleaning time ~ 2 min for 10 wt.% $PVDF_{534K}$-g-PEGMA after filtration of sodium alginate). To determine the flux after physical cleaning, we cleaned the membrane and then exposed it to foulant-free electrolyte solution according to standard conditioning practices (Kang, Asatekin et al. 2007).

3.2.9 AFM analysis

The surface roughness of membrane was determined using an Agilent 5500 AFM (Agilent Technologies, Inc., US). The acoustic alternating current (AC) tapping mode was used to characterize the membrane morphology, and the image acquisition and processing were completed with PicoView software (Version 6.1.3). Silicon cantilever probes (BudgetSensors, Bulgaria) with a nominal resonant frequency of 150 kHz and a force constant of 5 N/m were used for sample scanning. The cantilever probes were oscillated at an amplitude of approximately 2.0 V before engagement, and the piezo scanner stopped moving the sample toward the probe when the amplitude decreased by 10% owing to the tip-sample interactions. Once engaged, the oscillation amplitude was automatically adjusted by the servo system to 1.0–1.5 V for optimal imaging quality. The

typical scan rate used was 0.1–0.3 line/s (0.65–1.95 nm/s) with a scan size of 5 by 5 μm^2. At least seven replicates were performed for each membrane sample.

3.3 Results and discussions

3.3.1 XPS analysis

     The near-surface compositions of the PVDF membranes that were blended with 5 wt.%, 10 wt.% or 15 wt.% PVDF-g-PEGMA copolymer mixtures are shown in Figure 3.1. For all membranes, XPS analysis was conducted on the side of the membrane opposite to that in contact with the mirror (Hester, Banerjee et al. 2002). This is the active layer which filters out substances. The oxygen content increased with increasing PVDF-g-PEGMA according to the survey scan results, as shown in Table 3.2. There was no significant difference in the oxygen content between the PVDF membrane with $PVDF_{275K}$-g-PEGMA and that with $PVDF_{534K}$-g-PEGMA at the same amount of additive.
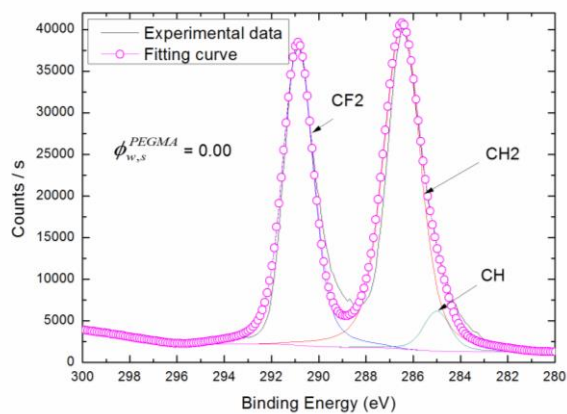
(a) PVDF-g-PEGMA 0 wt.%
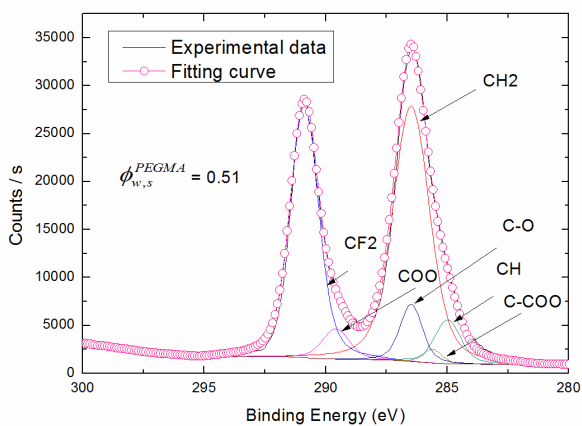
(b) PVDF$_{275K}$-g-PEGMA 5 wt.%
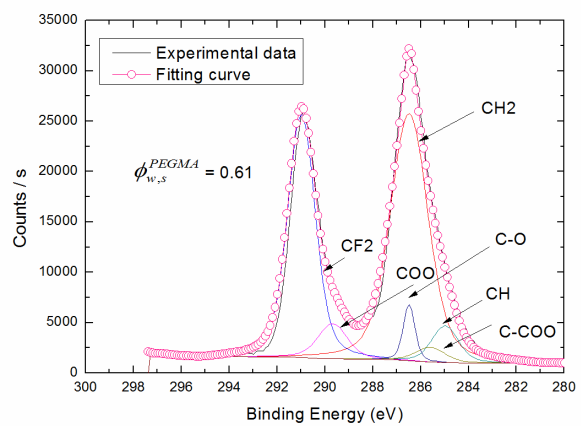
(c) PVDF$_{534K}$-g-PEGMA 5 wt.%
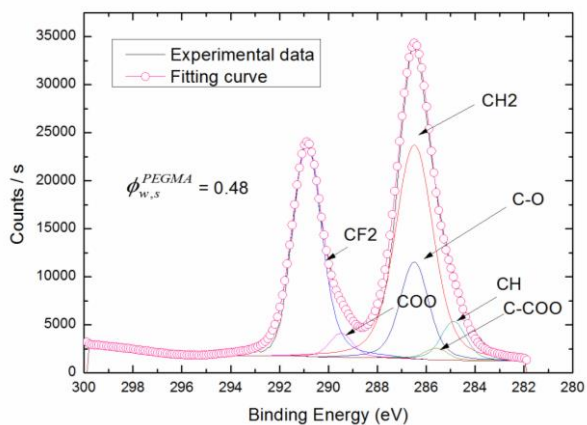
(d) PVDF$_{275K}$-g-PEGMA 10 wt.%
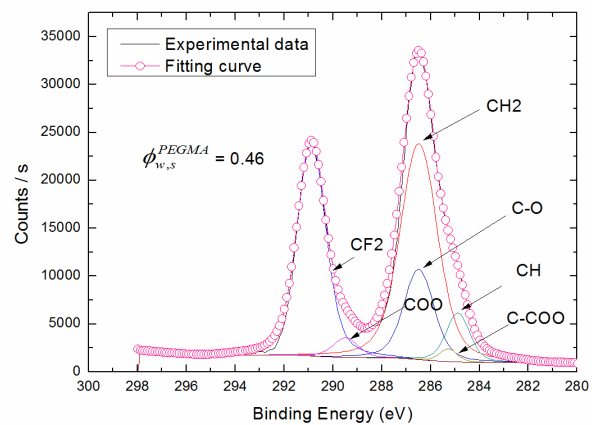
(e) PVDF$_{534K}$-g-PEGMA 10 wt.%
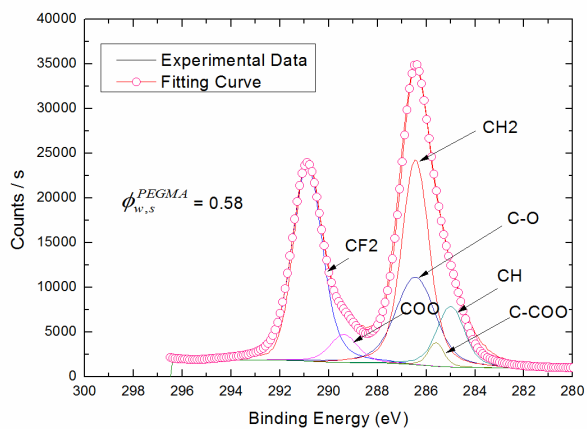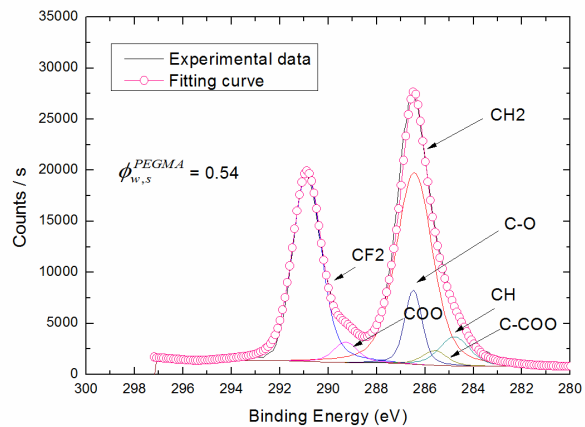
(f) PVDF$_{275K}$-g-PEGMA 15 wt.%   (g) PVDF$_{534K}$-g-PEGMA 15 wt.%

Figure 3.1. High-resolution XPS spectra for PVDF with the additives: (a) PVDF-g-PEGMA 0 wt.%, (b) PVDF$_{275K}$-g-PEGMA 5 wt.%, (c) PVDF$_{534K}$-g-PEGMA 5 wt.%, (d) PVDF$_{275K}$-g-PEGMA 10 wt.%, (e) PVDF$_{534K}$-g-PEGMA 10 wt.%, (f) PVDF$_{275K}$-g-PEGMA 15 wt.%, and (g) PVDF$_{534K}$-g-PEGMA 15 wt.%.

48

Table 3.2 The surface elemental compositions of PVDF/PVDF-g-PEGMA membranes with different additives.

Membrane with additive	F (%)	C (%)	O (%)
5 wt.% $PVDF_{275K}$-g-PEGMA	40.2	55.3	4.55
5 wt.% $PVDF_{534K}$-g-PEGMA	39.1	56.2	4.73
10 wt.% $PVDF_{275K}$-g-PEGMA	37.7	55.9	6.43
10 wt.% $PVDF_{534K}$-g-PEGMA	37.1	56.6	6.3
15 wt.% $PVDF_{275K}$-g-PEGMA	37.1	55.9	6.77
15 wt.% $PVDF_{534K}$-g-PEGMA	37.4	55.8	6.73

The near-surface mole fraction of PEGMA can be calculated from the following

equation (Hester, Banerjee et al. 2002)

$$X_S^{PEGMA} = \frac{A_{COO}}{A_{CF_2} + A_{COO}} \tag{1}$$

where A_{CF_2} and A_{COO} are the areas of the fitted CF_2 and COO peaks, respectively.

The near-surface weight fraction ($\phi_{w,s}^{PEGMA}$) of PEGMA was converted from the mole

fraction using the known molecular weights of PVDF and PEGMA. The weight fraction

of PEGMA is shown in Figure 3.1, weight fraction $\phi_{w,s}^{PEGMA}$ is 51 wt.%, 48 wt.%, and 58

wt.% when we have 5 wt.%, 10 wt.%, and 15 wt.% $PVDF_{275K}$-g-PEGMA and 61wt.%, 46

wt.%, and 54 wt.% when we have 5 wt.%, 10 wt.%, and 15 wt.% $PVDF_{534K}$-g-PEGMA

copolymer mixed with PVDF. The weight fraction of pure graft copolymer PVDF-g-

PEGMA is 67 ± 3 wt.% (Hester, Banerjee et al. 2002). Comparison of these values shows

that enrichment of the hydrophilic comb polymer PEGMA on the membrane surface. The

weight fraction of PEGMA is 0 wt.% when it is just PVDF as shown in Figure 3.1.

Theoretically, the 15 wt.% PVDF-g-PEGMA has the highest PEGMA content on the

membrane surface based on surface oxygen compositions. However, the weight

percentage of PEGMA is not highest for the 15 wt.% PVDF-g-PEGMA based on the

results of high-resolution XPS spectra. This is probably due to two main reasons: (1)

phase inversion occurs fast, so that PVDF-g-PEGMA molecules do not all have enough

time to migrate toward the interface, with PEGMA blocks turned toward the external

environment; (2) surface roughness (de Bernardez, Ferron et al. 1984) and inhomogeneity of the membrane could affect the XPS results.

3.3.2 Morphology

SEM images of PVDF/PVDF-g-PEGMA membranes are shown in Figure 3.2. The pore density of the membrane tends to become larger with a relatively constant pore size, as the amount of PVDF-g-PEGMA additive increases. Similar pore density changes are observed with increasing PVDF-g-POEM in PVDF without THF using N, N-dimethylacetamide (DMAc) as solvent (Hester, Banerjee et al. 2002). However, the surface morphology of PVDF with 10 wt.% or 15 wt.% PVDF-g-PEGMA is very different from those of Mayes groups(Hester, Banerjee et al. 2002) or membranes prepared without copolymer purification using NMP as solvent (Hester, Banerjee et al. 2002). Image Pro Plus V.7.0 software (Vashaw Scientific, Inc.) was used for image statistical analysis. The diameter of the periodic pillar-like structures or spheres is ~200 nm. Some spheres exist inside the PVDF matrix (Figure 3.3). This intriguing membrane structures was defect-free for 10 wt. % and15 wt. % PVDF-g-PEGMA because we examined these membranes at different locations under magnification of 2K×, 5 K×, 20 K×, and 100 K× (Figure 3.2g, h, i, j). The PVDF membrane has a pore size of $10 - 80$ nm, average pore size of 15.4 nm, maximum pore size of 79.8 nm, and low pore density of 2.2×10^{13} per m^2 (Figure 3.2a). The PVDF with 5 wt.% PVDF$_{534K}$-g-PEGMA has an average pore size of 23.6 nm and pore density of 2.6×10^{13} per m^2. The PVDF with 10 wt.% PVDF$_{534K}$-g-PEGMA has an average pore size of 28.1 nm and pore density of 1.3×10^{14} per m^2. The PVDF with 15 wt.% PVDF$_{534K}$-g-PEGMA has an average pore size of

30.7 nm. The mesopores density is about 1.6×10^{14} per m^2 for 15 wt.% PVDF$_{534K}$-g-PEGMA (Table 3.3) and is much higher than the previous results, which is at the same order of magnitude of triblock terpolymer self-assembling membrane (Phillip, Dorin et al. 2011). So the fabricated membranes show a potential of high performance based on SEM analysis (Figure 3.2 and Figure 3.3). The mechanisms for the observed morphological changes is very important for expanding applications or optimizing of this prepared membrane, however, it is out of the scope of this paper and need to be conducted in our future work.
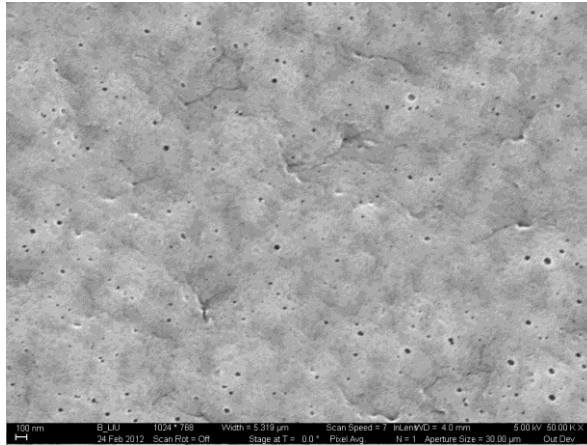
(a) 0 wt.% PVDF-g-PEGMA
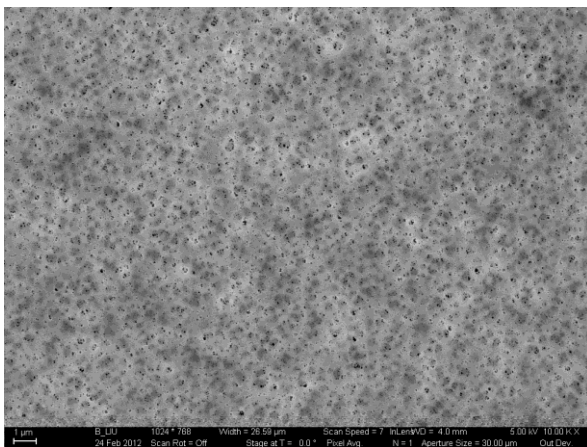
(b) 5 wt.% PVDF$_{275K}$-g-PEGMA

(c) 5 wt.% PVDF$_{534K}$-g-PEGMA

(d) 10 wt.% PVDF$_{275K}$-g-PEGMA

(e) 10 wt.% PVDF$_{534K}$-g-PEGMA

53

(f) 15 wt.% PVDF$_{275K}$-g-PEGMA   (g) 15 wt.% PVDF$_{534K}$-g-PEGMA at 20 K ×

(h) 2 K ×   (i) 5 K ×   (j) 100 K ×
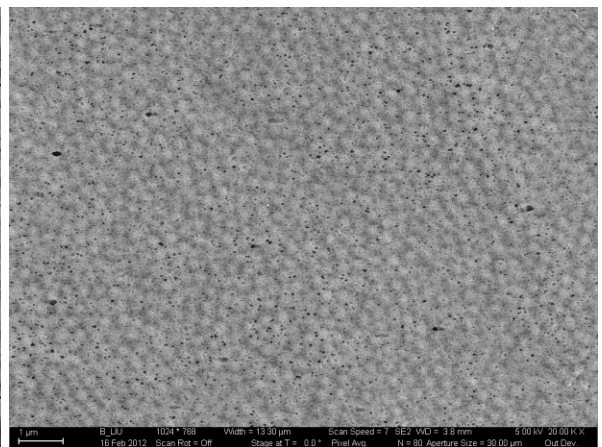
Figure 3.2. SEM images of the surface of PVDF membranes with PVDF$_{275K}$-g-PEGMA and PVDF$_{534K}$-g-PEGMA copolymer additives.

Table 3.3 Summary of pore size distribution statistics.

Membrane with additive	$D_{average}$ (nm)	D_{max} (nm)	Pore density (m^{-2})	ε (%)
0 wt.% PVDF-g-PEGMA	15	55	2.2×10^{13}	0.44
5 wt.% PVDF$_{275K}$-g-PEGMA	23	157	3.2×10^{13}	1.51
10 wt.% PVDF$_{275K}$-g-PEGMA	26	159	1.8×10^{14}	11.37
15 wt.% PVDF$_{275K}$-g-PEGMA	28	127	9.0×10^{13}	6.31
5 wt.% PVDF$_{534K}$-g-PEGMA	24	142	2.6×10^{13}	1.19
10 wt.% PVDF$_{534K}$-g-PEGMA	28	140	1.3×10^{14}	9.13
15 wt.% PVDF$_{534K}$-g-PEGMA	31	183	1.6×10^{14}	16.33
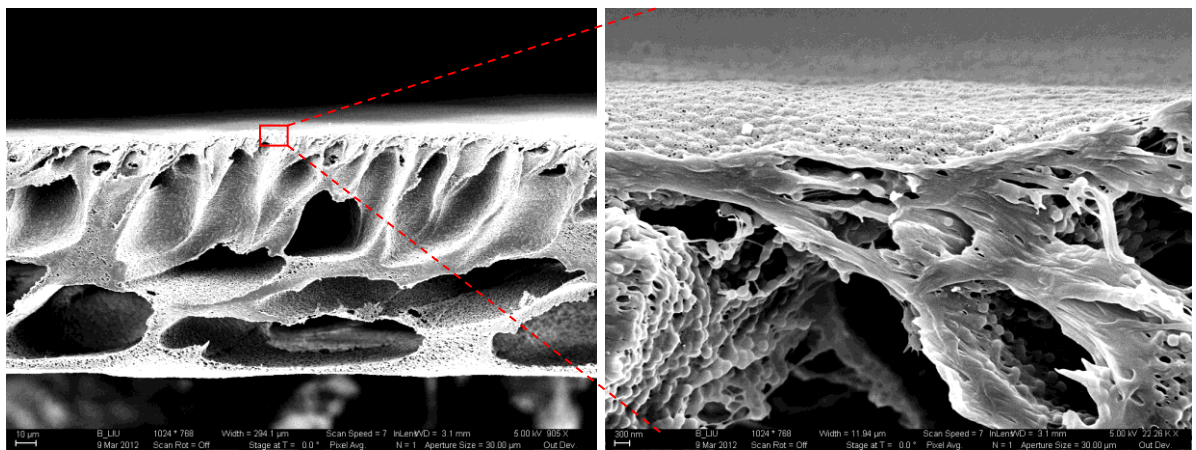
(a) Overall cross-section   (b) Cross-section near the surface

Figure 3.3. SEM image of the cross-section of PVDF membrane with 15 wt. % additives of $PVDF_{534k}$ -g-PEGMA.

3.3.3 Wettability

The dynamic water contact angle is presented in Figure 3.4 and it indicates that the PVDF membrane became some more hydrophilic with the addition of 5 wt.%, 10 wt.%, and 15 wt.% PVDF$_{534K}$-g-PEGMA. The contact angle declines linearly with the increasing time, except the 10 wt.% PVDF$_{534K}$-g-PEGMA. PEGMA is a hydrophilic part of copolymer. However, the more PVDF$_{534K}$-g-PEGMA was added to the PVDF, the more hydrophobic the membrane becomes even though high PVDF$_{534K}$-g-PEGMA addition means more oxygen on the membrane surface (more PEGMA on membrane surface) from XPS results (Table 3.2). This can be explained by obvious rougher surface (Herminghaus 2000, Tuteja, Choi et al. 2007), the increase in root mean square (RMS) roughness of different amounts of PVDF$_{534K}$-g-PEGMA addition is in the following order: 5 wt.% < 10 wt.% < 15 wt.%, as shown in Figure 3.5 and Figure 3.6. RMS roughness changing is a more significant parameter on hydrophilicity comparing with the effect of PEGMA content near the membrane surface. Interestingly, when these membranes were submerged in water for some time, the membrane became transparent, especially for 15 wt.% PVDF$_{534K}$-g-PEGMA.
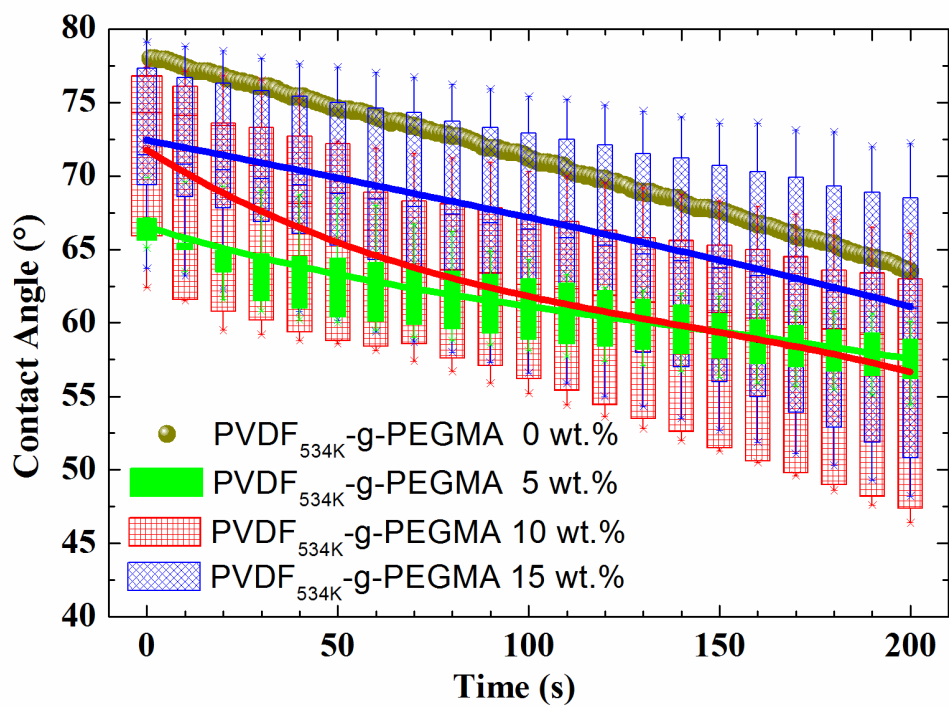
Figure 3.4. The variation of contact angle with time for different amounts (0, 5, 10 and 15 wt.%) of the additive $PVDF_{534K}$-g-PEGMA.

3.3.4 Roughness

The roughness of the PVDF membrane is affected significantly by the amount of PVDF-g-PEGMA added. The measured root mean square (RMS) roughness of the PVDF membrane was 12.80 ± 0.66 nm (Figure 3.5). The effect of the amount of PVDF-g-PEGMA on the RMS roughness of the PVDF membrane has similar changing trend for $PVDF_{275K}$-g-PEGMA and for $PVDF_{534K}$-g-PEGMA. The roughness first drops and then increases as addition increased. The roughness of $PVDF_{275K}$-g-PEGMA is higher than that of $PVDF_{534K}$-g-PEGMA. Figure 3.6 shows the surface morphology of the PVDF membrane with different amounts and molecular weights of the additives. A side by side comparison of $PVDF_{275K}$-g-PEGMA and $PVDF_{534K}$-g-PEGMA additives was presented. The amount of PVDF-g-PEGMA has a more significant effect on the morphology than does graft copolymer molecular weight for 10 wt.% and 15 wt.% $PVDF_{275K}$ and $PVDF_{534K}$. The PVDF membrane morphology is also shown in Figure 3.6.
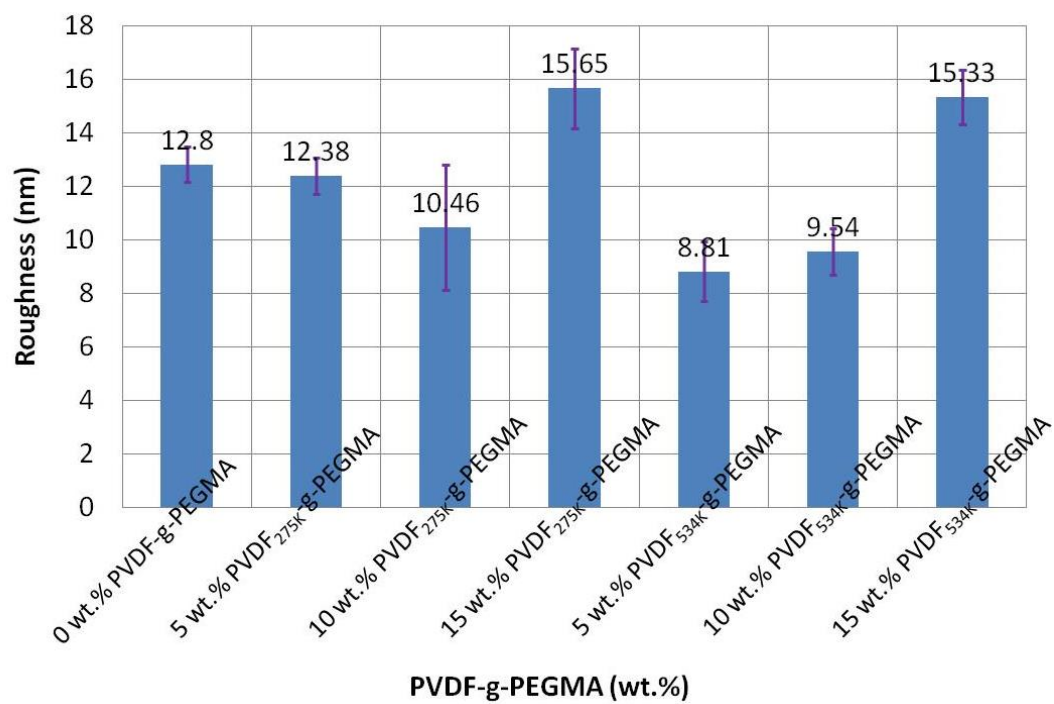
Figure 3.5. Roughness of the PVDF membrane with different PVDF-g-PEGMA additives.
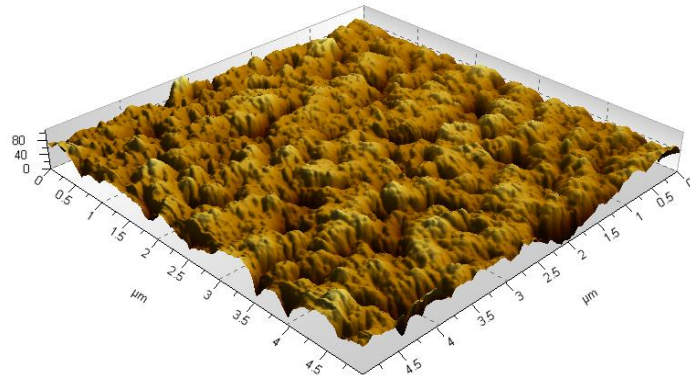
(a) 0 wt.% PVDF-g-PEGMA
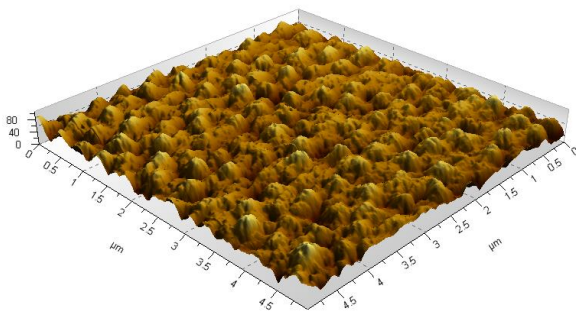
(b) 5 wt.% PVDF$_{275K}$-g-PEGMA
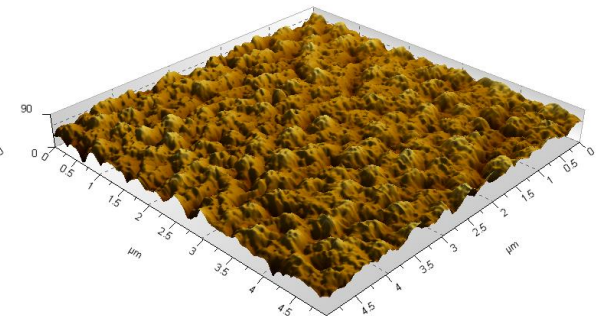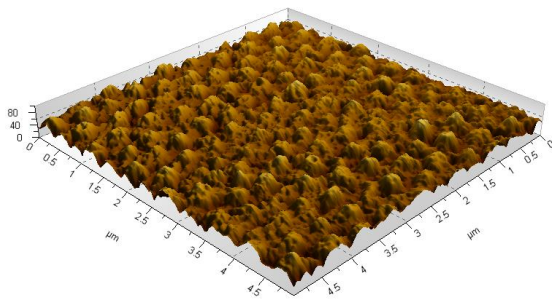
(c) 5 wt.% PVDF$_{534K}$-g-PEGMA

(d) 10 wt.% PVDF$_{275K}$-g-PEGMA
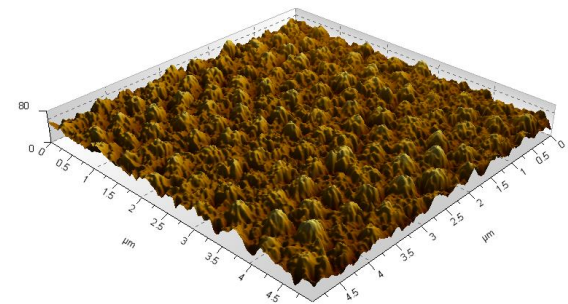
(e) 10 wt.% PVDF$_{534K}$-g-PEGMA
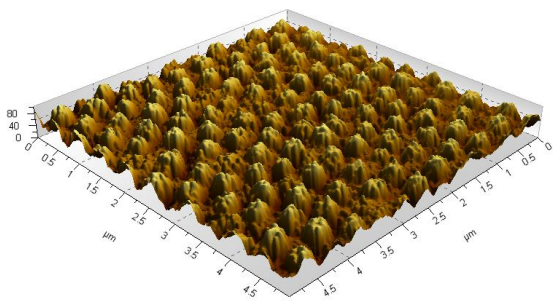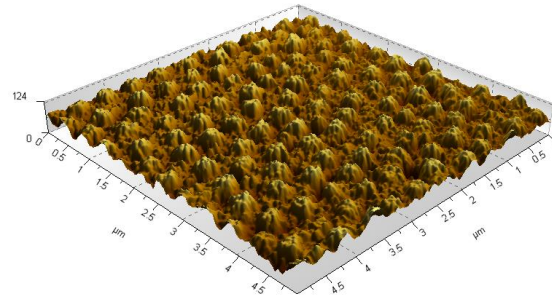
(f) 15 wt.% PVDF$_{275K}$-g-PEGMA   (g) 15 wt.% PVDF$_{534K}$-g-PEGMA

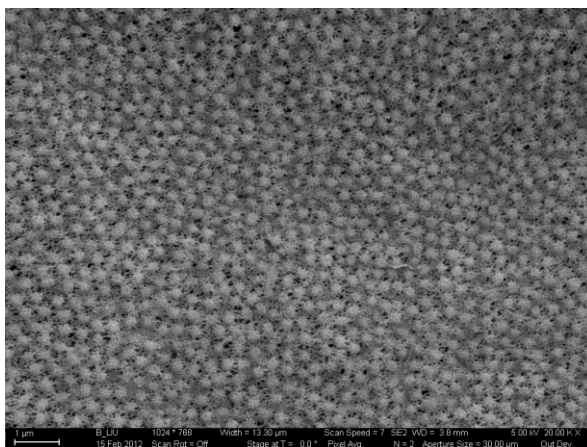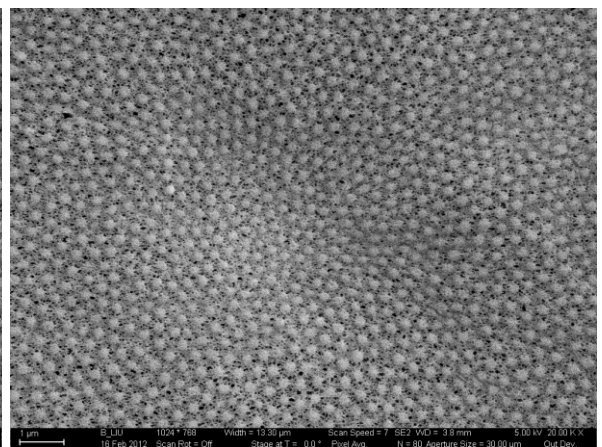**Figure 3.6.** AFM images of PVDF membranes with added (a) 0 wt.% PVDF-g-PEGMA, (b) 5 wt.% PVDF$_{275K}$-g-PEGMA, (c) 5 wt.% PVDF$_{534K}$-g-PEGMA, (d) 10 w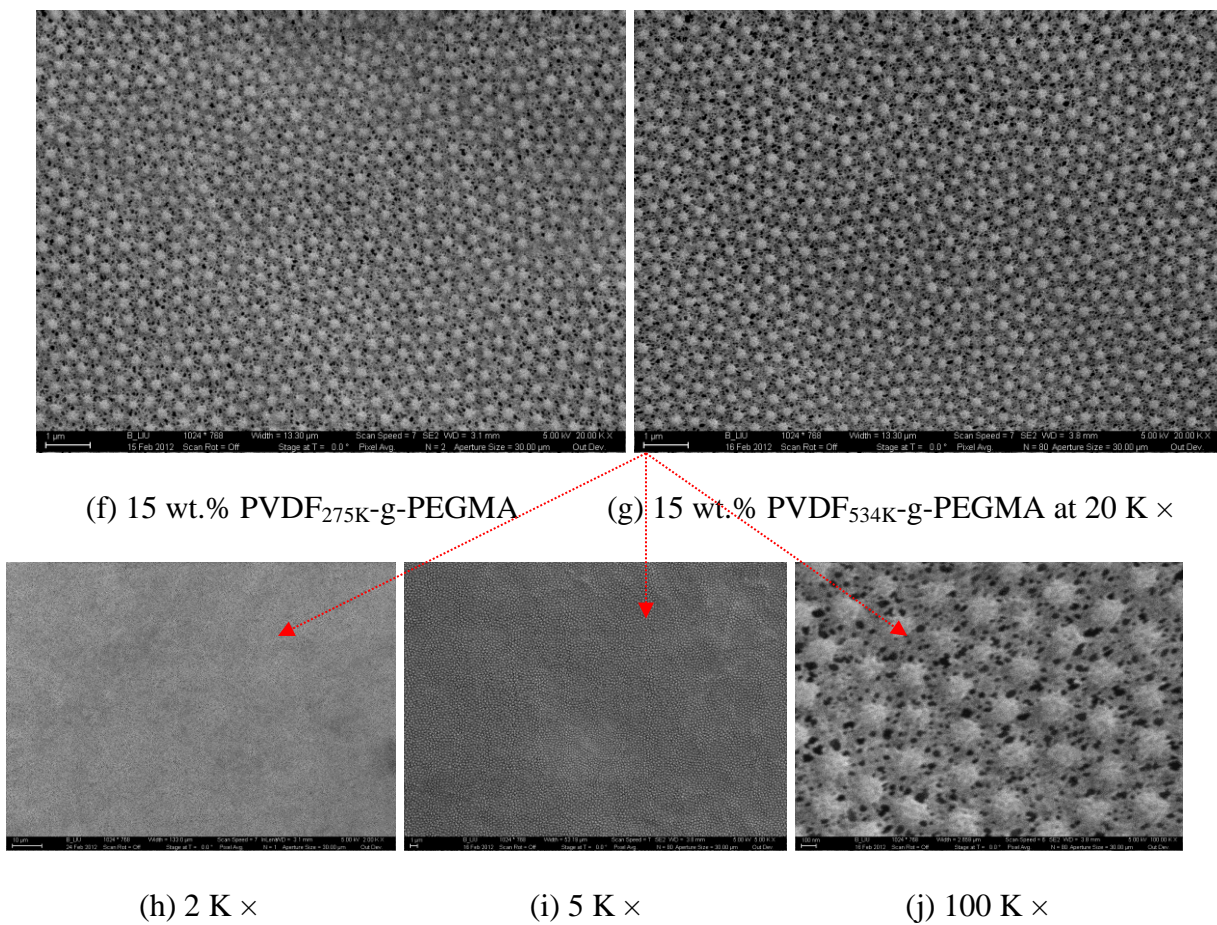t.% PVDF$_{275K}$-g-PEGMA, (e) 10 wt.% PVDF$_{534K}$-g-PEGMA, (f) 15 wt.% PVDF$_{275K}$-g-PEGMA, and (g) 15 wt.% PVDF$_{534K}$-g-PEGMA. The z-axis unit is nm.

3.3.5 Membrane permeate flux and removal efficiency

As shown in Figure 3.7a, the permeate fluxes of fabricated membranes for DI water with 5 wt.%, 10 wt.%, and 15 wt.% $PVDF_{534K}$-g-PEGMA under a constant applied pressure (0.07 MPa) had a large value, which are 1080 ($L/m^2 \cdot h \cdot bar$), 5110 ($L/m^2 \cdot h \cdot bar$), and 5170 ($L/m^2 \cdot h \cdot bar$), respectively. While for the virgin PVDF membrane no permeated water was detected under 0.07 MPa (10 psi). The highest flux of DI water is 116 $L/m^2 \cdot h$ under 1 bar (14.5 psi) of literature (Hashim, Liu et al. 2009), which is over one magnitude lower than our results even at a higher applied pressure. The permeate flux for DI water is obviously lower with 5 wt.% $PVDF_{534K}$-g-PEGMA than with 10 wt.% and 15 wt.%. These results are in agreement with the lower pore density of 5 wt.% $PVDF_{534K}$-g-PEGMA (as shown in Figure 3.2). The flux dropped dramatically within a few minutes when the feed foulant sodium alginate was added, which is probably due to pore constriction and pore blocking at the beginning of fouling experiment (Katsoufidou, Yiantsios et al. 2007). Overall, 15 wt.% $PVDF_{534K}$-g-PEGMA has a lower permeate flux drop than 10 wt.% $PVDF_{534K}$-g-PEGMA, and 5 wt.% $PVDF_{534K}$-g-PEGMA has the fastest flux drop. Using sodium alginate solution, the TOC removal efficiencies of PVDF membranes with 5 wt.%, 10 wt.%, and 15 wt.% $PVDF_{534K}$-g-PEGMA are 98.52%, 90.97%, and 87.19%, respectively (calculated from Figure 3.8a). The high removal efficiency can be attributed to the narrow pore size distribution, and it appears that there are no defects in the fabricated membrane. The molecular weight distribution of sodium alginate lies mainly in the range between 30 and 100 kDa based on measurements (Katsoufidou, Yiantsios et al. 2007) and the particle size of sodium alginate should be in the range of 15–80 nm. The average pore diameter of the fabricated membrane is

approximately 30.7 nm for 15 wt.% $PVDF_{534K}$-g-PEGMA. Therefore, the fabricated self-assembled membrane can easily remove most of the sodium alginate.
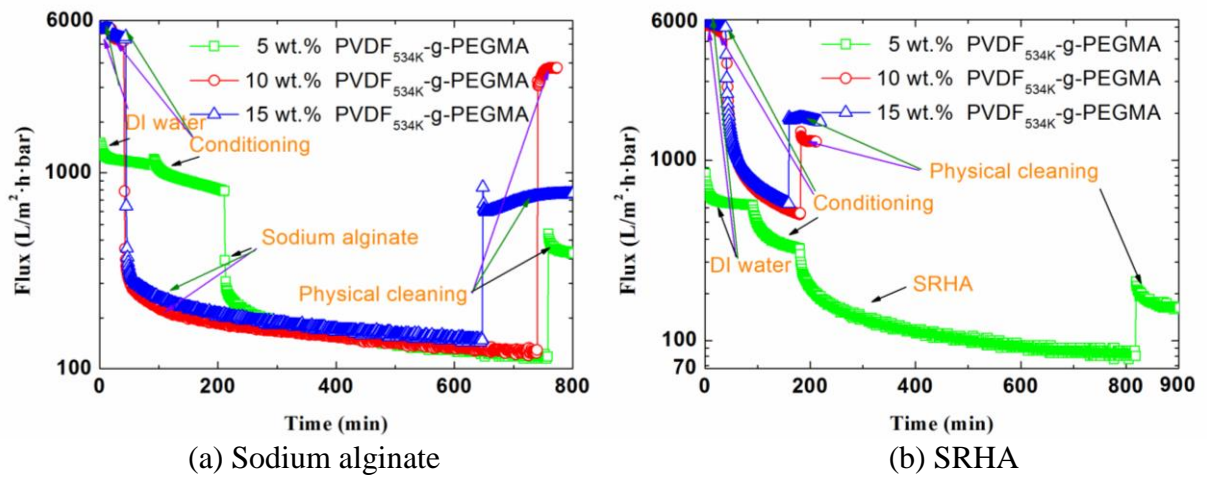
Figure 3.7. Effect of amount of PVDF$_{534K}$-g-PEGMA additives on flux performance of raw water containing (a) sodium alginate; (b) SRHA. All of these tests done on clean membranes.

	(a) Sodium alginate	(b) SRHA
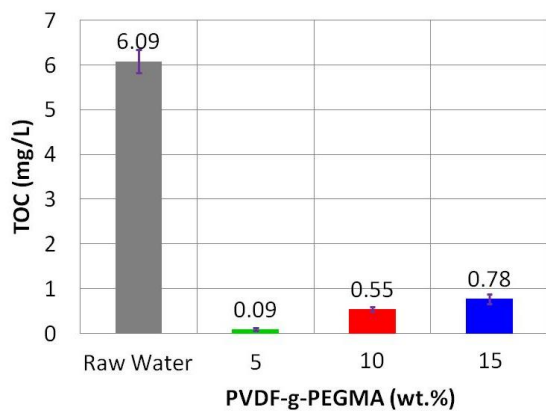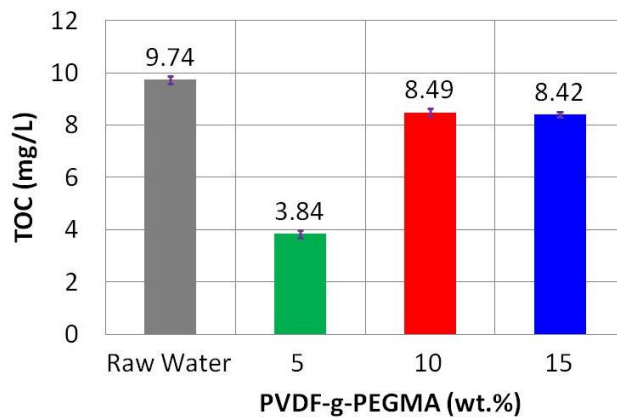
(a) Sodium alginate   (b) SRHA

Figure 3.8. TOC results of (a) sodium alginate- and (b) SRHA-containing raw water after 5 wt.%, 10 wt.%, and 15 wt.% $PVDF_{534K}$-g-PEGMA membrane filtration. Samples were taken after filtration of ~4 L raw water.

In the SRHA removal experiment, 10 wt.% and 15 wt.% PVDF$_{534K}$-g-PEGMA membranes had very high flux and low removal efficiency. The SRHA TOC removal efficiency was calculated from the raw water and filtrated water TOC values, as shown in Figure 3.8b; 5 wt.%, 10 wt.%, and 15 wt.% PVDF$_{534K}$-g-PEGMA membranes exhibited removal efficiencies of 60.6%, 12.83% and 13.55%, respectively. SRHA has a small molecular weight of 2600–3100 (a few nanometers); most of the particles can pass through the ~30.7 nm pores. However, the 5 wt.% PVDF$_{534K}$-g-PEGMA membrane exhibted a very different flux decline and removal efficiency from those of 10 wt.% and 15wt.% PVDF$_{534K}$-g-PEGMA membranes as shown in Figure 3.7b, and Figure 3.8b. The difference of surface roughness and pore distribution synergetic effect could lead to this results. The 5 wt.% PVDF$_{534K}$-g-PEGMA membrane is smoother than that of 10 wt.% and 15 wt.%, less particles deposit on smooth membranes (Vrijenhoek, Hong et al. 2001), so the flux decline rate is low. The low pore density and small pore size of 5 wt.% PVDF$_{534K}$-g-PEGMA membrane begins with a low flux.

After filtering of ~4 L sodium alginate, physical cleaning was employed to clean fouled membrane. The flux recovery for PVDF membrane with 5 wt.%, 10 wt.% and 15 wt.% PVDF$_{534K}$-g-PEGMA are 56%, 73% and 15%. Longer cleaning time of 2 min exhibits high flux recovery of 73%, which means the fabricated membranes have good anti-fouling property. The purpose of this randomly selected longer cleaning for 10 wt.% PVDF$_{534K}$-g-PEGMA is to see how high the flux recovery can be at longer cleaning time, not for the effect of cleaning time on flux recovery. After filtering of ~4 L SRHA, the flux recovery for PVDF membrane with 5 wt.%, 10 wt.% and 15 wt.% PVDF$_{534K}$-g-PEGMA are 62%, 31% and 39% by physical cleaning. Overall, it seems that 5 wt.%

membrane has a higher flux recovery at the same cleaning conditions. This may be due to the fact that (1) smooth surface, and (2) low pore density.

If calcium is added to the SRHA feed it is possible to obtain large TOC removal efficiency. As shown in Figure 3.9 and Figure 3.10, 2 mM $CaCl_2$ and 10 mM $Ca(OH)_2$ were added to SRHA in two different tests. The removal efficiencies calculated from Fig. 4.10 are 77.72% and 72.07% for 2 mM $CaCl_2$ and 10 mM $Ca(OH)_2$, respectively. For the 10 mM $Ca(OH)_2$ addition the pH was 12, but then we added HCl to adjust pH to 6.9. The permeate flux is very high, as shown in Figure 3.9. After membrane performance test, an obvious fouling layer was formed in the presence of the 10 mM $Ca(OH)_2$; however, this layer can be washed out easily. For the 2 mM $CaCl_2$ addition (raw water pH ~ 6.9), the permeate flux drops dramatically and the fouling layer is not easy to wash out. The fouling layer formed in the presence of Ca^{2+} is very compact. Calcium forms intramolecular complexes with humic acid (predominantly with carboxylic groups). Humic acid molecules formed into a "cross-linked" structure in the fouling layer owing to intermolecular bridging between Ca^{2+} and carboxylic groups, each humic acid molecule strongly associated with the humic acid molecules around it (Li and Elimelech 2004).
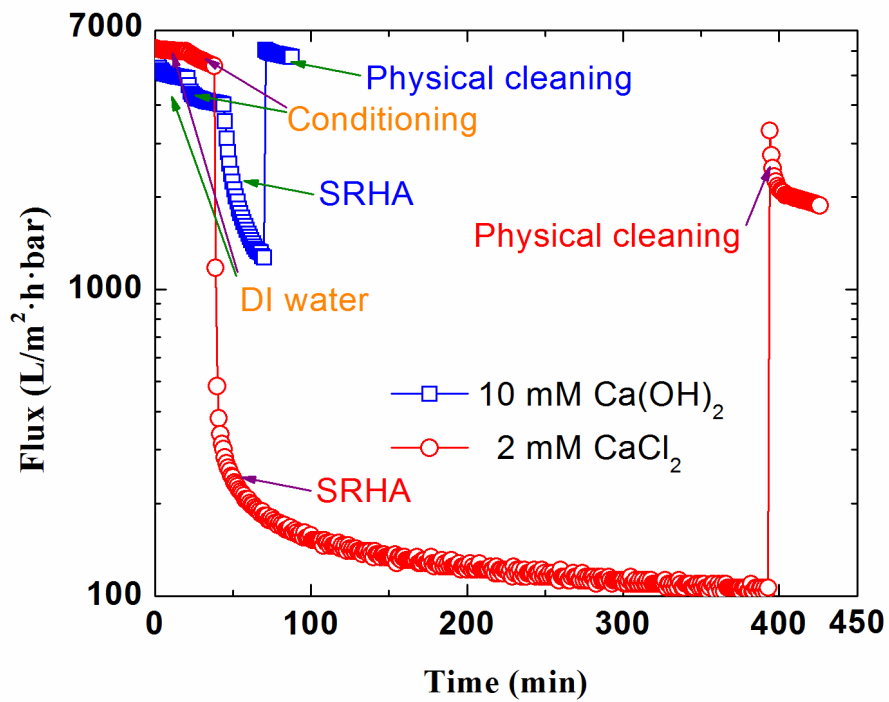
Figure 3.9. Effect of calcium hydroxide and calcium chloride on flux performance with 10 wt.% PVDF$_{534K}$-g-PEGMA membrane filtration. All of these tests done on clean membranes.
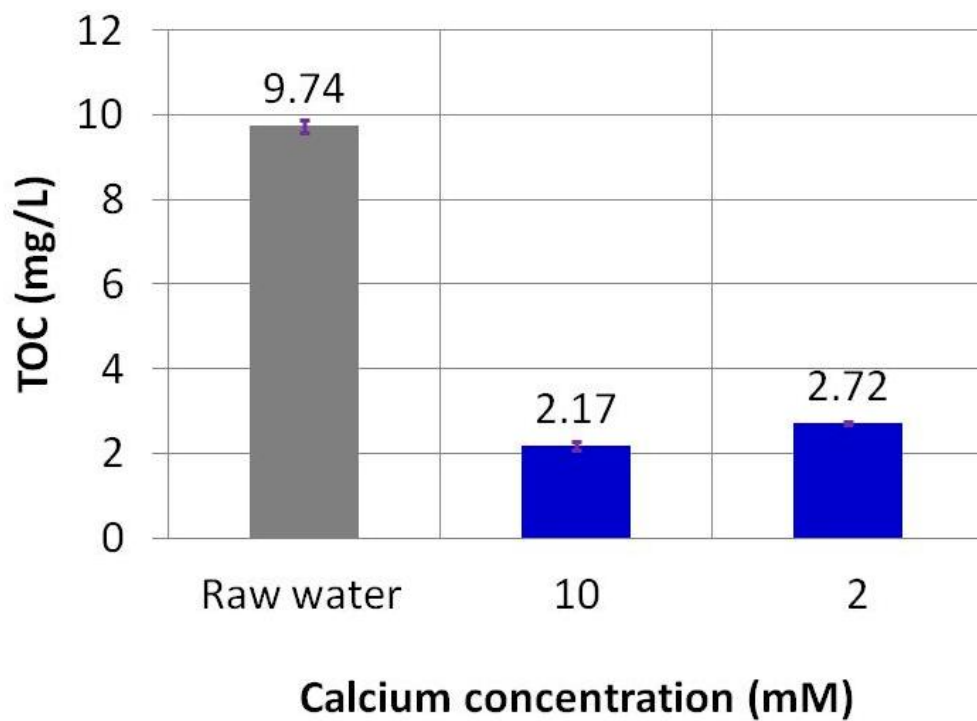
Figure 3.10. TOC results of raw water, 10 mM calcium hydroxide solution, and 2 mM calcium chloride solution after 10 wt.% $PVDF_{534K}$-g-PEGMA membrane filtration.

3.4 Conclusions

In this research, we focused on preparing and characterizing defect-free high-performance ultrafiltration membranes. The key of this synthesis method is blending the base polymer with derivatives of the polymer and tailoring the membrane casting conditions. The membrane characteristics and performance were systematically examined when adding different molecular weights ($PVDF_{275K}$-g-PEGMA, $PVDF_{534K}$-g-PEGMA) and the amounts (5 wt.%, 10 wt.%, and 15 wt.%) of copolymer. The amount of PVDF-g-PEGMA has a more significant effect on the membrane morphology and performance than does graft copolymer molecular weights within the parameters of this experiment.

The fabricated membranes exhibit an intriguing morphology with ~200 nm diameter of the periodic pillar-like structures connected by a porous mesh, high flux of 5170 ($L/m^2 \cdot h \cdot bar$) under low transmembrane pressure (0.07 MPa) and high removal efficiencies of SA (over 87%) and SRHA (over 72% with calcium). The superior performance of defect-free ultrafiltration membranes is due to its special structures. Optimization of the polymer concentration, the relative amount of solvents or varying the temperature of the water bath could further advance its applications in water treatment.

The membrane shows periodic morphology properties similar to those self-assembling membranes, but a little larger pore size distribution and different morphology. The mechanism for this membrane could probably be crystallization of semi-crystalline polymer or self-assembling, which will be further investigated in our research group.

CHAPTER 4

FORMING MECHANISM STUDY OF UNIQUE PILLAR-LIKE AND DEFECT-FREE PVDF ULTRAFILTRATION MEMBRANES WITH HIGH FLUX

4.1 Introduction

Common polymers used to prepare membranes include polyvinylidene fluoride (PVDF), polytetrafluoroethylene (PTFE), polyethersulfone (PES), polypropylene (PP), polyvinyl chloride (PVC), and polysulfone (PSF) (Yang, Xu et al. 2005, Chakrabarty, Ghoshal et al. 2008, Teoh and Chung 2009, Zhang, Chen et al. 2009, Darvishmanesh, Tasselli et al. 2011, Liu, Chen et al. 2012, Pezeshk, Rana et al. 2012). In recent years, PVDF membranes have been used in many applications owing to their good physical and chemical resistance properties (Deshmukh and Li 1998, Yeow, Field et al. 2002, Yeow, Liu et al. 2004, Tan, Tan et al. 2006). Several methods have been employed to increase the hydrophilicity and fouling resistance of PVDF membranes. These methods include surface coating (Akthakul, Salinaro et al. 2004), surface grafting (Wang, Tan et al. 2002, Liu, Du et al. 2007), and blending with amphiphilic copolymers(Hester and Mayes 2002, Zhao, Qian et al. 2008). However, surface coating and surface grafting have several disadvantages. For instance, surface coating uses physical adsorption to coat on the membrane a thin layer of water-soluble polymers or surfactants from a solution. The coating is usually unstable and can be washed away during operation of the membrane. To introduce functional groups on the membrane surface, surface grafting requires an extra step to introduce functional groups on the membrane surface which makes surface

grafting inapplicable to large-scale industrial manufacture (Schäfer, Fane et al. 2005, Liu, Xu et al. 2009, Zhou, Liu et al. 2009). Blending amphiphilic copolymers synthesizes a hydrophilic and anti-fouling membrane in a single-step, which has potential for production at industrial scale. In this method, amphiphilic copolymers with both hydrophilic and hydrophobic segments are blended with the casting solutions during the membrane synthesis process. Hydrophobic segments in the copolymer can physically combine with the membrane backbone matrix, whereas hydrophilic segments can increase the membrane's hydrophilicity (Hester, Banerjee et al. 1999, Zhao, Qian et al. 2008). Several amphiphilic copolymers have been successfully applied in the casting process to improve the hydrophilicity of the membranes (Hester, Banerjee et al. 2002, Chen, Ying et al. 2003, Akthakul, Salinaro et al. 2004, Zhao, Zhu et al. 2007, Zhao, Qian et al. 2008, Hashim, Liu et al. 2009, Li, Zhao et al. 2009, Liu, Xu et al. 2009). PEGylated or PEG-based functionalities incorporating poly(ethylene glycol) methyl ether methacrylate (PEGMA) have been added to PVDF membranes, and these membranes show good hydrophilicity and high resistance to fouling, as demonstrated in several previous studies (Chang, Shih et al. 2011, Chiag, Chang et al. 2012, Venault, Chang et al. 2012). Therefore, PEGMA was selected as the hydrophilic grafting segment in this study.

Overall, the purpose of this study is to understand the formation mechanism of pillar-like structures. It is essential to understand the reason of forming pillar-like structures since it will not only guide us on how to improve the performance of current prepared membrane but it will also help us to make the whole casting process more feasible for a larger-scale production. Therefore, we continued our previous research (Liu, Chen et al. 2013) on producing defect-free high-performance PVDF membranes

with pillar-like structures. The outstanding characteristics of these membranes, such as high flux and sodium alginate (SA) removal efficiency, are attributed to narrow pore size distribution, high surface porosity, and the unique surface feature of approximately 200 nm between each pillar-like structure. All the pores are distributed in the spaces between pillar-like structures, which mean that surface pore diameters on membranes are less than 200 nm. The absence of large pores indicates that the membrane is defect-free. In addition, the PVDF membranes we produced had up to 15% surface porosity, much higher than other PVDF membranes described in the literature (up to 4.8%) (Hester and Mayes 2002). To study formation mechanism of pillar-like structure from solvent aspect, we changed the solvent from a mixture of N,N-dimethylformamide (DMF) and tetrahydrofuran (THF) to pure DMF and then to pure 1-methyl-2-pyrrolidinone (NMP). We also used ternary phase diagram to verify the effect of solvent. Regarding additives for membrane synthesis, we first used a copolymer solution containing impurities as an exploratory test, and then changed to a purified copolymer powder. Furthermore, we added additional NMP or PEGMA to the casting solution to simulate the use of copolymer solution in the casting process in order to reconfirm the influence of NMP and PEGMA. The cast PVDF membranes were characterized by scanning electron microscopy (SEM) for morphology, X-ray photoelectron spectroscopy (XPS) for surface composition of membrane, contact angle measurement for hydrophilicity, fourier transform infrared attenuated reflection spectroscopy (FTIR-ATR) for the presence of PVDF-g-PEGMA, and atomic force microscopy (AFM) for roughness and adhesive force. The performance of the membranes, including permeation flux and sodium

alginate (SA) rejection, were also studied. Finally, the target plot method was used to help us to choose the membrane with the best performance from all casted membranes.

4.2 Experimental

4.2.1 Materials

Poly(vinylidene fluoride) (PVDF, approximately 534,000 g/mol in M_w), poly(ethylene glycol) methyl ether methacrylate (PEGMA, M_n = 475 g/mol), copper (I) chloride (CuCl), 4-4′-dimethyl-2-2′-dipyridyl (DMDP), silicone oil, NMP, THF, DMF, hydrochloric acid (HCl), petroleum ether, and methanol were purchased from Sigma-Aldrich, USA. All solvents and chemicals were reagent grade, and all reagents were used as received.

4.2.2 Model foulant

SA was purchased from Sigma-Aldrich (USA) for use as a model compound for extracellular polymeric substances (EPS) (Katsoufidou, Yiantsios et al. 2008). The SA stock solution was prepared in a flask by adding SA to deionized water and mixing until completely dissolved. The SA stock solution of 2 g/L was stored at 4°C for future use. In all fouling experiments, the SA concentrations were determined using a Shimadzu total organic carbon (TOC) analyzer (Shimadzu Co., Japan).

4.2.3 Synthesis of graft copolymer PVDF-g-PEGMA

The steps used to synthesize the copolymer PVDF-g-PEGMA were similar to those previously published (Hester, Banerjee et al. 2002, Hashim, Liu et al. 2009). First, 5 g of PVDF were dissolved in 40 mL of NMP in a conical flask at 50ºC for 24 h and stirred using a magnetic stirrer. PEGMA (50 mL), the catalyst CuCl (0.04 g), and the initiator DMDP (0.23 g) were added to the flask after the solution was cooled to room temperature. A rubber septum was used to seal the flask, and nitrogen gas was bubbled through the solution for 30 min and stirred using a magnetic stirrer. Then the flask was put in a silicon oil bath at 90ºC for 19 h and stirred using a magnetic stirrer. The copolymer mixture was at that point ready to use for the exploratory test. The copolymer mixture contained NMP, unreacted PEGMA, CuCl, and the initiator DMDP. The amount of copolymer present in the mixture was calculated on the basis of 20% PEGMA conversion ratio (Hester, Banerjee et al. 2002, Hashim, Liu et al. 2009, Liu, Chen et al. 2013). To purify the copolymer mixture for the second set of synthesis, a mixture of 0.1 mL of HCl, 1 part petroleum ether, and 1 part methanol was used to precipitate the graft copolymer followed by a filtration process. The recovered polymer was redissolved in NMP and reprecipitated in petroleum ether/methanol repetitively for three times. Finally, the polymer was dried under vacuum for 12 h at 25°C for future use (Hester, Banerjee et al. 2002). Detailed characterizations of PVDF-g-PEGMA can be found in other studies (Hester, Banerjee et al. 2002, Akthakul, Salinaro et al. 2004). The copolymer mixture and the purified polymer were both used as additives in this research.

4.2.4. Preparation of PVDF membranes

The casting solutions were prepared in 125 mL conical flasks while heating at 60°C and stirring at 500 rpm (Corning, USA). After 24 h of heating and mixing, the casting solutions were degassed without mixing for at least 2 h until no gas bubbles were observed. A doctor blade (Universal blade applicator, Paul N. Gardner Company, Inc., Pompano Beach, FL) with a gate height of 200 μm was used to cast the solution on a first-grade surface optical mirror. The mirror was left in air for 10 s before it was immersed for 48 h in a 25°C coagulation bath that contained deionized water. The cast membranes were then air dried for 24 h. Membranes were prepared from casting solutions according to the compositions listed in Table 4.1.

Table 4.1 The composition of the casting solutions.

Membrane ID	PVDF (g)	Main solvent DMF (g)	Main solvent NMP (g)	Main solvent THF (g)	Additive type Purified PVDF-g-PEGMA (g)	Additive type PVDF-g-PEGMA from mixture (g)	Extra solvent PEGMA (mL)	Extra solvent NMP (mL)	Additive/PVDF wt/wt (%)
a. Pure PVDF	9	28.7	-	12.3	-	-	-	-	-
b. M[1] P-g-P D/T = 7/3[2]	9	27.755	-	11.895	-	1.35	-	-	15
c. M P-g-P DMF	9	39.65	-	-	-	1.35	-	-	15
d. M P-g-P NMP	9	-	39.65	-	-	1.35	-	-	15
e. P[3] P-g-P DMF	9	39.65	-	-	1.35	-	-	-	15
f. P P-g-P NMP	9	-	39.65	-	1.35	-	-	-	15
g. P P-g-P NMP F[4]P	9	-	39.65	-	1.35	-	5.4	-	15
h. P P-g-P DMF FN	9	39.65	-	-	1.35	-	-	5.4	15
i. P P-g-P DMF FN FP	9	39.65	-	-	1.35	-	5.4	5.4	15

[1]: M means PVDF-g-PEGMA from mixture; [2]: D/T = 7/3 means the weight/weight ratio of DMF/THF is 7/3; [3]: P means purified PVDF-g-PEGMA; [4]: F means extra solvent.

4.2.5 Membrane morphology

The morphology of the membrane surface was examined with SEM (Zeiss Ultra 60; Carl Zeiss NTS, USA). Membranes were positioned on stubs with carbon dots and then sputter coated with an ~2 nm gold layer before imaging. An acceleration voltage of 5 kV was used to examine coated samples at different magnifications. Average pore diameter ($D_{average}$), maximum observed pore diameter (D_{max}), pore density, and surface porosity (ε) were obtained from SEM images using the Image-Pro Plus 7.0 (Media Cybernetics, USA). The surface porosity was defined as the ratio between the total area enclosed by pores and that of the entire area.

4.2.6 Determination of the cloud point

Cloud point data were measured by titration method. The solution to be titrated was prepared in a sealable bottle and kept stirring at 60 °C. Non-solvent (DI water) was slowly added into the solution until the polymer solution became irreversibly turbid as detected visually (Tiraferri, Yip et al. 2011).

4.2.7 XPS analysis

The X-ray photoelectron spectroscopy (XPS, Thermo K-Alpha XPS system) was used to study the near-surface compositions of PVDF membrane to a depth of less than 5 nm. Survey spectra were collected over 0-1350 eV, and high-resolution scan with a resolution of 0.1 eV were also collected.

4.2.8 Liquid sessile drop contact angle analysis

Liquid sessile drop dynamic contact angle measurements on the membrane were performed at 25°C using a Ramé-hart Model 250 goniometer (Ramé-hart Instrument Co., USA). The static and dynamic water contact angles were measured by placing 2 µL of deionized water on the membrane surface. At least five independent measurements were taken at different locations on a membrane sample. The average values are reported.

4.2.9 FTIR-ATR

The presence of PVDF-g-PEGMA in the PVDF membranes was analyzed by using a Fourier transform infrared (FTIR) spectrometer (Perkin Elmer, Spectrum One equipped with an attenuated total reflection (ATR) attachment). Samples were placed on the sample holder, and all spectra were recorded in the wave number range from 4000 to 650 cm^{-1} by cumulating 32 scans at a resolution of 2 cm^{-1}.

4.2.10 AFM analysis

The surface roughness of the cast membrane was measured using an Agilent 5500 AFM (Agilent Technologies, Inc., USA). Membrane samples were fixed on a specimen holder, and 5 μm × 5 μm areas were scanned in the acoustic alternating current (AC) tapping mode. At least five replicates were performed for each membrane sample. The average values with standard errors are reported.

4.2.11 Flux performance

A dead-end filtration cell (Millipore, USA) with an effective membrane area of 28.7 cm^2 was used for membrane flux performance testing. The filtration cell had a cell volume of 200 mL, and it was connected to a 5 L dispensing vessel. All filtration experiments were performed under a constant pressure of 0.14 MPa (20 psi) by applying compressed nitrogen gas. The permeate weight data was measured and collected once per minute using Collect 6.1 software (Cambridgesoft, USA) and an Ohaus Adventurer Pro Balance AV8101 (Ohaus, USA).

The membrane fouling test procedure was as follows. First, the membrane was soaked in DI water for 48 h. Second, the membrane was compacted using approximately 4 L of DI water under a pressure of 0.14 MPa. Third, the membrane was conditioned using 4 L of a 10 mM NaCl solution.

Fourth, the feed solution containing 20 mg/L SA and 10 mM NaCl was added to the filtration cell, and each fouling test ran for at least for 6 h. A stirring plate (Corning, USA) was used to minimize concentration polarization during the filtration test. A magnetic stirrer was hung from the top to prevent ruining the membrane. At the end of

the fouling test, the surface of the testing membrane was physically cleaned by rinsing with DI water for 1 min.

4.2.12 Interaction force measurements

The interactions between the SA foulant and membranes b, c, d, and i (Table 1) were investigated by using an AFM (Multimode NanoScope IIId, Bruker Nano Inc. Germany) to measure the interaction forces between a carboxylate-modified latex (CML) colloid probe and the membrane surfaces. The CML colloid probe (Invitrogen, USA) was used as a surrogate for SA because the predominant functional groups of alginate are carboxylic acid groups (Ang, Lee et al. 2006, Chen, Mylon et al. 2006). The membrane sample preparation and interaction measurements were similar to those in a recent study by Tang et al. (Tang, Gu et al. 2013). The CML colloid had a diameter of 16 μm and was attached using an epoxy adhesive to a tipless silicon-nitride cantilever with a spring constant of 0.06 N/m (Bruker, Camarillo, USA). The colloid probes were oxidized in a UV-ozone chamber (Procleaner[TM] 110, BioForce Nanosciences, Inc., Ames, USA) for 15 min before use. All force measurements were conducted in a glass fluid cell. A solution of 10 mM NaCl with pH 5.9 (unadjusted pH) was injected into the fluid cell with a syringe, and force was measured by bringing the colloid probe toward the membrane surface and then retracting the probe after contact. The scan rate and ramp size were 0.49 Hz and 1.0 μm, respectively. For each membrane, 5 force measurements were conducted at each of 15 locations. Force–separation curves were obtained from the retraction force measurements, and the work of adhesion can be calculated by integrating the area under the retraction force profiles (Tang, Gu et al. 2013). Because the retraction forces

82

measured for membranes b, c, d, and i were attractive, the work of adhesion represents the energy required to pull the CML probe away from the membrane surface after contact (Tang, Gu et al. 2013).

4.3 Results and discussion

4.3.1 Membrane morphology

SEM images of all cast PVDF membranes are shown in Figure 4.1, Figure 4.2, and Figure 4.3. The statistics of pore size distribution are summarized in Table 4.2. The pure PVDF membrane (a) has a surface porosity of 0.10%, average pore size of 6 ± 3 nm, maximum pore size of 23 nm, and pore density of 2.6×10^{13} m^{-2}. Based on our previous experiment, we used a mixture of DMF and THF as the solvent for the casting solution (Liu, Chen et al. 2013). The main disadvantage of this solvent mixture is that THF is highly flammable (Canal, Ramnial et al. 2008) and volatile (Kang, Jung et al. 2008); when mixed with air, it can be explosive (Coetzee and Chang 1985). This may cause safety issues during industrial production (Chemicals 1992). To determine if THF can be replaced with a much safer solvent, we changed the solvent from a mixture of DMF/THF (Figure 4.1B, membrane b) to pure DMF (Figure 4.1C, membrane c) and then to pure NMP (Figure 4.1D, membrane d) while keeping other variables the same. Figure 4.1 shows the surface morphology of membranes cast with different solvents.
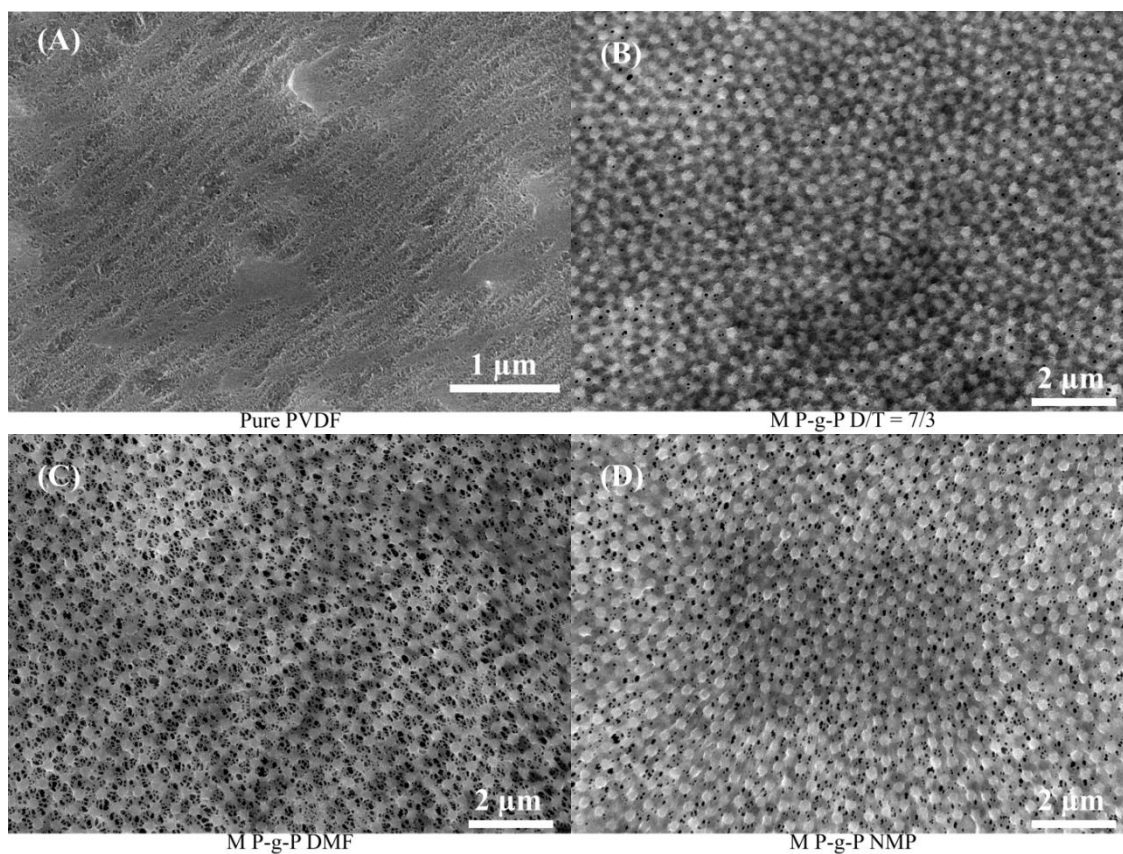
Figure 4.1. SEM images of membrane top surfaces: (A) membrane a. pure PVDF, (B) membrane b. M P-g-P D/T = 7/3, (C) membrane c. M P-g-P DMF, and (D) membrane d. M P-g-P NMP (Table 4.1).

As shown in Figure 4.1, membranes b, c, and d had pillar-like structure with similar features on their surfaces. The distance between neighbor pillar-like structure was approximately 200 nm, and all pores were located between pillar-like structures. However, the surface porosities of the three membranes were different. Table 4.2 shows that membranes b, c, and d had surface porosities of 5.67%, 14.69%, and 4.46%, respectively. The effect of solvent can explain the difference in surface porosity. Based on the results of cloud point test, casting solutions of membrane b, c and d need 14wt%, 12wt% and 15wt% of non-solvent (DI water) to reach the cloud point, respectively. The results of cloud point test showed that casting solution of membrane c which used DMF as solvent was the closest to the binodal curve, followed by membrane b and then membrane d. A rapid phase inversion happened rather than a delayed phase inversion if the casting dope was closer to the binodal curve (Kosuri and Koros 2008). Therefore, phase inversion happened fastest in membrane c, followed by membrane b and then membrane d. A faster phase inversion normally resulted in larger pores and higher surface porosity (Young and Chen 1995). Because pillar-like structure exists in membrane b as well as in c and d, the presence of THF (membrane b) during the casting process is not essential for pillar-like formation.

Table 4.2 Summary of pore size distribution statistics.

Membrane ID	$D_{average}$ (nm)	D_{max} (nm)	Pore density (m^{-2})	ε (%)
a. Pure PVDF	6 ± 3	23	2.6×10^{13}	0.10
b. M P-g-P D/T = 7/3	34 ± 19	126	5.2×10^{13}	5.67
c. M P-g-P DMF	75 ± 23	166	3.1×10^{13}	14.69
d. M P-g-P NMP	42 ± 23	146	2.6×10^{13}	4.46
e. P P-g-P DMF	69 ± 21	151	7.3×10^{12}	2.97
f. P P-g-P NMP	15 ± 5	49	2.9×10^{12}	0.07
g. P P-g-P NMP FP	36 ± 19	122	2.6×10^{13}	3.15
h. P P-g-P DMF FN	76 ± 20	141	4.9×10^{12}	2.19
i. P P-g-P DMF FN FP	38 ± 25	185	4.5×10^{13}	7.00

Because the copolymer mixture contained PVDF-g-PEGMA, NMP, PEGMA, CuCl, and DMDP, our next step was to eliminate other residual chemicals introduced during the casting process. Therefore, two membranes were cast with purified PVDF-g-PEGMA powder (membranes e and f) for comparison with membranes cast with the copolymer mixture (membranes c and d). Figure 4.2A shows that membrane e cast with purified PVDF-g-PEGMA using DMF as solvent did not contain pillar-like structure. However, pillar-like structures were observed on membrane f (Figure 4.2B) cast with purified PVDF-g-PEGMA using NMP as solvent. Both membrane c (Figure 4.1C) and membrane e (Figure 4.2A) used DMF as solvent, but the additives were different, with one being copolymer mixture (membrane c) and the other being purified PVDF-g-PEGMA powder (membrane e). Because no pillar-like structures were observed on membrane e, we conclude that DMF is not essential for forming PILLAR-LIKE STRUCTURE. Both membrane d (Figure 4.1D) and membrane f (Figure 4.2B) used NMP as solvent, and pillar-like structures were observed on both. Therefore, the key to form pillar-like structure structures is the presence of both PVDF-g-PEGMA and NMP in the casting solution. Figure 4.3 showed ternary diagram of PVDF-g-PEGMA in different solvents (DMF or NMP). As shown in Figure 4.3, it was clear that NMP was a better solvent than DMF for PVDF-g-PEGMA because the DMF binodal line was closer to the pure polymer-solvent axis than the NMP binodal line. Thus, phase inversion process happened faster in the casting solution when DMF was used as solvent (membrane e) than when NMP was used as solvent (membrane f). In other words, when DMF was used as solvent, PEGMA segments did not have enough time to migrate to the surface. On the other hand, when NMP was used as solvent, PEGMA segments from PVDF-g-PEGMA

had more time to migrate to the surface and repel with each other to form pillar-like structure. This result can also be verified from XPS data as shown in Table 4.3. With more PEGMA segments migrating to the surface, the membrane f had 4.67% oxygen content, higher than 1.19% oxygen content of the membrane e.
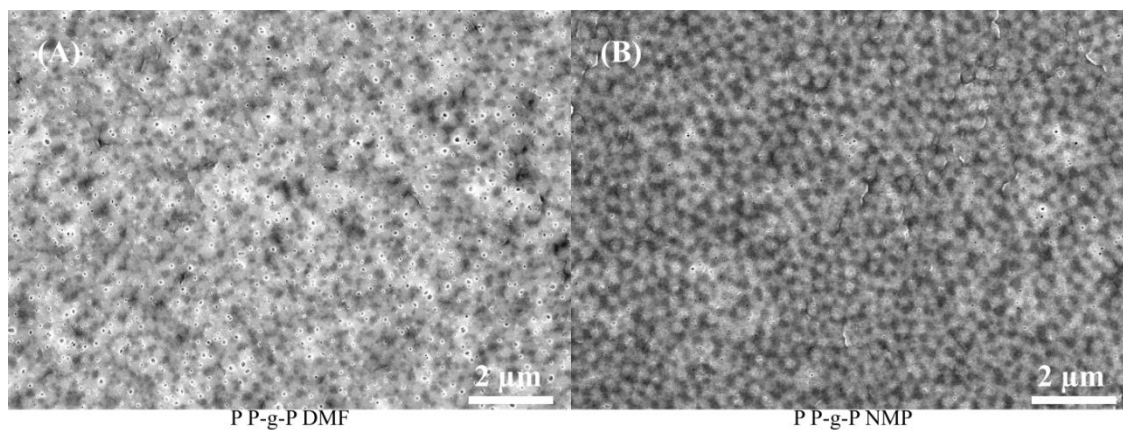
(A) P P-g-P DMF

(B) P P-g-P NMP

Figure 4.2. SEM images of membrane top surfaces: (A) membrane e. P P-g-P DMF and (B) membrane f. P P-g-P NMP (Table 4.1).
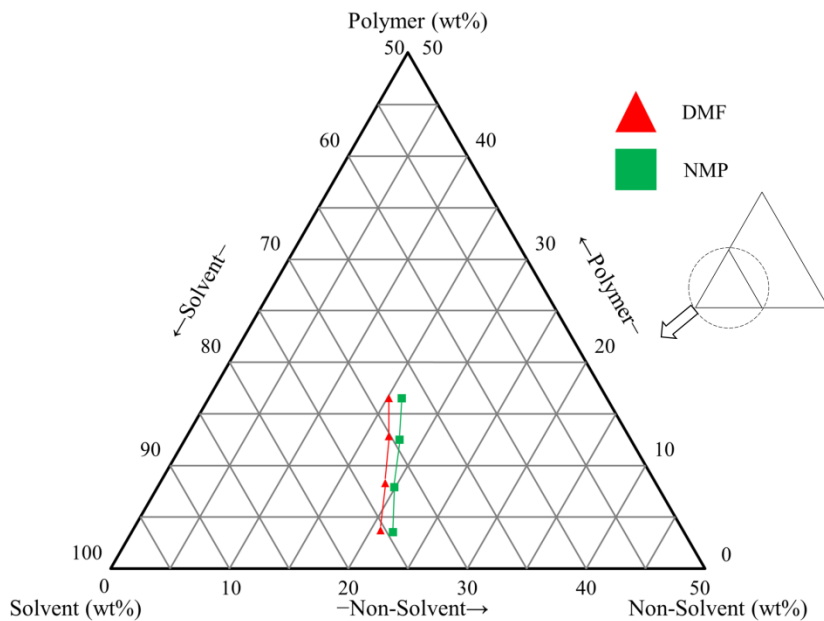
Figure 4.3. Ternary phase diagram with cloud points for PVDF-g-PEGMA/solvent/water system at 60 °C.

Membrane f has less obvious pillar-like structure than membrane d. The presence of PEGMA in the casting solution might cause this. Membrane d used the copolymer mixture as the additive, whereas membrane f used purified copolymer. The copolymer mixture contains some residual NMP and PEGMA, but purified PVDF-g-PEGMA does not. NMP was used as solvent for both membrane d and f. Therefore, the residual PEGMA should be an important factor in the difference between membranes d and f. To confirm the effect of PEGMA, we cast membrane g under the same casting conditions but with additional PEGMA in the casting solution. Membranes h and i were cast using DMF as solvent to reconfirm the effects of NMP and PEGMA.

Pillar-like structures on membrane g (Fig. 4.4A) are more obvious than those on membrane f. Thus, the role of PEGMA is clear: During the phase inversion process, PVDF segments in PVDF-g-PEGMA physically combine with PVDF backbone material while the PEGMA segments migrate to the surface. The free PEGMA molecules not only brought more PEGMA segments from PVDF-g-PEGMA to the surface, but also increased the repulsion forces between all PEGMA segments. The result was more obvious pillar-like structure on the membrane surface. Table 4.3 also confirmed that more PEGMA migrated to the surface for the membrane g than the membrane f. As shown in Table 4.3, the oxygen content of the membrane g was 6.86%, while the oxygen content of the membrane f was 4.67%. Several studies also showed that the same segments in the copolymer repelled each other during the phase inversion process (Nunes, Sougrat et al. 2010, Stuart, Huck et al. 2010, Yin, Yao et al. 2013).

P P-g-P NMP FP

P P-g-P DMF FN
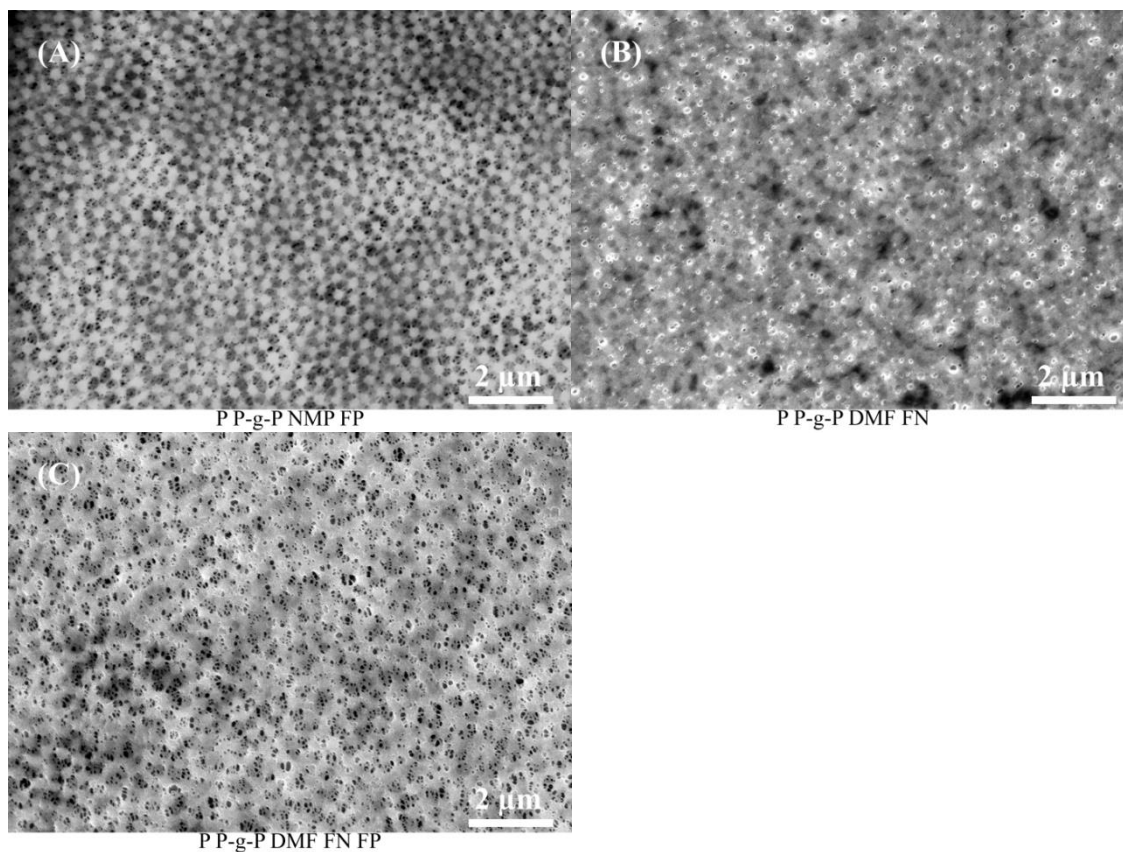
P P-g-P DMF FN FP

Figure 4.4. SEM images of membrane top surfaces: (A) membrane g. P P-g-P NMP FP, (B) membrane h. P P-g-P DMF FN, and (C) membrane i. P P-g-P DMF FN FP (Table 4.1).

Membranes h (Figure 4.4B) and i (Figure 4.4C) further confirm the effects of NMP and PEGMA. No pillar-like structures are found on membrane h, whereas membrane i has pillar-like structure. Although PVDF-g-PEGMA and NMP both exist in the casting solution of membrane h, the repulsion force was not high enough to form pillar-like structure because there were fewer PEGMA on the membrane surface. After extra PEGMA was added to the casting solution, the repulsion force on the membrane surface was high enough to form pillar-like structure (membrane i). The movement of PEGMA segments for the membranes e, h and i can also be verified from Table 4.3. The oxygen content from the highest to the lowest were the membranes i, h, and then e. Comparison of the oxygen content of the membranes e and h confirmed that NMP slowed the phase inversion process as more PEGMA migrate to the surface. Comparison of the oxygen content of the membranes h and i reconfirmed that more PEGMA segments from PVDF-g-PEGMA were brought to the surface by free PEGMA molecules.

Overall, the mechanism of pillar-like structure formation is as follows: During the phase inversion process, the PVDF segments in PVDF-g-PEGMA physically combine with the PVDF backbone material while the hydrophilic segments of PEGMA migrate to the surface of the membrane. NMP is needed to form pillar-like structure. Once NMP is added to the casting solution, PEGMA segments in PVDF-g-PEGMA have more time to migrate to the surface due to a slower phase inversion process. These PEGMA segments repelled each other on the membrane surface during the phase inversion process. Free PEGMA molecules not only bring more PEGMA segments in PVDF-g-PEGMA to the surface but also increase the repulsion forces between all PEGMA segments.

4.3.2 XPS analysis

The near-surface compositions of prepared PVDF membranes are shown in Table 4.3. XPS analysis was conducted on the active layer of the membrane. The oxygen content of membrane indicates the migration level of PEGMA. Theoretical oxygen content can be calculated based on the chemical structure of PVDF-g-PEGMA and the composition of casting solution (Hester, Banerjee et al. 2002). According to the FTIR-ATR data, no residual PEGMA left on the membrane. Assuming all solvent in the polymeric thin film goes into the coagulation bath during the phase inversion, and chemical composition is uniformed through the entire membrane, the theoretical oxygen content for membrane b to i is in the range from 3.29% to 3.84%. Comparing the theoretical oxygen content with the experimental data, more PEGMA segments moved to the surface on membrane b, c, d, f and i. Membrane e and h have a lower oxygen content might because of phase inversion happens to fast that PEGMA do not have enough time to migrate to the surface before the active layer formed. As the more PEGMA migrates to the surface, the higher oxygen content should be observed.

Table 4.3 The surface elemental compositions of PVDF membranes.

Membrane ID	F (%)	C (%)	O (%)
b. M P-g-P D/T = 7/3	35.91	57.72	6.37
c. M P-g-P DMF	38.11	56.04	5.84
d. M P-g-P NMP	36.89	56.63	6.49
e. P P-g-P DMF	45.33	53.48	1.19
f. P P-g-P NMP	37.50	57.83	4.67
g. P P-g-P NMP FP	36.46	56.68	6.86
h. P P-g-P DMF FN	43.75	53.88	2.36
i. P P-g-P DMF FN FP	39.41	55.42	5.17

4.3.3 Contact angle measurement

Contact angle measurement is the most convenient method to characterize the hydrophilicity and wetting ability of membrane surface. Such measurements are affected by capillary forces within pores, roughness and heterogeneity (Taniguchi and Belfort 2002). However, the relative hydrophilicity of each membrane can be compared with its static contact angle and dynamic contact angle. A more hydrophilic membrane has a smaller initial contact angle and a quicker decrease rate of static contact angle.

Hydrophilicities of pure PVDF and modified PVDF membranes were characterized via static contact angle and dynamic contact angle, and the data are reported in Table 4.4 and Figure 4.5, respectively. From Figure 4.5, the contact angles that decline linearly with time faster indicate higher membrane hydrophilicity. From Table 4.4, all PVDF membranes containing PVDF-g-PEGMA in the casting solution have better wettability than the pure PVDF membrane. The better hydrophilicity is attributed to hydrophilic PEGMA segments on the membrane surface. The contact angle results reconfirm the presence of PVDF-g-PEGMA in membranes b to i.

Table 4.4 Static contact angle measurements.

Membrane ID	Contact angle (°)
a. Pure PVDF	90.2 ± 1.0
b. M P-g-P D/T = 7/3	69.4 ± 4.4
c. M P-g-P DMF	72.3 ± 3.3
d. M P-g-P NMP	74.2 ± 4.7
e. P P-g-P DMF	67.7 ± 1.1
f. P P-g-P NMP	74.2 ± 1.7
g. P P-g-P NMP FP	67.6 ± 2.9
h. P P-g-P DMF FN	73.1 ± 3.7
i. P P-g-P DMF FN FP	75.3 ± 2.5
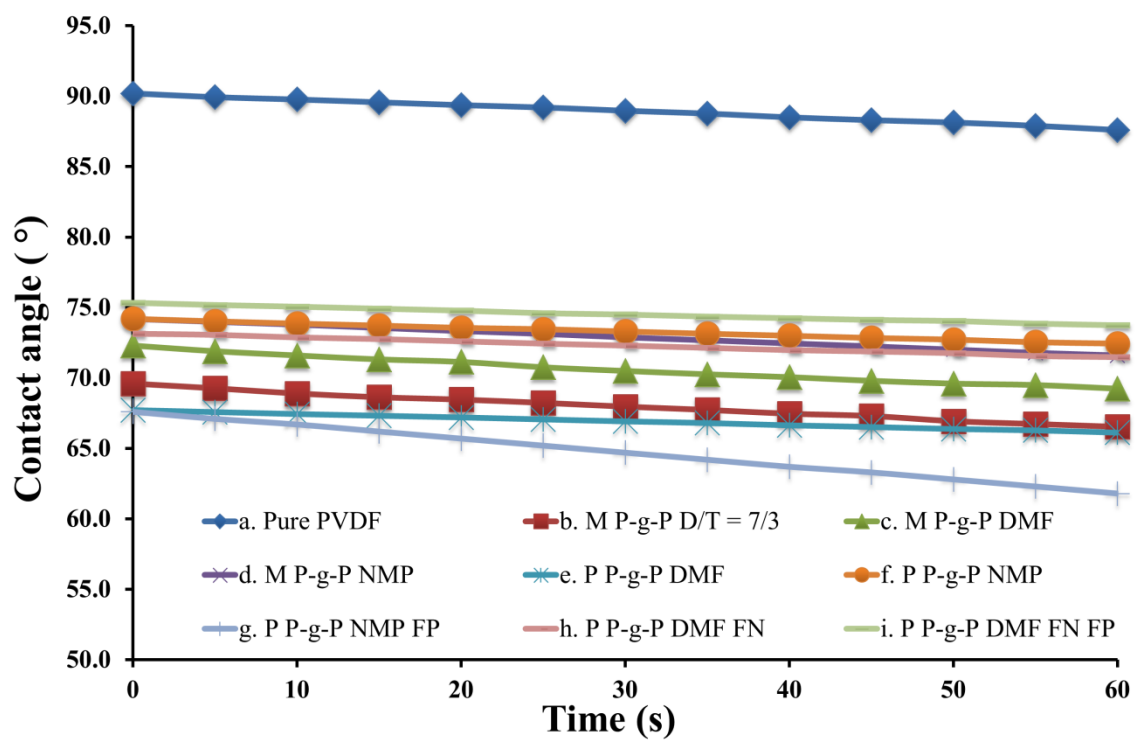
Figure 4.5. Changes in contact angle with time.

4.3.4 FTIR-ATR analysis

FTIR-ATR analysis was used to characterize the crystalline phase of PVDF and to verify the presence of PVDF-g-PEGMA on the membrane surface. Vibrational band at 765 cm^{-1} refer to α phase, and vibrational band at 840 cm^{-1} refer to β phase (Salimi and Yousefi 2003, Gregorio 2006). Crystalline phase of PVDF in membrane a (Pure PVDF) is α phase and crystalline phase of PVDF in all other modified PVDF membranes (membrane b to membrane i) is a mixture of α phase and β phase. Since a mixture of α phase and β phase is observed from membrane b to membrane i, crystalline phase of PVDF do not significantly influence the formation of pillar-like structure. The characteristic C=O stretching band represented by the peak at 1727 cm^{-1} was observed on membranes b, c, d, g and i but not on membranes e, f, and h. This might be due to limited equipment sensitivity. Based on the previous contact angle measurement results, membranes e, f and h had smaller contact angles than the pure PVDF membrane (membrane a), which proved the presence of amphiphilic copolymer PVDF-g-PEGMA on the cast membranes. In addition, no obvious peak was observed at 1642 cm^{-1}, which represents the C=C stretch. Thus, unreacted monomer in the unpurified mixture was removed during the coagulation bath. Similar results were obtained in other studies, which suggest the presence of PVDF-g-PEGMA on all modified PVDF membrane surfaces.(Chen, Liu et al. 2006, Liu, Du et al. 2007, Choi, Kwon et al. 2012, Hashim, Liu et al. 2012).
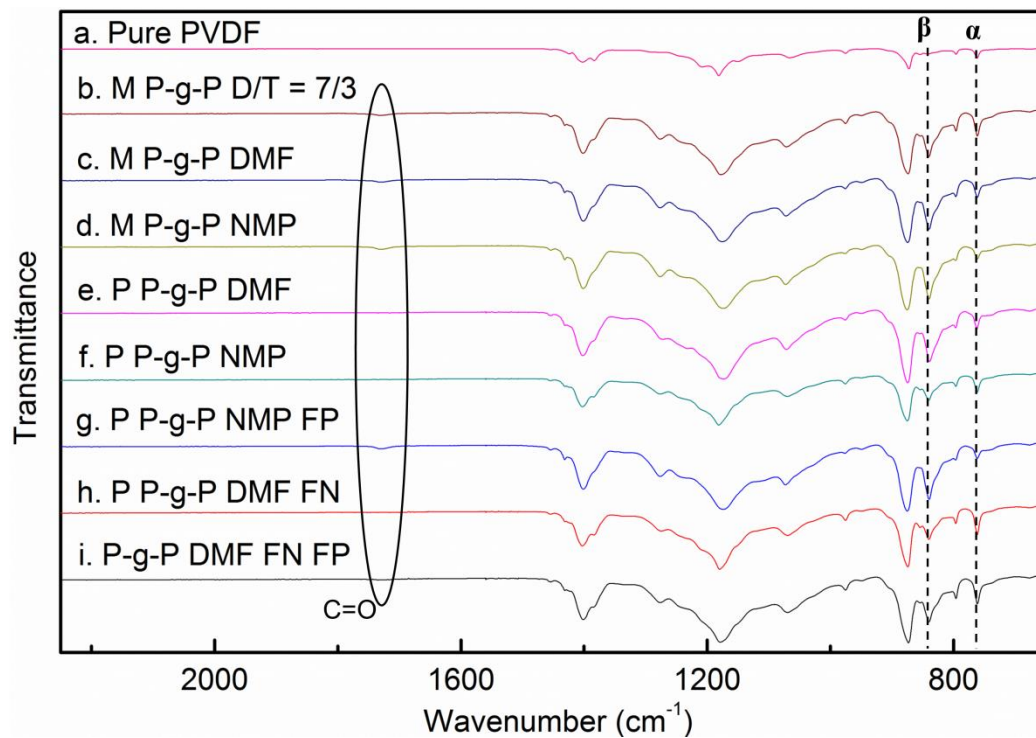
Figure 4.6. FTIR-ATR spectra of pure PVDF and modified PVDF membranes.

4.3.5 Roughness

The roughnesses of the PVDF membranes are shown in Figure 4.7. The measured root mean square (RMS) roughness of the pure PVDF (membrane a) was 34.0 ± 7.3 nm. Pillar-like structure did not significantly influence the surface roughness. Figure 4.8 shows the surface morphology of the PVDF membranes; consistent with SEM results, more obvious Pillar-like structure can be seen in membranes b, c, d, g, and i (Figure 4.1B, Figure 4.1C, Figure 4.1D, Figure 4.4A, and Figure 4.4C).
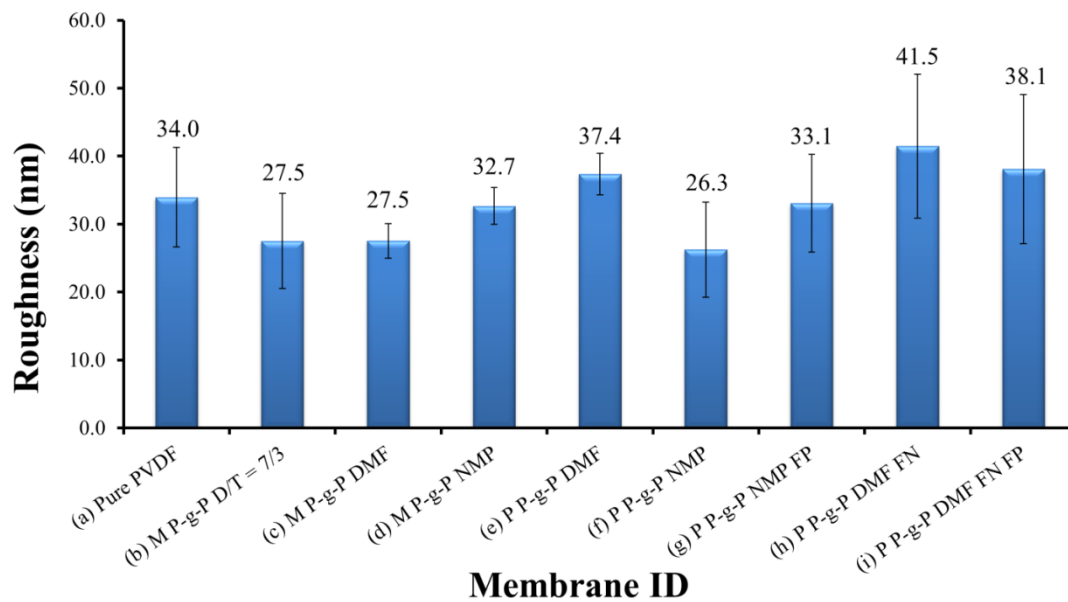
Figure 4.7. Roughnesses of the PVDF membranes.

(a)

(b)

(c)

(d)

(e)

103

(f)

(g)

(h)

(i)
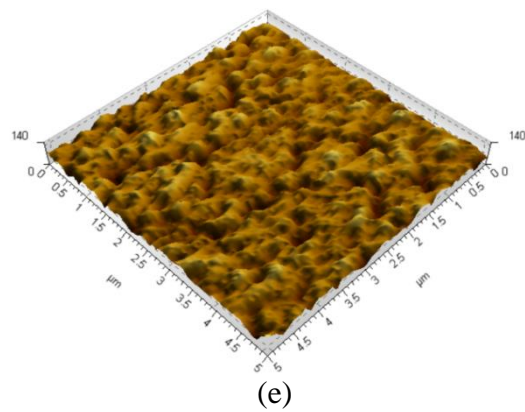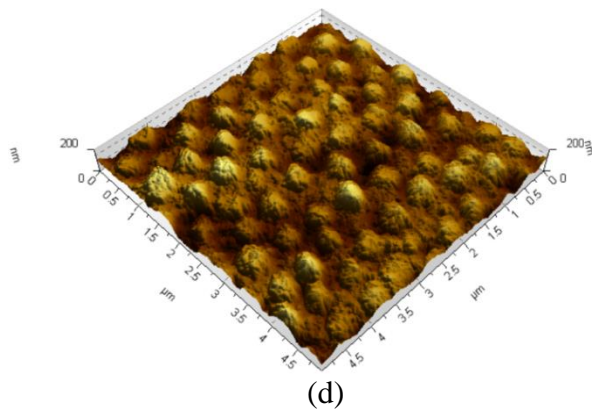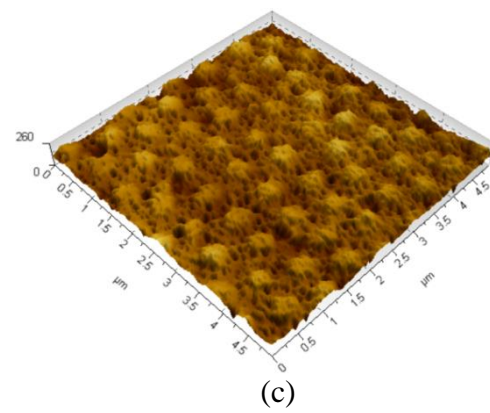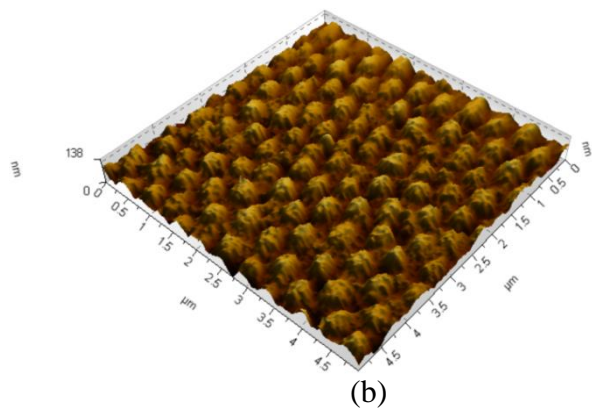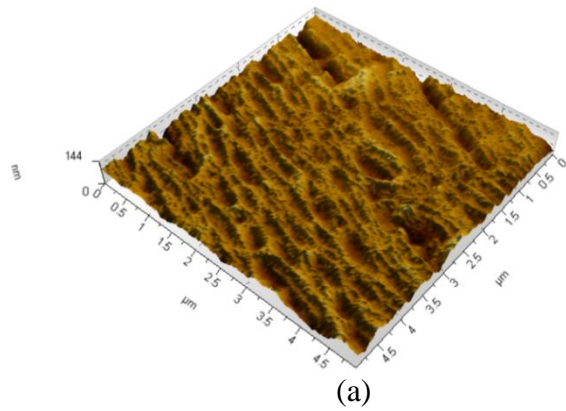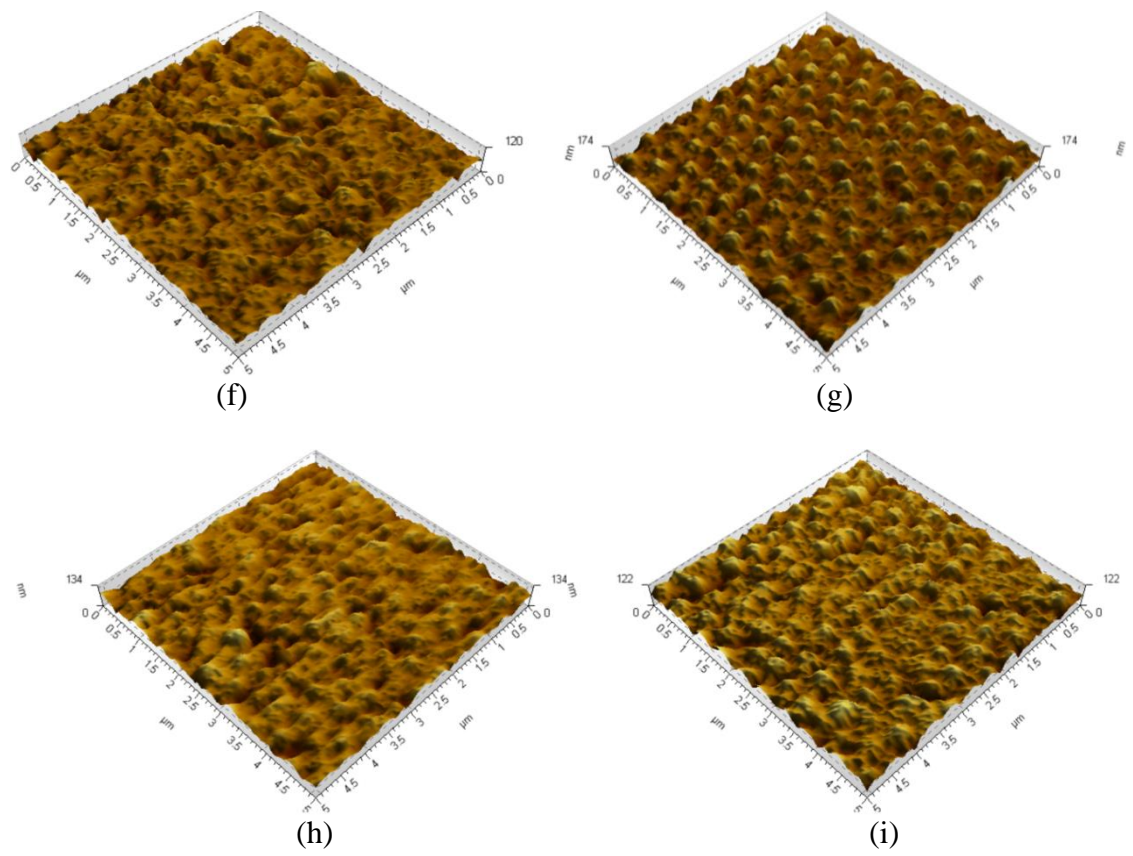
Figure 4.8. AFM images of PVDF membranes.

4.3.6 Membrane permeate flux and removal efficiency

The effects of copolymer composition and solvent on PVDF membrane performance were investigated by pure water permeation and SA filtration studies. Under an applied constant pressure of 0.14 MPa, no water permeation was observed for membranes a, e, and f, whereas b, c, d, g, and i had very high pure water fluxes of 374 $L/m^2/h/bar$, 2173 $L/m^2/h/bar$, 949 $L/m^2/h/bar$, 800 $L/m^2/h/bar$, and 3270 $L/m^2/h/bar$, respectively, as shown in Figure 4.9 and Table 4.5. The pure water flux of membrane h was orders of magnitude lower than that of membranes b, c, d, g, and i from the very beginning. The highest pure water flux for a PVDF membrane we can find in the literature is 116 $L/m^2/h/bar$ (Hashim, Liu et al. 2009), much smaller than our results. After physical cleaning, membranes b, c, d, g, and i had recovery fluxes of 135 $L/m^2/h/bar$, 1195 $L/m^2/h/bar$, 446 $L/m^2/h/bar$, 600 $L/m^2/h/bar$, and 818 $L/m^2/h/bar$, respectively. Of those five membranes, g had the highest flux recovery ratio, 75%, probably because of its better hydrophilicity, as shown in Figure 4.5. The SA rejection results are shown in Figure 4.10. Based on measurements, the molecular weight of SA ranges between 30 and 100 kDa (Katsoufidou, Yiantsios et al. 2007), and the SA particle size should have a diameter in the range of 15–80 nm. Membranes b, c, d, g, and i had SA rejections of 87%, 89%, 94%, 94%, and 91%, respectively. The high rejection rate can be attributed to the narrow pore size distribution and small average pore diameter, as shown in Table 4.2. The above results showed that there were no defects in the fabricated membrane.
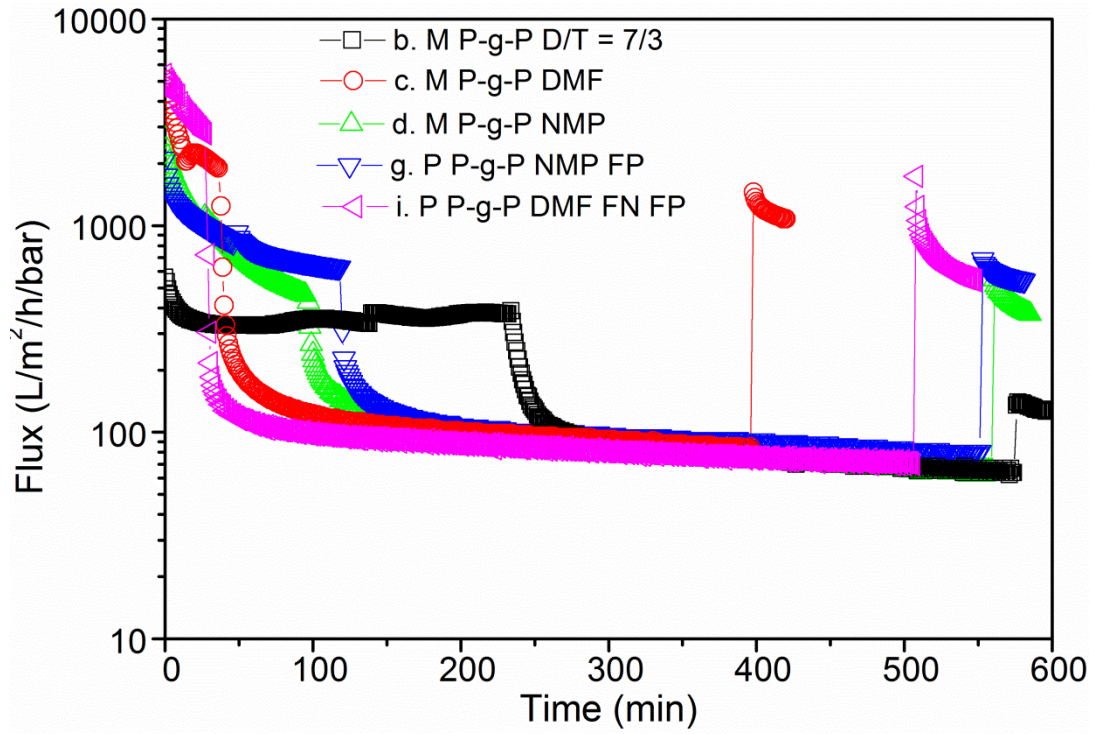
Figure 4.9. Flux performance of PVDF membranes.

Table 4.5 Flux performance of PVDF membranes.

Membrane ID	Pure water flux (L/m^2/h/bar)	Recovery flux (L/m^2/h/bar)	Recovery ratio (%)
b. M P-g-P D/T = 7/3	374	135	36
c. M P-g-P DMF	2173	1195	55
d. M P-g-P NMP	949	446	47
g. P P-g-P NMP FP	800	600	75
i. P P-g-P DMF FN FP	3270	818	25
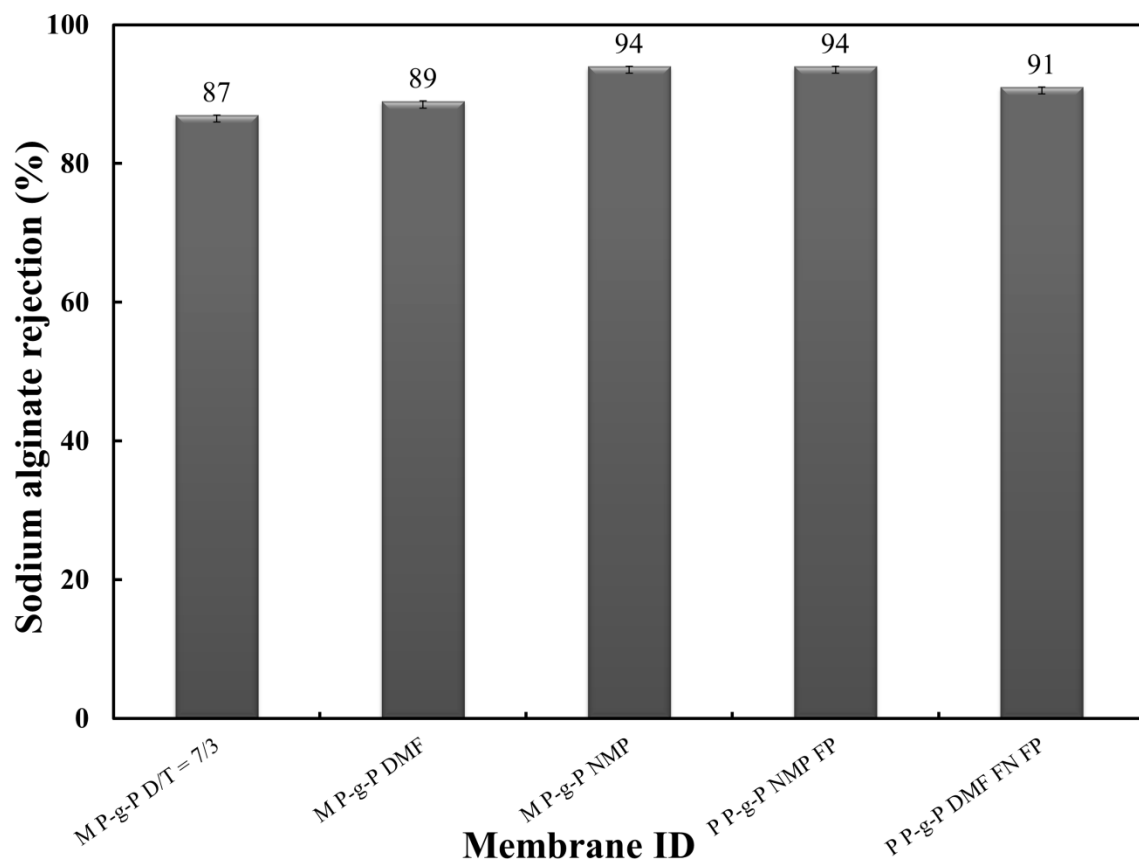
Figure 4.10. Rejection profile of sodium alginate.

4.3.7 Interaction force measurements

Figure 4.11 presents distributions of the work of adhesion for membranes b, c, d, and i obtained in 10 mM NaCl and at pH 7.0. Adhesion interactions were observed during all pull-off events for the four membranes. The adhesion potential energy that measured for membranes b and c was approximately 180×10^{-18} J, whereas the largest for membrane d was approximately 400×10^{-18} J. The adhesion potential energy for membrane i was considerably higher at more than 900×10^{-18} J. Comparing the average works of adhesion for the four membranes, the most anti-adhesive are membranes b and c (which are similar), followed by membrane d, and the least anti-adhesive is membrane i. The measured flux recovery ratios (Table 4.5) agree with these anti-adhesive properties, except in the case of membrane b. The membrane with the lowest adhesion potential energy should have the highest flux recovery ratio. Membrane c had lowest adhesion potential energy and had the highest flux recovery ratio of 55%. Membrane b had a low adhesion potential energy but had a lower flux recovery ratio than membrane c. This might be because the copolymers were not well distributed on the surface of membrane b and thus some parts of the surface were more hydrophilic than others. Overall, the anti-adhesive properties agree with the flux recovery ratios for membranes c, d, and i.
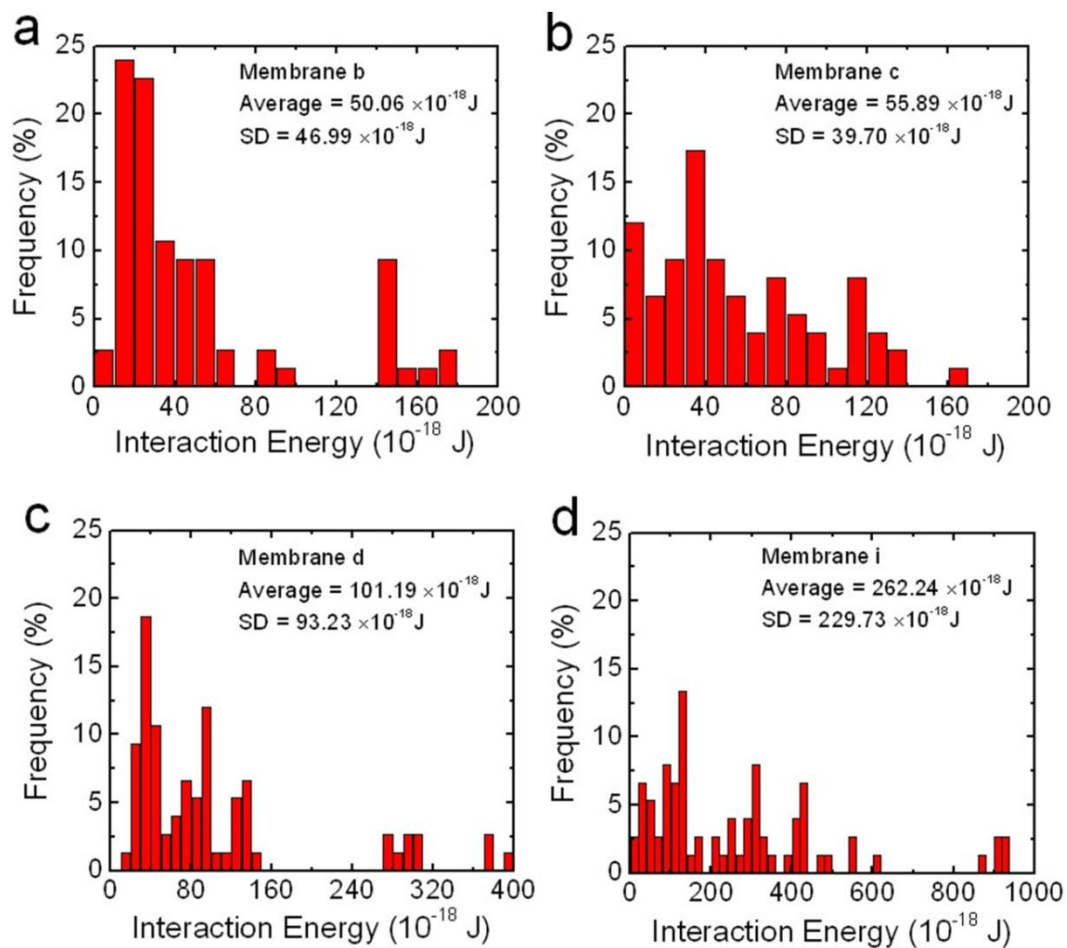
Figure 4.11. Distributions of work of adhesion for (a) membrane b, (b) membrane c, (c) membrane d, and (d) membrane i. All measurements were performed in 10 mM NaCl and at pH 5.9.

4.4 Conclusions

In this paper, we investigated the formation mechanism of pillar-like structure from aspects of solvent and additive. The pillar-like structure formation mechanism is as follows: During the phase inversion process, PVDF segments in the copolymer PVDF-g-PEGMA physically combine with the PVDF backbone material while hydrophilic PEGMA segments expand on the surface. Once NMP exists in the casting solution, PEGMA segments have more time to migrate to the surface during phase inversion process. These PEGMA segments on the surface repelled each other on the membrane surface and form the pillar-like structure.

To determine which cast membrane is best suited for industrial production, we used a target plot. The membrane properties and performance were ranked from level 1 (the innermost ring on the target) to level 10 (the outermost ring); level 1 indicates ideal properties. Then the points corresponding to the rankings were connected. Shapes corresponding to membranes with better performance are located closer to the central point. Surface porosity, contact angle, roughness, pure water flux, pure water flux after physical cleaning, flux recovery rate, and SA removal efficiency were used as parameters in our target plot. A detailed scale parameter setting can be found in Table 4.6, Table 4.7 and Table 4.8. To simplify the selection process, we averaged the values of the seven parameters with the same weight and selected the membrane with the lowest average value. Other users can weight each parameter for their own purposes. Figure 4.12 shows the target plot of our cast membranes. Based on the average parameter values, membrane c had the best performance.

Table 4.6 Level setting for target plot.

	L1	L2	L3	L4	L5	L6	L7	L8	L9	L10
Porosity (%)	18+	16-18	14-16	12-14	10-12	8-10	6-8	4-6	2-4	0-2
Contact Angle (°)	0-10	10-20	20-30	30-40	40-50	50-60	60-70	70-80	80-90	90+
Roughness (nm)	0-5	5-10	10-15	15-20	20-25	25-30	30-35	35-40	40-45	45+
Pure Water flux ($L/m^2/h$)	2700+	2400-2700	2100-2400	1800-2100	1500-1800	1200-1500	900-1200	600-900	300-600	0-300
Flux Recovery Rate (%)	90-100	80-90	70-80	60-70	50-60	40-50	30-40	20-30	10-20	0-10
SA Removal Efficiency (%)	90-100	80-90	70-80	60-70	50-60	40-50	30-40	20-30	10-20	0-10

Table 4.7 Membrane performance data from the test.

	Surface Porosity (%)	Contact Angle (°)	Roughness (nm)	Pure Water Flux (L/m^2/h)	Pure Water Flux After Physical Cleaning (L/m^2/h)	Flux Recovery Ratio (%)	SA Removal Efficiency (%)
b. M P-g-P D/T = 7/3	5.67	69.4	27.5	515	184	36	87
c. M P-g-P DMF	14.69	72.3	27.5	2997	1658	55	89
d. M P-g-P NMP	4.46	74.2	32.7	1309	619	47	94
g. P P-g-P NMP FP	3.15	67.6	33.1	1104	826	75	94
i. P P-g-P DMF FN FP	7.00	75.3	38.1	4510	1148	25	91

Table 4.8 Converted membrane performance data in target plot scale.

	Surface Porosity	Contact Angle	Roughness	Pure Water Flux	Pure Water Flux After Physical Cleaning	Flux Recovery Ratio	SA Removal Efficiency	Average Value
b. M P-g-P D/T = 7/3	8	7	6	9	10	7	2	7.0
c. M P-g-P DMF	3	8	6	1	5	5	2	4.3
d. M P-g-P NMP	8	8	7	6	8	6	1	6.3
g. P P-g-P NMP FP	9	7	7	7	8	3	1	6.0
i. P P-g-P DMF FN FP	7	8	8	1	7	8	1	5.7
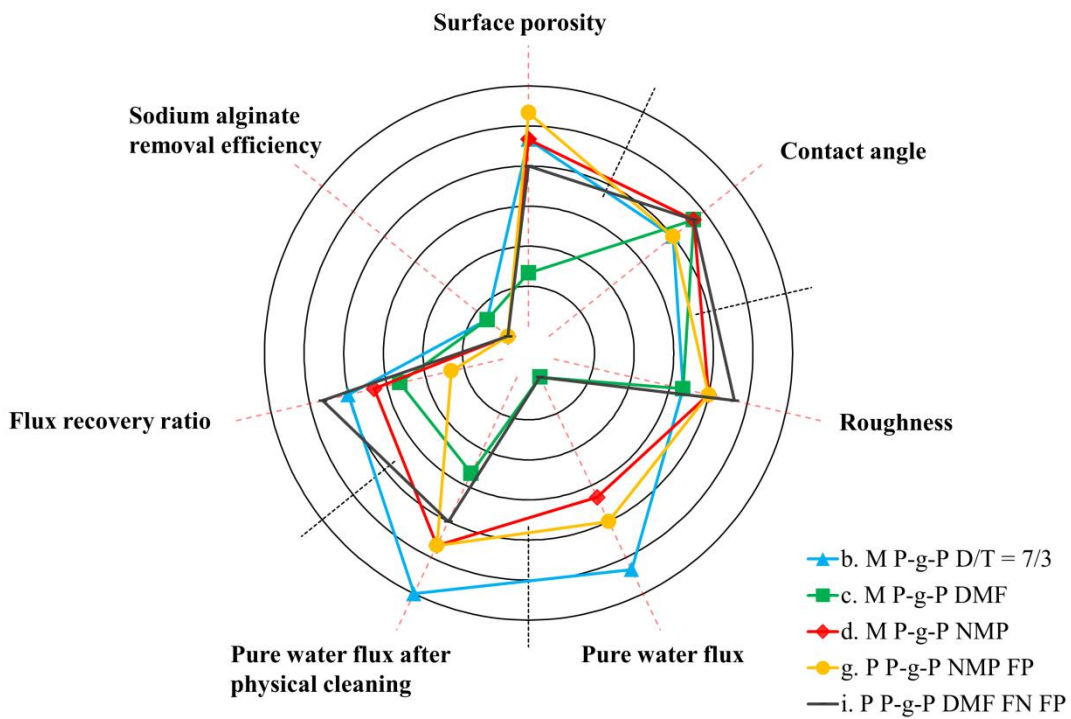
Figure 4.12. Target plot for comparing the properties and performance of cast membranes.

The cast membrane c had a pure water flux of 2173 $L/m^2/h/bar$ under a constant pressure of 0.14 MPa and an SA removal efficiency of 89%. After simple physical cleaning, its membrane flux recovery rate was 55% with a flux of 1195 $L/m^2/h/bar$. Both the pure water flux and the recovery flux are much higher than those of other PVDF membranes described in the literature.

CHAPTER 5

THE EFFECT OF PEGMA DOSE ON HIGH PERFORMANCE

ULTRAFILTRATION PVDF MEMBRANE

5.1 Introduction

Membrane technologies have been increasingly applied in water and wastewater treatment plants since the last few decades because of the technological improvement and cost reduction. Compared to conventional treatment plants, membrane plants require smaller land use, produce fewer by-products, produce effluent water at consistent and high quality (Baker 1991). According to Freedonia Group's research, the global membrane filtration market will reach $25 billion by 2017, with an 9.2 percent annual growth rate (Ng August 7, 2013).

One major challenge of the membrane technology is fouling during the filtration process. Membrane fouling is an undesirable phenomenon since it reduces the efficiency the of membrane filtration process. The cause of membrane's susceptibility to fouling is the hydrophobic property of membrane bone material. Therefore, in order to minimize membrane fouling, several techniques have been used to improve the fouling resistance of membranes. These techniques can be classified into coating, surface polymerization, adsorption and blending modification (Zhao, Zheng et al. 2012). Blending modification blends amphiphilic graft copolymers with the membrane bone material in the casting solution during the membrane casting process. This type of copolymer has good compatibility with the membrane bone material and improves membrane hydrophilicity to increase fouling resistance. The hydrophilic segments of amphiphilic copolymer tend

117

to expand on the membrane surface during the phase inversion process, while the hydrophobic segments physically combine with the membrane bone material. Several studies show that amphiphilic copolymers can improve the fouling resistance of membranes. For instance, polyacrylonitrile-graft-poly(ethylene oxide) (PAN-g-PEO) and polysulfone-graft-poly(ethylene glycol) (PSF-g-PEG) have been used to improve the hydrophilicity of PAN membrane and PSF membrane, respectively (Park, Acar et al. 2006, Kang, Asatekin et al. 2007).

Among the common membrane materials such as cellulose acetates (CA), polyamide (PA), polyvinylidene fluoride (PVDF), polytetrafluoroethylene (PTFE), polyethersulfone (PES), polypropylene (PP) and polysulfone (PSF), PVDF has attracted much interest due to its good physical and chemical properties such as high resistance to acids, bases, solvents, and chlorine (Yeow, Field et al. 2002, Tan, Tan et al. 2006, Chakrabarty, Ghoshal et al. 2008, Yu, Cheng et al. 2013, Zhang, Wang et al. 2013).

One method to improve the hydrophilicity of PVDF membrane is blending with amphiphilic copolymers. Several studies have shown that the amphiphilic copolymer of poly(vinylidene fluoride) (PVDF) backbone grafted with poly(ethylene glycol) methyl ether methacrylate (PEGMA) (PVDF-g-PEGMA) can improve the hydrophilicity of PVDF membranes (Hester, Banerjee et al. 2002, Asatekin, Menniti et al. 2006, Liu, Chen et al. 2006).

The amount of polymer or copolymer additive has a significant impact on membrane properties and performance (Ma, Shi et al. 2011). However, there is little research on the effect of hydrophilic PEGMA additive to the properties and performance of membranes. In this study, we investigate the influence of PEGMA dose on PVDF membranes. We prepare PVDF membranes with different amounts of PEGMA in casting solutions and then compare the performances of these prepared membranes.

5.2 Experimental

5.2.1 Materials

Poly(vinylidene fluoride) (PVDF, Mw ~ 534,000 g/mol), Poly(ethylene glycol) methyl ether methacrylate (PEGMA, Mn = 475 g/mol), copper(I) chloride (CuCl), 4-4′-dimethyl-2-2′-dipyridyl (DMDP), silicone oil, and N,N-Dimethylformamide (DMF) were purchased from Sigma-Aldrich. All solvents and chemicals were reagent grade, and all reagents were used as received.

5.2.2 Model foulant

Sodium alginate (SA) was purchased from Sigma-Aldrich (St. Louis, MO) and used as the model for extracellular polymeric substances (EPS) (Katsoufidou, Yiantsios et al. 2008). Stock solution of sodium alginate was prepared in flask by adding sodium alginate to deionized water and mixing until completely dissolved. The stock solution of 2 g/L sodium alginate was stored at 4°C for future use. In all fouling experiments, the sodium alginate concentrations were determined using a Shimadzu total organic carbon (TOC) analyzer (Shimadzu Co.).

5.2.3 Preparation of PVDF membranes

The step to synthesize the copolymer PVDF-g-PEGMA was similar to those previously published (Hashim, Liu et al. 2009). The detailed characterization of copolymer PVDF-g-PEGMA can be found from other literature (Akthakul, Salinaro et al. 2004).

Membranes were prepared from casting solutions containing PVDF, PVDF-g-PEGMA copolymer mixture additives and DMF according to the compositions listed in Table 5.1. The concentration of PVDF bone materials was kept at 18 wt% throughout all the experiments.

The casting solutions were prepared in 125 mL conical flasks while heating at 80 °C and stirring at 500 rpm using digital stirring hot plates (Corning, MA). After 24 hours of heating and mixing, the casting solutions were degassed without mixing for at least 2 hours until no gas bubbles were observed. A doctor blade (Universal blade applicator, Paul N. Gardner Company, Inc., Pompano Beach, FL) with a gate height of 200 μm was used to cast the solution on a first-grade surface optical mirror. The mirror was left in the air for 10 s before it was immersed in a 25°C coagulation bath which contains deionized water. After 48 hours in the coagulation bath, the membranes were then air-dried for 24 hours.

Table 5.1 The composition of the casting solutions.

Membrane ID	PVDF (g)	DMF (g)	Additive (g)	PEGMA (mL)
Pure PVDF	9	41	-	-
PVDF-0 PEGMA	9	39.65	1.35	-
PVDF-1.8 PEGMA	9	39.65	1.35	1.8
PVDF-3.6 PEGMA	9	39.65	1.35	3.6

5.2.4 XPS analysis

The X-ray photoelectron spectroscopy (XPS, Thermo K-Alpha XPS system) was used to study the near-surface compositions of PVDF membrane to a depth of less than 5 nm. Survey spectra were collected over 0-1350 eV, and high-resolution scan with a resolution of 0.1 eV was also collected.

5.2.5 Liquid sessile drop contact angle analysis

Liquid sessile drop dynamic contact angle measurements on the membrane were performed at 25 °C using a Ramé-hart Model 250 goniometer (Ramé-hart Instrument Co, Succasunna, USA). The dynamic water contact angle was measured by placing 2 µL of deionized water on the dry membrane surface. The average of at least five independent measurements at different sites of one membrane was used.

5.2.6 Membrane morphology

The morphology of the prepared membrane surface was examined with scanning electron microscopy (SEM) (Zeiss Ultra 60; Carl Zeiss NTS, LLC North America). These membranes were positioned on stubs with carbon dots, and sputter coated with a ~2 nm gold layer. An acceleration voltage of 5 kV was used to examine the coated samples at different magnifications. Average pore diameter ($D_{average}$), maximum observed pore diameter (D_{max}), and surface porosity (ε) were obtained from SEM images using Image-Pro Plus7.0 (Media Cybernetics, Silver Spring, MD). The surface porosity is defined as the ratio between the total areas enclosed by pores to that of the entire area.

5.2.7 Determination of the cloud point

Cloud point data were measured by the titration method. The solution to be titrated was prepared in a sealable bottle and kept stirring at 60 °C. Non-solvent (DI water) was slowly added into the solution until the polymer solution became irreversibly turbid as detected visually (Xu, Zhang et al. 2014).

5.2.8 AFM analysis

The surface roughness of casted membranes was measured by using an Agilent 5500 AFM (Agilent Technologies, Inc., US). Membrane samples were fixed on a specimen holder and 5 μm × 5 μm areas were scanned in the acoustic alternating current (AC) tapping mode. At least five replicates were performed for each membrane sample.

5.2.9 Flux performance

A dead-end filtration cell (Millipore) with an effective membrane area of 28.7 cm^2 was used in this research. The filtration cell had a cell volume of 200 mL, and it was connected with a 5L dispensing vessel. All the filtration experiments were performed under constant pressure of 0.14 MPa (20 psi) by applying compressed nitrogen gas. The permeate weight was measured and collected every minute by using Collect 6.1 software and an Ohaus Adventurer Pro Balance AV8101.

The experimental procedures used for each fouling test were as follows. First, the membrane was soaked in DI water for 48 hours before the test. Then the membrane was compacted using ~ 4 liters of DI water under 0.14 MPa pressure. After filtrating the DI water, the membrane was conditioned by passing through a 10 mM NaCl solution with a filtration volume of 4 liters.

For the fouling test, the feed solution was added into the filtration cell, and each fouling test ran at least for 6 hours. A stirring plate (PC-410D, Corning, MA) was used to minimize concentration polarization during the filtration test. A solution containing 20 mg/L of sodium alginate (SA) and 10mM NaCl was used for the fouling test. At the end of the fouling test, physical cleaning was applied to clean the surface of the membrane. The fouled membrane was rinsed with DI water for 1 min. In order to determine the recovery flux after physical cleaning, the membrane was exposed to foulant-free electrolyte solution according to the standard conditioning practice (Kang, Asatekin et al. 2007).

5.3 Results and discussions

5.3.1 XPS analysis

The near-surface compositions of prepared PVDF membranes are shown in Table 5.2. XPS analysis was conducted on the active layer of the membrane. The oxygen content of membrane indicates the migration level of PEGMA. As more PEGMA migrate to the surface, higher oxygen content should be observed. Based on the results, as more PEGMA is added into the casting solution, more PEGMA have migrated to the surface during phase inversion.

Table 5.2 The surface elemental compositions of PVDF membranes.

membrane ID	F (%)	C (%)	O (%)
PVDF-0 PEGMA	36.56	56.79	6.65
PVDF-1.8 PEGMA	35.97	57.26	6.76
PVDF-3.6 PEGMA	35.18	57.63	7.19

5.3.2 Contact angle measurement

The hydrophilicity of prepared PVDF membranes was characterized by contact angle measurement. Surface roughness, heterogeneity and capillary forces within pores can affect contact angle measurement (Taniguchi and Belfort 2002). However, static contact angle and dynamic contact angle can be used to compare the relative hydrophilicity of each membrane. A smaller initial contact angle and a quicker decrease rate of dynamic contact angle indicate better hydrophilicity.

The dynamic contact angle measurements are presented in Figure 5.1. The initial contact angle of pure PVDF membrane, PVDF-0 PEGMA, PVDF-1.8 PEGMA and PVDF-3.6 PEGMA are 90 °, 62 °, 57 ° and 56 °, respectively. The results demonstrate that prepared membranes become more hydrophilic as more PEGMA is added into the casting solution.
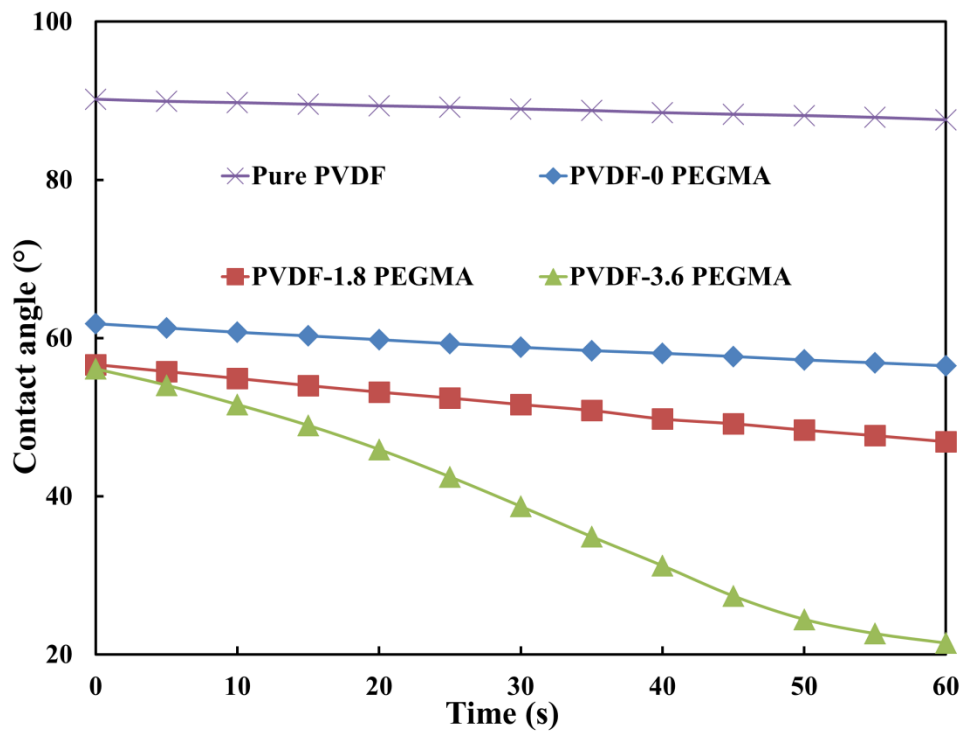
Figure 5.1. Changes in contact angle with time.

5.3.3 Membrane morphology

SEM images of prepared PVDF membranes are shown in Figure 5.2. The Image Pro Plus software is used to characterize membrane surface property. The statistics of pore size distribution, including average pore diameter ($D_{average}$), maximum pore diameter (D_{max}), and surface porosity (ε), are summarized in Table 5.3. The pure PVDF membrane has an average pore size of 6 nm, maximum pore size of 23 nm and surface porosity of 0.05%. Both the maximum pore size and the surface porosity of prepared PVDF membranes decreased as more PEGMA was added into the casting solution. The PVDF-0 PEGMA has an average pore size of 37 nm and surface porosity of 6.40%. The PVDF-1.8 PEGMA has an average pore size of 37 nm and surface porosity of 4.58%. The PVDF-3.6 PEGMA has an average pore size of 29 nm and surface porosity of 0.65%. The difference of surface porosity and pore size can be explained by the rate of phase inversion process. Based on the results of cloud point test, the casting solutions of PVDF-0 PEGMA, PVDF-1.8 PEGMA and PVDF-3.6 PEGMA need 17.4 wt%, 16.1 wt% and 13.6 wt% of non-solvent (DI water) to reach the cloud point, respectively. The results of cloud point test show that the casting solution of PVDF-3.6 PEGMA was the closest to the binodal curve, followed by PVDF-1.8 PEGMA and then PVDF-0 PEGMA. In other words, because of the shift of binodal boundary, the nonsolvent advances into the polymer solution film more slowly, while the vitrification front moves more quickly relative to the nonsolvent front. This phenomenon causes the decrease in pore size and surface porosity (Tiraferri, Yip et al. 2011).
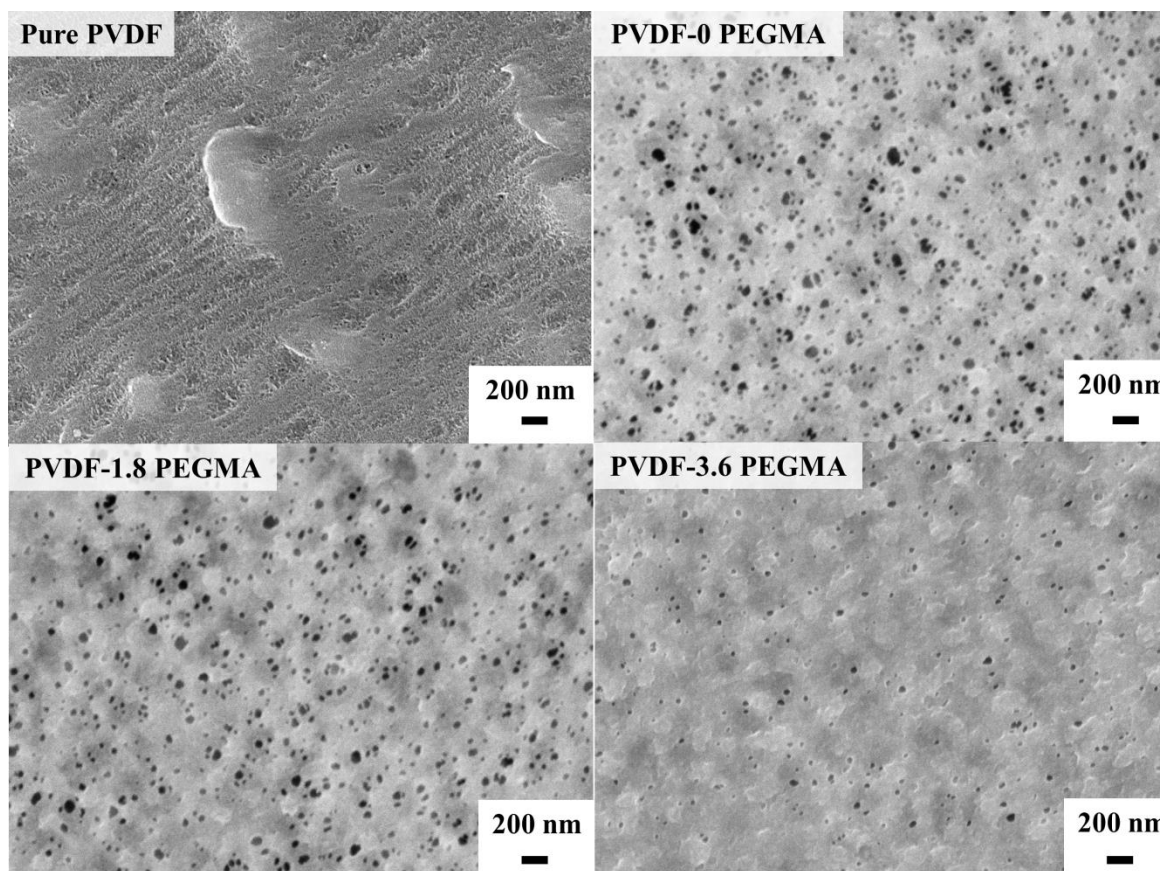
Figure 5.2. SEM images prepared PVDF membrane surface.

Table 5.3 Summary of pore size distribution statistics.

Membrane ID	$D_{average}$ (nm)	D_{max} (nm)	ε (%)
Pure PVDF	6	23	0.05
PVDF-0 PEGMA	37	115	6.40
PVDF-1.8 PEGMA	37	99	4.58
PVDF-3.6 PEGMA	29	56	0.65

5.3.4 Roughness

The measured root mean square (RMS) roughness of pure PVDF membrane is 12.5 ± 0.7 nm. The surface roughnesses of prepared PVDF membranes increase as more PEGMA is added to the casting solution. . The RMS of fabricated PVDF membrane with 0 mL PEGMA, 1.8 mL PEGMA and 3.6 mL PEGMA are 6.2 ± 1.8 nm, 8.8 ± 1.3 nm and 11.3 ± 2.0 nm, respectively.

5.3.5 Membrane permeate flux and removal efficiency

As shown in Figure 5.3 and Table 5.4, the initial fluxes of PVDF-0 PEGMA, PVDF-1.8 PEGMA and PVDF-3.6 PEGMA for DI water are 3519 L/m^2/h/bar, 985 L/m^2/h/bar and 518 L/m^2/h/bar, respectively. No permeate is collected for pure PVDF membrane under 0.14 MPa. The highest DI water flux for a PVDF membrane found in literature is 116 L/m^2/h/bar (Hashim, Liu et al. 2009), which is much smaller than our results. Pure water flux decreases and flux recovery ratio increases as more PEGMA is added into the casting solution. These results are consistent with what we observed from SEM images. As more PEGMA is added into the casting solutions, both pore size and surface porosity decrease.

The removal ratio of SA for PVDF-0 PEGMA, PVDF-1.8 PEGMA and PVDF-3.6 PEGMA are 80%, 85% and 85%, respectively.

After filtering sodium alginate, one minute of physical cleaning is used to clean the membrane surface. The flux recovery ratio for PVDF-0 PEGMA, PVDF-1.8 PEGMA and PVDF-3.6 PEGMA are 30%, 90% and 96%, respectively. The result of flux recovery ratio is consistent with membrane hydrophilicity results, as membrane with better hydrophilicity should have better fouling resistance.
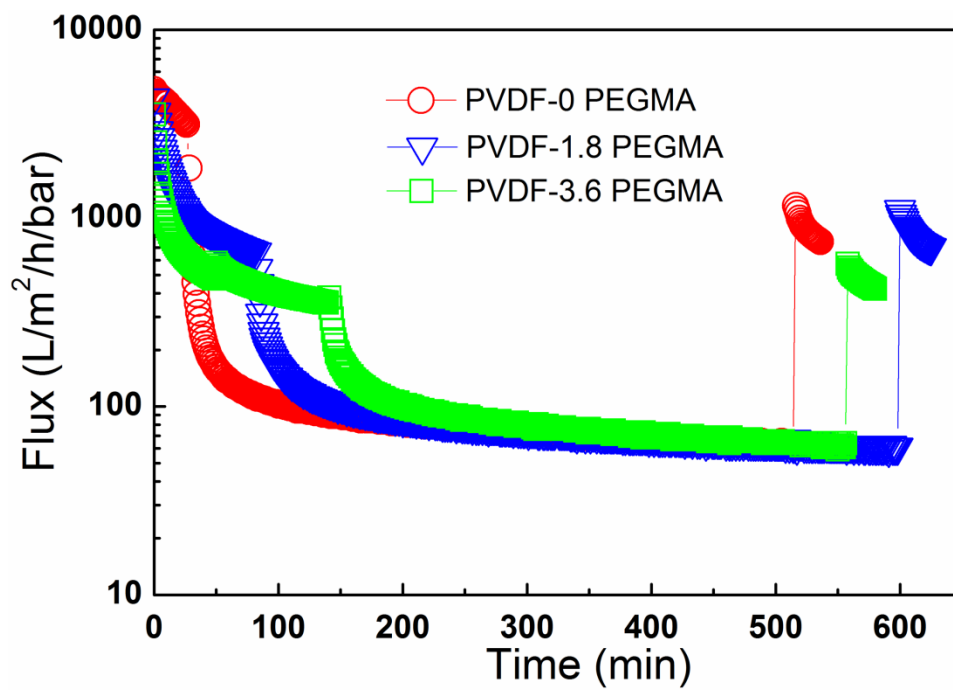
Figure 5.3. Flux performance of PVDF membranes.

Table 5.4 Flux performance of PVDF membranes

Membrane ID	Pure water flux (L/m^2/h/bar)	Recovery flux (L/m^2/h/bar)	Flux recovery ratio (%)	SA rejection ratio (%)
PVDF-0 PEGMA	3519	1062	30	80
PVDF-1.8 PEGMA	985	887	90	85
PVDF-3.6 PEGMA	518	498	96	85

5.4 Conclusions

In this part, we investigated the influence of PEGMA dose on PVDF membrane, with the main goal to increase the anti-fouling property of PVDF membranes. Our major findings are listed as follows:

- The dose of PEGMA in the casting solution affects the hydrophilicity, roughness and surface porosity of PVDF membrane. As more PEGMA is used in casting solution, the hydrophilicity and roughness of prepared PVDF membrane increases while surface porosity decreases;

- Pure water flux decreases as more PEGMA is used, which results in decreased membrane surface porosity; the pure water flux of fabricated PVDF membrane with 0 mL PEGMA, 1.8 mL PEGMA and 3.6 mL PEGMA are 3519 $L/m^2/h/bar$, 985 $L/m^2/h/bar$ and 518 $L/m^2/h/bar$, respectively;

- The flux recovery ratio of fabricated PVDF membrane with 0 mL PEGMA, 1.8 mL PEGMA and 3.6 mL PEGMA are 30%, 90% and 96%, respectively;

- The TOC (sodium alginate) rejection ratio of fabricated PVDF membrane with 0 mL PEGMA, 1.8 mL PEGMA and 3.6 mL PEGMA are 80%, 85% and 85%, respectively.

CHAPTER 6

CONCLUSIONS AND FUTURE WORK

6.1 Conclusions

To better promote the large-scale implementation of membrane technologies, it is vital to overcome the challenges faced by current membranes. For current ultrafiltration membranes, membrane lifetime and membrane fouling are two major challenges. During the membrane filtration process, membrane fouling caused by natural organic matter is an inevitable phenomenon, and physical cleaning or chemical cleaning have to be used to recover the performance of membrane. As a result, these cleaning processes shorten the lifetime of membranes. Therefore, the motivation of this study is to overcome two major challenges faced by ultrafiltration membrane with a simple and cost effective method to facilitate future large scale production. We choose PVC and PVDF materials as backbone materials because of their outstanding physical and chemical properties. And we use the phase inversion method to synthesize our membranes because this method is simple and easy to be applied for large scale production.

The PVC and PVDF membranes were synthesized via the phase inversion method by using amphiphilic copolymer to improve hydrophilicity. The properties of synthesized membranes were characterized from various aspects: surface morphology was characterized by SEM, chemical composition was characterized by FTIR-ATR and XPS, hydrophilicity was characterized by contact angle, and surface roughness was characterized by AFM.

This study presents one of the first syntheses of unique pillar-like and defect-free PVDF ultrafiltration membranes with high flux. Furthermore, the forming mechanism of pillar-like structure was investigated, and the influence of PEGMA was also studied.

The key findings of this study are:

A. For PVC membranes: With the increase of Pluronic F 127 content from 0 wt% to 10 wt%, the oxygen content on the membrane surface increased and then reached an asymptote when 8 wt% or greater Pluronic F 127 was used; the pore size and pore density both decreased; the membrane surface became more hydrophilic as indicated by lower contact angles; and the flux declined by 30% when Pluronic F 127 reached 10 wt%.

B. High performance PVDF membranes with unique pillar-like structures are synthesized by adding PVDF-g-PEGMA in the casting solutions. The unique pillar-like structures ensure high surface porosity and defect free surface property.

C. I investigated the formation mechanism of pillar-like structure from the aspects of solvent and additive. During the phase inversion process, PVDF segments in the copolymer PVDF-g-PEGMA physically combine with the PVDF backbone material while hydrophilic PEGMA segments expand on the surface. Once NMP exists in the casting solution, PEGMA segments have more time to migrate to the surface during the phase inversion process. These PEGMA segments on the surface repelled each other on the membrane surface and form the pillar-like structure.

D. The influence of PEGMA in the casting solution was studied. The dose of PEGMA in the casting solution affects the hydrophilicity, roughness and surface porosity of PVDF membrane. As more PEGMA is used in casting solution, the hydrophilicity and roughness of the prepared PVDF membrane increases while surface porosity decreases, and pure water flux.

6.2 Future work

Based on the results from this study, I recommend the following directions for future studies.

A. Further research could be done on the influence of the coagulation bath. In the current research, DI water was used for coagulation bath in order to minimize the variables. However, coagulation bath is another important factor that can influence the formation of membrane. Therefore, parameters such as the composition of the coagulation bath, and the temperature of the coagulation bath can be studied to improve the performance of current.

B. Improvement on the mechanical strength of PVDF membranes can be done to prevent the dramatic drop of the initial flux. The flux of synthesized PVDF membrane dropped by nearly half of its initial value during the first 20 minutes test. This phenomenon might be caused by the compression of the membrane. Therefore, improving membrane's mechanical strength might help to increase membrane flux.

C. Synthesis of PVC and PVDF hollow fiber membranes based on the current

casting composition and condition is recommended. Although it is more

complicated to synthesize hollow fiber membrane than flat membrane since there

are more variables involved (e.g., bore fluid, air gap,etc), hollow fiber membrane

has a wider range of applications than flat membrane for large-scale facilities.

REFERENCES

Adout, A., S. Kang, A. Asatekin, A. M. Mayes and M. Elimelech (2010). "Ultrafiltration Membranes Incorporating Amphiphilic Comb Copolymer Additives Prevent Irreversible Adhesion of Bacteria." Environ. Sci. Technol. **44**(7): 2406-2411.

Adout, A., S. Kang, A. Asatekin, A. M. Mayes and M. Elimelech (2010). "Ultrafiltration Membranes Incorporating Amphiphilic Comb Copolymer Additives Prevent Irreversible Adhesion of Bacteria." Environmental Science & Technology **44**(7): 2406-2411.

Akthakul, A., R. F. Salinaro and A. M. Mayes (2004). "Antifouling polymer membranes with subnanometer size selectivity." Macromolecules **37**(20): 7663-7668.

Alexandridis, P., V. Athanassiou, S. Fukuda and T. A. Hatton (1994). "Surface-activity of poly(ethylene oxide)-block-poly(propylene oxide)-block-poly(ethylene oxide) copolymers." Langmuir **10**(8): 2604-2612.

Ang, W. S., S. Y. Lee and M. Elimelech (2006). "Chemical and physical aspects of cleaning of organic-fouled reverse osmosis membranes." Journal of Membrane Science **272**(1-2): 198-210.

Asatekin, A., S. Kang, M. Elimelech and A. Mayes (2007). "Anti-fouling ultrafiltration membranes containing polyacrylonitrile-graft-poly(ethylene oxide) comb copolymer additives." Journal of Membrane Science **298**(1-2): 136-146.

Asatekin, A., S. Kang, M. Elimelech and A. M. Mayes (2007). "Anti-fouling ultrafiltration membranes containing polyacrylonitrile-graft-poly (ethylene oxide) comb copolymer additives." Journal of Membrane Science **298**(1-2): 136-146.

Asatekin, A., A. Menniti, S. Kang, M. Elimelech, E. Morgenroth and A. M. Mayes (2006). "Antifouling nanofiltration membranes for membrane bioreactors from self-assembling graft copolymers." Journal of Membrane Science **285**(1-2): 81-89.

Auschra, C. and R. Stadler (1993). "Synthesis of block copolymers with poly(methyl methacrylate) - P(B-b-MMA), P(EB-b-MMA), P(S-b-B-b-MMA) and P(S-b-EB-b-MMA)." Polymer Bulletin **30**(3): 257-264.

Baker, J. S. and L. Y. Dudley (1998). "Biofouling in membrane systems - A review." Desalination **118**(1-3): 81-89.

Baker, R. (2012). Membrane technology and applications, John Wiley & Sons.

Baker, R. W. (1991). "Membrane separation systems recent developments and future directions." from http://www.knovel.com/knovel2/Toc.jsp?BookID=312.

Bartels, C. R., M. Wilf, K. Andes and J. Iong (2005). "Design considerations for wastewater treatment by reverse osmosis." Water Science and Technology **51**(6-7): 473-482.

Bates, F. S. and G. H. Fredrickson (1999). "Block copolymers - Designer soft materials." Physics Today **52**(2): 32-38.

Bellona, C. and J. E. Drewes (2007). "Viability of a low-pressure nanofilter in treating recycled water for water reuse applications: A pilot-scale study." Water Research **41**(17): 3948-3958.

Brindle, K. and T. Stephenson (1996). "The application of membrane biological reactors for the treatment of wastewaters." Biotechnology and Bioengineering **49**(6): 601-610.

Canal, J. P., T. Ramnial, L. D. Langlois, C. D. Abernethy and J. A. C. Clyburne (2008). "A three-step laboratory sequence to prepare a carbene complex of silver(I) chloride." Journal of Chemical Education **85**(3): 416-419.

Chakrabarty, B., A. K. Ghoshal and A. K. Purkait (2008). "Preparation, characterization and performance studies of polysulfone membranes using PVP as an additive." Journal of Membrane Science **315**(1-2): 36-47.

Chang, Y., Y. J. Shih, C. Y. Ko, J. F. Jhong, Y. L. Liu and T. C. Wei (2011). "Hemocompatibility of Poly(vinylidene fluoride) Membrane Grafted with Network-Like and Brush-Like Antifouling Layer Controlled via Plasma-Induced Surface PEGylation." Langmuir **27**(9): 5445-5455.

Chemicals, D. (1992). Material Safety Data Sheet, Tetrahydrofuran, Mar.

Chen, K. L., S. E. Mylon and M. Elimelech (2006). "Aggregation kinetics of alginate-coated hematite nanoparticles in monovalent and divalent electrolytes." Environmental Science & Technology **40**(5): 1516-1523.

Chen, Y. W., D. M. Liu, Q. L. Deng, X. H. He and X. F. Wang (2006). "Atom transfer radical polymerization directly from poly(vinylidene fluoride): Surface and antifouling properties." Journal of Polymer Science Part a-Polymer Chemistry **44**(11): 3434-3443.

Chen, Y. W., L. Ying, W. H. Yu, E. T. Kang and K. G. Neoh (2003). "Poly(vinylidene fluoride) with grafted poly(ethylene glycol) side chains via the RAFT-mediated process and pore size control of the copolymer membranes." Macromolecules **36**(25): 9451-9457.

Chiag, Y.-C., Y. Chang, W.-Y. Chen and R.-c. Ruaan (2012). "Biofouling Resistance of Ultrafiltration Membranes Controlled by Surface Self-Assembled Coating with PEGylated Copolymers." Langmuir **28**(2): 1399-1407.

Childress, A. E. and M. Elimelech (2000). "Relating nanofiltration membrane performance to membrane charge (electrokinetic) characteristics." Environmental Science & Technology **34**(17): 3710-3716.

Choi, H., Y. Kwon, Y. Jung, S. Hong and T. Tak (2012). "Preparation and Characterization of Antifouling Poly(vinylidene fluoride) Blended Membranes." Journal of Applied Polymer Science **123**(1): 286-291.

Coetzee, J. F. and T. H. Chang (1985). "Purification of Solvents for Electroanalysis - Tetrahydrofuran and Dioxane." Pure and Applied Chemistry **57**(4): 633-638.

Darvishmanesh, S., F. Tasselli, J. C. Jansen, E. Tocci, F. Bazzarelli, P. Bernardo, P. Luis, J. Degreve, E. Drioli and B. Van der Bruggen (2011). "Preparation of solvent stable polyphenylsulfone hollow fiber nanofiltration membranes." Journal of Membrane Science **384**(1-2): 89-96.

Daufin, G., J.-P. Escudier, H. Carrere, S. Berot, L. Fillaudeau and M. Decloux (2001). "Recent and emerging applications of membrane processes in the food and dairy industry." Food and Bioproducts Processing **79**(2): 89-102.

de Bernardez, L. S., J. Ferron, E. C. Goldberg and R. H. Buitrago (1984). "The effect of surface roughness on XPS and AES." Surface Science **139**(2-3): 541-548.

Delgado, C., G. E. Francis and D. Fisher (1992). "The uses and porperties of PEG-linked proteins." Critical Reviews in Therapeutic Drug Carrier Systems **9**(3-4): 249-304.

Deshmukh, S. P. and K. Li (1998). "Effect of ethanol composition in water coagulation bath on morphology of PVDF hollow fibre membranes." Journal of Membrane Science **150**(1): 75-85.

Fontananova, E., J. C. Jansen, A. Cristiano, E. Curcio and E. Drioli (2006). "Effect of additives in the casting solution on the formation of PVDF membranes." Desalination **192**(1-3): 190-197.

Frenzel, I., D. F. Stamatialis and M. Wessling (2006). "Water recycling from mixed chromic acid waste effluents by membrane technology." Separation and Purification Technology **49**(1): 76-83.

Frigge, M., D. C. Hoaglin and B. Iglewicz (1989). "SOME IMPLEMENTATIONS OF THE BOXPLOT." American Statistician **43**(1): 50-54.

Gin, D. L. and R. D. Noble (2011). "Designing the Next Generation of Chemical Separation Membranes." Science **332**(6030): 674-676.

Goosen, M. F. A., S. S. Sablani, H. Ai-Hinai, S. Ai-Obeidani, R. Al-Belushi and D. Jackson (2004). "Fouling of reverse osmosis and ultrafiltration membranes: A critical review." Separation Science and Technology **39**(10): 2261-2297.

Gregorio, R. (2006). "Determination of the alpha, beta, and gamma crystalline phases of poly(vinylidene fluoride) films prepared at different conditions." Journal of Applied Polymer Science **100**(4): 3272-3279.

Hamilton-Brown, P., T. Gengenbach, H. J. Griesser and L. Meagher (2009). "End Terminal, Poly(ethylene oxide) Graft Layers: Surface Forces and Protein Adsorption." Langmuir **25**(16): 9149–9156.

Hashim, N. A., F. Liu, M. R. M. Abed and K. Li (2012). "Chemistry in spinning solutions: Surface modification of PVDF membranes during phase inversion." Journal of Membrane Science **415**: 399-411.

Hashim, N. A., F. Liu and K. Li (2009). "A simplified method for preparation of hydrophilic PVDF membranes from an amphiphilic graft copolymer." Journal of Membrane Science **345**(1-2): 134-141.

Herminghaus, S. (2000). "Roughness-induced non-wetting." Europhysics Letters **52**(2): 165-170.

Herzberg, M., S. Kang and M. Elimelech (2009). "Role of Extracellular Polymeric Substances (EPS) in Biofouling of Reverse Osmosis Membranes." Environmental Science & Technology **43**(12): 4393-4398.

Hester, J. F., P. Banerjee and A. M. Mayes (1999). "Preparation of protein-resistant surfaces on poly(vinylidene fluoride) membranes via surface segregation." Macromolecules **32**(5): 1643-1650.

Hester, J. F., P. Banerjee, Y. Y. Won, A. Akthakul, M. H. Acar and A. M. Mayes (2002). "ATRP of amphiphilic graft copolymers based on PVDF and their use as membrane additives." Macromolecules **35**(20): 7652-7661.

Hester, J. F. and A. M. Mayes (2002). "Design and performance of foul-resistant poly(vinylidene fluoride) membranes prepared in a single-step by surface segregation." Journal of Membrane Science **202**(1-2): 119-135.

Huang, H., K. Schwab and J. G. Jacangelo (2009). "Pretreatment for Low Pressure Membranes in Water Treatment: A Review." Environmental Science & Technology **43**(9): 3011-3019.

Jackson, E. A. and M. A. Hillmyer (2010). "Nanoporous membranes derived from block copolymers: from drug delivery to water filtration." Acs Nano **4**(7): 3548-3553.

Judd, S. (2008). "The status of membrane bioreactor technology." Trends in Biotechnology **26**(2): 109-116.

Judd, S. and C. Judd (2011). "The MBR Book Principles and Applications of Membrane Bioreactors for Water and Wastewater Treatment Preface." Mbr Book: Principles and Applications of Membrane Bioreactors for Water and Wastewater Treatment, 2nd Edition: Vii-X.

Kang, M., R. Jung, H. S. Kim and H. J. Jin (2008). "Preparation of superhydrophobic polystyrene membranes by electrospinning." Colloids and Surfaces a-Physicochemical and Engineering Aspects **313**: 411-414.

Kang, S., A. Asatekin, A. Mayes and M. Elimelech (2007). "Protein antifouling mechanisms of PAN UF membranes incorporating PAN-g-PEO additive." Journal of Membrane Science **296**(1-2): 42-50.

Kang, S., A. Asatekin, A. M. Mayes and M. Elimelech (2007). "Protein antifouling mechanisms of PAN UF membranes incorporating PAN-g-PEO additive." Journal of Membrane Science **296**(1-2): 42-50.

Kato, M., M. Kamigaito, M. Sawamoto and T. Higashimura (1995). "Polymerization of methyl methacrylate with the carbon tetrachloride/dichlorotris-(triphenylphosphine)ruthenium(II) methylaluminum bis(2,6-di-tert-butylphenoxide) initiating system - possibility of living radical polymerization." Macromolecules **28**(5): 1721-1723.

Katsoufidou, K., S. G. Yiantsios and A. J. Karabelas (2007). "Experimental study of ultrafiltration membrane fouling by sodium alginate and flux recovery by backwashing." Journal of Membrane Science **300**(1-2): 137-146.

Katsoufidou, K., S. G. Yiantsios and A. J. Karabelas (2008). "An experimental study of UF membrane fouling by humic acid and sodium alginate solutions: the effect of backwashing on flux recovery." Desalination **220**(1–3): 214-227.

Kim, M. S., S. J. Lee, J. U. Kang and K. J. Bae (2005). "Preparations of polypropylene membrane with high porosity in supercritical CO2 and its application for PEMFC." Journal of Industrial and Engineering Chemistry **11**(2): 187-193.

Kosuri, M. R. and W. J. Koros (2008). "Defect-free asymmetric hollow fiber membranes from Torlon (R), a polyamide-imide polymer, for high-pressure CO2 separations." Journal of Membrane Science **320**(1-2): 65-72.

Li, B., W. Zhao, Y. L. Su, Z. Y. Jiang, X. Dong and W. P. Liu (2009). "Enhanced desulfurization performance and swelling resistance of asymmetric hydrophilic pervaporation membrane prepared through surface segregation technique." Journal of Membrane Science **326**(2): 556-563.

Li, Q. L. and M. Elimelech (2004). "Organic fouling and chemical cleaning of nanofiltration membranes: Measurements and mechanisms." Environmental Science & Technology **38**(17): 4683-4693.

Listiarini, K., W. Chun, D. D. Sun and J. O. Leckie (2009). "Fouling mechanism and resistance analyses of systems containing sodium alginate, calcium, alum and their combination in dead-end fouling of nanofiltration membranes." Journal of Membrane Science **344**(1-2): 244-251.

Liu, B., C. Chen, T. Li, J. Crittenden and Y. Chen (2013). "High performance ultrafiltration membrane composed of PVDF blended with its derivative copolymer PVDF-g-PEGMA." Journal of Membrane Science **445**(0): 66-75.

Liu, B., C. Chen, W. Zhang, J. Crittenden and Y. Chen (2012). "Low-cost antifouling PVC ultrafiltration membrane fabrication with Pluronic F 127: Effect of additives on properties and performance." Desalination **307**(0): 26-33.

Liu, B., C. Chen, W. Zhang, J. C. Crittenden and Y. Chen (2012). "Low-cost antifouling PVC ultrafiltration membrane fabrication with Pluronic F 127: Effect of additives on properties and performance." Desalination **307**: 26-33.

Liu, B. C., C. Chen, T. Li, J. Crittenden and Y. S. Chen (2013). "High performance ultrafiltration membrane composed of PVDF blended with its derivative copolymer PVDF-g-PEGMA." Journal of Membrane Science **445**: 66-75.

Liu, B. C., C. Chen, W. Zhang, J. Crittenden and Y. S. Chen (2012). "Low-cost antifouling PVC ultrafiltration membrane fabrication with Pluronic F 127: Effect of additives on properties and performance." Desalination **307**: 26-33.

Liu, B. C., C. Chen, W. Zhang, J. Crittenden and Y. S. Chen (2013). "Low-cost antifouling PVC ultrafiltration membrane fabrication with Pluronic F 127: Effect of additives on properties and performance (vol 307, pg 26, 2012)." Desalination **311**: 244-244.

Liu, D. M., Y. W. Chen, N. Zhang and X. H. He (2006). "Controlled grafting of polymer brushes on poly(vinylidene fluoride) films by surface-initiated atom transfer radical polymerization." Journal of Applied Polymer Science **101**(6): 3704-3712.

Liu, F., C.-H. Du, B.-K. Zhu and Y.-Y. Xu (2007). "Surface immobilization of polymer brushes onto porous poly(vinylidene fluoride) membrane by electron beam to improve the hydrophilicity and fouling resistance." Polymer **48**(10): 2910-2918.

Liu, F., Y. Y. Xu, B. K. Zhu, F. Zhang and L. P. Zhu (2009). "Preparation of hydrophilic and fouling resistant poly(vinylidene fluoride) hollow fiber membranes." Journal of Membrane Science **345**(1-2): 331-339.

Liu, Y., B. Q. He, J. X. Li, R. D. Sanderson, L. Li and S. B. Zhang (2011). "Formation and structural evolution of biphenyl polyamide thin film on hollow fiber membrane during interfacial polymerization." Journal of Membrane Science **373**(1-2): 98-106.

Ma, Y., F. Shi, J. Ma, M. Wu, J. Zhang and C. Gao (2011). "Effect of PEG additive on the morphology and performance of polysulfone ultrafiltration membranes." Desalination **272**(1): 51-58.

Manttari, M., K. Viitikko and M. Nystrom (2006). "Nanofiltration of biologically treated effluents from. the pulp and paper industry." Journal of Membrane Science **272**(1-2): 152-160.

Mei, S., C. F. Xiao and X. Y. Hu (2011). "Preparation of Porous PVC Membrane via a Phase Inversion Method from PVC/DMAc/Water/Additives." Journal of Applied Polymer Science **120**(1): 557-562.

Mulder, M. (1991). Basic principles of membrane technology. Dordrecht, Netherlands; Boston, Kluwer Academic.

Ng, W., Ed. (August 7, 2013). Global Membrane Filtration Market Will Surpass $25 Billion in 2017, THOMASNET.

Nunes, S. P., R. Sougrat, B. Hooghan, D. H. Anjum, A. R. Behzad, L. Zhao, N. Pradeep, I. Pinnau, U. Vainio and K. V. Peinemann (2010). "Ultraporous Films with Uniform Nanochannels by Block Copolymer Micelles Assembly." Macromolecules **43**(19): 8079-8085.

Pabby, A. K., S. S. Rizvi and A. M. S. Requena (2008). Handbook of membrane separations: chemical, pharmaceutical, food, and biotechnological applications, CRC press.

Park, J. Y., M. H. Acar, A. Akthakul, W. Kuhlman and A. M. Mayes (2006). "Polysulfone-graft-poly(ethylene glycol) graft copolymers for surface modification of polysulfone membranes." Biomaterials **27**(6): 856-865.

Pasche, S., M. Textor, L. Meagher, N. D. Spencer and H. J. Griesser (2005). "Relationship between Interfacial Forces Measured by Colloid-Probe Atomic Force Microscopy and Protein Resistance of Poly(ethylene glycol)-Grafted Poly(l-lysine) Adlayers on Niobia Surfaces." Langmuir **21**(14): 6508-6520.

Peinemann, K. V., V. Abetz and P. F. W. Simon (2007). "Asymmetric superstructure formed in a block copolymer via phase separation." Nature Materials **6**(12): 992-996.

Petersen, R. J. (1993). "COMPOSITE REVERSE-OSMOSIS AND NANOFILTRATION MEMBRANES." Journal of Membrane Science **83**(1): 81-150.

Pezeshk, N., D. Rana, R. M. Narbaitz and T. Matsuura (2012). "Novel modified PVDF ultrafiltration flat-sheet membranes." Journal of Membrane Science **389**: 280-286.

Phillip, W. A., R. M. Dorin, J. Werner, E. M. V. Hoek, U. Wiesner and M. Elimelech (2011). "Tuning Structure and Properties of Graded Triblock Terpolymer-Based Mesoporous and Hybrid Films." Nano Letters **11**(7): 2892-2900.

Phillip, W. A., M. A. Hillmyer and E. L. Cussler (2010). "Cylinder Orientation Mechanism in Block Copolymer Thin Films Upon Solvent Evaporation." Macromolecules **43**(18): 7763-7770.

Phillip, W. A., B. O'Neill, M. Rodwogin, M. A. Hillmyer and E. L. Cussler (2010). "Self-Assembled Block Copolymer Thin Films as Water Filtration Membranes." Acs Applied Materials & Interfaces **2**(3): 847-853.

Rana, D. and T. Matsuura (2010). "Surface Modifications for Antifouling Membranes." Chemical Reviews **110**(4): 2448-2471.

Rana, D. and T. Matsuura (2010). "Surface Modifications for Antifouling Membranes." Chem. Rev. **110**: 2448–2471.

Rasanen, E., N. B. Nystrom, J. Sahlstein and O. Tossavainen (2002). "Comparison of commercial membranes in nanofiltration of sweet whey." Lait **82**(3): 343-356.

Salimi, A. and A. A. Yousefi (2003). "FTIR studies of beta-phase crystal formation in stretched PVDF films." Polymer Testing **22**(6): 699-704.

Schäfer, A. I., A. G. Fane and T. D. Waite (2005). Nanofiltration : principles and applications. Oxford, Elsevier.

Shannon, M. A., P. W. Bohn, M. Elimelech, J. G. Georgiadis, B. J. Mariñas and A. M. Mayes (2008). "Science and technology for water purification in the coming decades." Nature **452**(7185): 301-310.

Smart, T., H. Lomas, M. Massignani, M. V. Flores-Merino, L. R. Perez and G. Battaglia (2008). "Block copolymer nanostructures." Nano Today **3**(3-4): 38-46.

Stuart, M. A. C., W. T. S. Huck, J. Genzer, M. Muller, C. Ober, M. Stamm, G. B. Sukhorukov, I. Szleifer, V. V. Tsukruk, M. Urban, F. Winnik, S. Zauscher, I. Luzinov and S. Minko (2010). "Emerging applications of stimuli-responsive polymer materials." Nature Materials **9**(2): 101-113.

Su, Y., W. Cheng, C. Li and Z. Jiang (2009). "Preparation of antifouling ultrafiltration membranes with poly(ethylene glycol)-graft-polyacrylonitrile copolymers." Journal of Membrane Science **329**(1-2): 246–252.

Tan, X. Y., S. P. Tan, W. K. Teo and K. Li (2006). "Polyvinylidene fluoride (PVDF) hollow fibre membranes for ammonia removal from water." Journal of Membrane Science **271**(1-2): 59-68.

Tang, C. Y. Y., Y. N. Kwon and J. O. Leckie (2007). "Probing the nano- and micro-scales of reverse osmosis membranes - A comprehensive characterization of physiochemical properties of uncoated and coated membranes by XPS, TEM, ATR-FTIR, and streaming potential measurements." Journal of Membrane Science **287**(1): 146-156.

Tang, L., W. Y. Gu, P. Yi, J. L. Bitter, J. Y. Hong, D. H. Fairbrother and K. L. Chen (2013). "Bacterial anti-adhesive properties of polysulfone membranes modified with polyelectrolyte multilayers." Journal of Membrane Science **446**: 201-211.

Taniguchi, M. and G. Belfort (2002). "Correcting for surface roughness: Advancing and receding contact angles." Langmuir **18**(16): 6465-6467.

Taniguchi, M. and G. Belfort (2004). "Low protein fouling synthetic membranes by UV-assisted surface grafting modification: varying monomer type." Journal of Membrane Science **231**(1-2): 147-157.

Teoh, M. M. and T. S. Chung (2009). "Micelle-like macrovoids in mixed matrix PVDF-PTFE hollow fiber membranes." Journal of Membrane Science **338**(1-2): 5-10.

Tian, J. Y., Z. L. Chen, Y. L. Yang, H. Liang, J. Nan and G. B. Li (2010). "Consecutive chemical cleaning of fouled PVC membrane using NaOH and ethanol during ultrafiltration of river water." Water Research **44**(1): 59-68.

Tiraferri, A., N. Y. Yip, W. A. Phillip, J. D. Schiffman and M. Elimelech (2011). "Relating performance of thin-film composite forward osmosis membranes to support layer formation and structure." Journal of Membrane Science **367**(1-2): 340-352.

Tuteja, A., W. Choi, M. L. Ma, J. M. Mabry, S. A. Mazzella, G. C. Rutledge, G. H. McKinley and R. E. Cohen (2007). "Designing superoleophobic surfaces." Science **318**(5856): 1618-1622.

Van der Bruggen, B. (2009). "Chemical Modification of Polyethersulfone Nanofiltration Membranes: A Review." Journal of Applied Polymer Science **114**(1): 630-642.

Van der Bruggen, B., K. Everaert, D. Wilms and C. Vandecasteele (2001). "Application of nanofiltration for removal of pesticides, nitrate and hardness from ground water: rejection properties and economic evaluation." Journal of Membrane Science **193**(2): 239-248.

Venault, A., Y. Chang, D. M. Wang and J. Y. Lai (2012). "Surface anti-biofouling control of PEGylated poly(vinylidene fluoride) membranes via vapor-induced phase separation processing." Journal of Membrane Science **423**: 53-64.

Venault, A., Y. H. Liu, J. R. Wu, H. S. Yang, Y. Chang, J. Y. Lai and P. Aimar (2014). "Low-biofouling membranes prepared by liquid-induced phase separation of the PVDF/polystyrene-b-poly (ethylene glycol) methacrylate blend." Journal of Membrane Science **450**: 340-350.

Vrijenhoek, E. M., S. Hong and M. Elimelech (2001). "Influence of membrane surface properties on initial rate of colloidal fouling of reverse osmosis and nanofiltration membranes." Journal of Membrane Science **188**(1): 115-128.

Wang, J. S. and K. Matyjaszewski (1995). "CONTROLLED LIVING RADICAL POLYMERIZATION - ATOM-TRANSFER RADICAL POLYMERIZATION IN THE PRESENCE OF TRANSITION-METAL COMPLEXES." Journal of the American Chemical Society **117**(20): 5614-5615.

Wang, P., K. L. Tan, E. T. Kang and K. G. Neoh (2001). "Synthesis, characterization and anti-fouling properties of poly(ethylene glycol) grafted poly(vinylidene fluoride) copolymer membranes." Journal of Materials Chemistry **11**(3): 783-789.

Wang, P., K. L. Tan, E. T. Kang and K. G. Neoh (2002). "Antifouling poly(vinylidene fluoride) microporous membranes prepared via plasma-induced surface grafting of poly(ethylene glycol)." Journal of Adhesion Science and Technology **16**(2): 111-127.

Wang, Y. and F. Li (2011). "An Emerging Pore-Making Strategy: Confined Swelling-Induced Pore Generation in Block Copolymer Materials." Advanced Materials **23**(19): 2134-2148.

Wang, Y. Q., T. Wang, Y. L. Su, F. B. Peng, H. Wu and Z. Y. Jiang (2005). "Remarkable reduction of irreversible fouling and improvement of the permeation properties of poly(ether sulfone) ultrafiltration membranes by blending with Pluronic F127." Langmuir **21**: 11856-11862.

Xu, J. A. and Z. L. Xu (2002). "Poly(vinyl chloride) (PVC) hollow fiber ultrafiltration membranes prepared from PVC/additives/solvent." Journal of Membrane Science **208**(1-2): 203-212.

Xu, L. R., C. Zhang, M. Rungta, W. L. Qiu, J. Q. Liu and W. J. Koros (2014). "Formation of defect-free 6FDA-DAM asymmetric hollow fiber membranes for gas separations." Journal of Membrane Science **459**: 223-232.

Yang, Q., Z. K. Xu, Z. W. Dai, J. L. Wang and M. Ulbricht (2005). "Surface modification of polypropylene microporous membranes with a novel glycopolymer." Chemistry of Materials **17**(11): 3050-3058.

Yang, S. Y., J. Park, J. Yoon, M. Ree, S. K. Jang and J. K. Kim (2008). "Virus filtration membranes prepared from nanoporous block copolymers with good dimensional stability under high pressures and excellent solvent resistance." Advanced Functional Materials **18**(9): 1371-1377.

Yang, S. Y., I. Ryu, H. Y. Kim, J. K. Kim, S. K. Jang and T. P. Russell (2006). "Nanoporous membranes with ultrahigh selectivity and flux for the filtration of viruses." Advanced Materials **18**(6): 709-+.

Yang, S. Y., J. A. Yang, E. S. Kim, G. Jeon, E. J. Oh, K. Y. Choi, S. K. Hahn and J. K. Kim (2010). "Single-file diffusion of protein drugs through cylindrical nanochannels." Acs Nano **4**(7): 3817-3822.

Yeow, M. L., R. W. Field, K. Li and W. K. Teo (2002). "Preparation of divinyl-PDMS/PVDF composite hollow fibre membranes for BTX removal." Journal of Membrane Science **203**(1-2): 137-143.

Yeow, M. L., Y. T. Liu and K. Li (2004). "Morphological study of poly(vinylidene fluoride) asymmetric membranes: Effects of the solvent, additive, and dope temperature." Journal of Applied Polymer Science **92**(3): 1782-1789.

Yi, Z., L. P. Zhu, Y. F. Zhao, B. K. Zhu and Y. Y. Xu (2012). "An extending of candidate for the hydrophilic modification of polysulfone membranes from the compatibility consideration: The polyethersulfone-based amphiphilic copolymer as an example." Journal of Membrane Science **390**: 48-57.

Yin, J., X. Yao, J.-Y. Liou, W. Sun, Y.-S. Sun and Y. Wang (2013). "Membranes with Highly Ordered Straight Nanopores by Selective Swelling of Fast Perpendicularly Aligned Block Copolymers." ACS Nano.

Young, T. H. and L. W. Chen (1995). "Pore formation mechanism of membranes from phase inversion process." Desalination **103**(3): 233-247.

Yu, H. Y., Y. Kang, Y. L. Liu and B. X. Mi (2014). "Grafting polyzwitterions onto polyamide by click chemistry and nucleophilic substitution on nitrogen: A novel approach to enhance membrane fouling resistance." Journal of Membrane Science **449**: 50-57.

Yu, S. C., Q. B. Cheng, C. M. Huang, J. Liu, X. Y. Peng, M. H. Liu and C. J. Gao (2013). "Cellulose acetate hollow fiber nanofiltration membrane with improved permselectivity prepared through hydrolysis followed by carboxymethylation." Journal of Membrane Science **434**: 44-54.

Zavala-Rivera, P., K. Channon, V. Nguyen, E. Sivaniah, D. Kabra, R. H. Friend, S. K. Nataraj, S. A. Al-Muhtaseb, A. Hexemer, M. E. Calvo and H. Miguez (2012). "Collective osmotic shock in ordered materials." Nature Materials **11**(1): 53-57.

Zhang, P. Y., Z. L. Xu, H. Yang, Y. M. Wei, W. Z. Wu and D. G. Chen (2013). "Preparation and characterization of PVDF-P(PEGMA-r-MMA) ultrafiltration blend membranes via simplified blend method." Desalination **319**: 47-59.

Zhang, X. Z., Y. S. Chen, A. H. Konsowa, X. S. Zhu and J. C. Crittenden (2009). "Evaluation of an innovative polyvinyl chloride (PVC) ultrafiltration membrane for wastewater treatment." Separation and Purification Technology **70**(1): 71-78.

Zhang, Y., Z. Wang, W. F. Lin, H. T. Sun, L. G. Wu and S. F. Chen (2013). "A facile method for polyamide membrane modification by poly(sulfobetaine methacrylate) to improve fouling resistance." Journal of Membrane Science **446**: 164-170.

Zhao, Y.-H., Y.-L. Qian, B.-K. Zhu and Y.-Y. Xu (2008). "Modification of porous poly(vinylidene fluoride) membrane using amphiphilic polymers with different structures in phase inversion process." Journal of Membrane Science **310**(1-2): 567-576.

Zhao, Y. H., Y. L. Qian, B. K. Zhu and Y. Y. Xu (2008). "Modification of porous poly(vinylidene fluoride) membrane using amphiphilic polymers with different structures in phase inversion process." Journal of Membrane Science **310**(1-2): 567-576.

Zhao, Y. H., B. K. Zhu, L. Kong and Y. Y. Xu (2007). "Improving hydrophilicity and protein resistance of poly(vinylidene fluoride) membranes by blending with amphiphilic hyperbranched-star polymer." Langmuir **23**(10): 5779-5786.

Zhao, Z. G., J. F. Zheng, M. J. Wang, H. Y. Zhang and C. C. Han (2012). "High performance ultrafiltration membrane based on modified chitosan coating and electrospun nanofibrous PVDF scaffolds." Journal of Membrane Science **394**: 209-217.

Zhou, M., H. Liu, J. E. Kilduff, R. Langer, D. G. Anderson and G. Belfort (2009). "High-Throughput Membrane Surface Modification to Control NOM Fouling." Environ. Sci. Technol. **43**: 3865-3871.

Zhou, M. Y., H. W. Liu, J. E. Kilduff, R. Langer, D. G. Anderson and G. Belfort (2009). "High-Throughput Membrane Surface Modification to Control NOM Fouling." Environmental Science & Technology **43**(10): 3865-3871.